2

Binding and specificity of Aluminium in proteins

E. Rezabal

December 26, 2007

Acknowledgments

This research was funded by Euskal Herriko Unibertsitatea (the University of the Basque Country) and Eusko Jaurlaritza (the Basque Government).

The SGI/IZO-SGIker UPV/EHU (supported by the National Program for the Promotion of Human Resources within the National Plan of Scientific Research, Development and Innovations, Fondo Social Europeo and MCyT) is gratefully acknowledged for generous allocation of computational resources in Spain.

Contents

Part 1 Introduction

1
Sarrera

1.1
Biosferan aurkitzen den aluminioaren jatorria

Bizitzarako beharrezkoa ez den arren, aluminioak ingurune biologikoetan duen konzentrazio altua ulertzeko, bere ziklo biogeokimikoa izan behar da kontutan, zeina lehen aldiz C. Exley-ek osatu baitzuen [1] (ikus 2.1 irudia). Lurrazalean aurki daitezkeen elementuen artean, aluminioa da hirugarrena ugaritasunean, oxigeno eta silizioaren ondoren, noski, lurrazalaren % 8-a aluminioak osatzen baitu [2]. Litosferak iragazgaiztasun haundia du eta aluminioari oso ondo eusten dio biosferatik kanpo, bertan ziklatzen den aluminioaren % 99.999-a litosferan bertan geratzen da. Feldespato, kaolinita edo aluminosilikatua bezalako lehen eta bigarren mailako mineraletatik igaro eta fase koloidalak osatu ondoren, zenbait sedimentazio prozesuri esker, aluminioa lurrazalera itzuliko da prezipitazio eta disoluzio sail desberdinen bidez. Hau da, ziklatutako aluminioaren zati bat beti disoluzioan aurkitzen da; bertan, aluminioak ondoren konposatu disolbagaitzak osatuko dituzten espezieak osa ditzake, edo bestela, molekula organikoei lotu eta konposatu disolbagarriak sor ditzake [3], horrela, ziklo biotikora iritsiz.

Edozein izaki bizidunetan aurki daiteke aluminioa, biosfera osoan zehar. Halere, oraindik ez zaio funtzio biologikorik ezagutzen giza gorputzean, eta beste gainontzeko izakitan izan ditzakeen funtzioei buruz ere, oso informazio gutxi dago [1]. Sistema biologikoetarako metal tribalenteak ez dira egokiak, berauen neurri txiki eta karga haundiaren ondorioz euren ligando trukaketa abiadura oso baxua delako. Aluminioa oso txikia eta karga handikoa da, horrexegatik, ez du izan inoiz sistema biologikoan erabilgarritasunik [4, 5]. Funtzio gabezia honek litosferak metala sistema biologikoetatik at mantentzeko duen gaitasunaren ondorio eta era berean, froga gisa har daiteke.

Hala eta guztiz ere, biosferan aluminioaren konzentrazioa oso altua da, bizitzarako beharrezkoak diren beste metalenarekin alderatuta, eta hau ez dator bat, ez bere ziklo litosferikoaren ezaugarriekin ezta funtzio biologikoaren

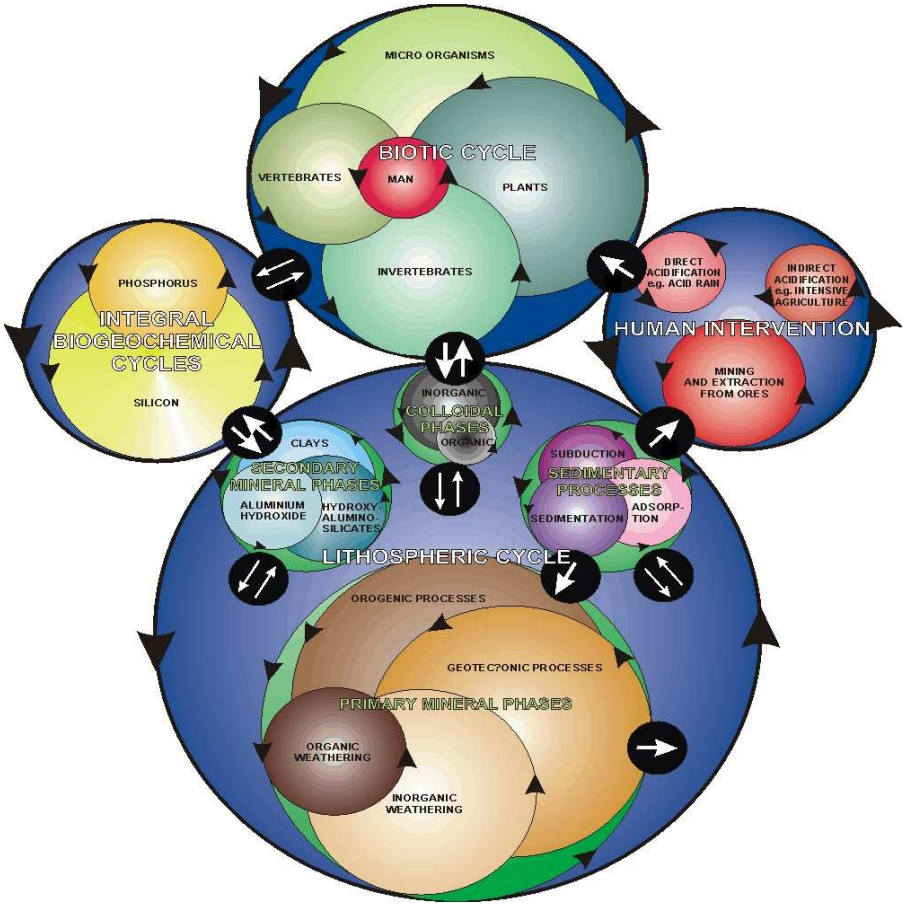

Fig. 1.1 Aluminioaren ziklo biogeokimikoa [1]

gabeziarekin ere. Izan ere, gizakiak zerikusi handia izan du aluminioaren eskuragarritasun biologikoaren handitzean eta, ondorioz, baita biosferan aurki daitekeen aluminio konzentrazioan ere. Bi modutan eragin du gizakiak:

Alde batetik, ingurunean azidotasuna eraginez. Honek, azidotasunak alegia, litosferaren higadura areagotu egin du, eta ondorioz, lurraren tanpoi izaera gutxitu egin da [3]. Aluminioaren kimikan pH-ak eragin handia du, honen disolbagarritasuna ingurune alkalino edo azidoetan haunditu egin daiteke eta. Halakoetan, euri azidoa deritzanak aluminioa litosferatik atera eta uretara eramango du, lurrera, eta lurrazpiko eta lurrazaleko uretara iritsiaz. Horrela handitu da nabarmen aluminioaren eskuragarritasuna [2].

Bestalde, XIX. mendearen bukaeraz geroztik, gure gizartean oso erabilia izan da aluminioa. Gaur egun, edaten dugu uretan, industrian, sendagaietan,

txertoetan, zain bidezko elikaduran [6], kosmetikoetan [7, 8], etab.etan aurki dezakegu. Aluminio-iturri hauek, era berean, ingurunean aurki daitekeen Al konzentrazioa handitu egiten dute.

1.2 Aluminioa giza gorputzean

Egunean 10-30 mg aluminio sartzen dugu gorputzean batazbeste, baina behin gorputzean aurkitzen duen lehen oztopoa hestea da, honek oso gutxi xurgatzen baitu (5-10μg). Odolera iristen den kopuru hau, faktore ugariren eraginpean dago: besteak beste, hestean bertan aurki dezakegun zitrato, Ca, Mg, Si edo D bitamina konzentrazioa, gorputzean daukagun burdina, edo hormona paratiroidea, besteak beste [9]. Honetaz gain, aluminio konzentrazio altuak, iraitz aparatuaren arazoak, adinak, etab.ek ere, xurgatutako aluminio kopurua areagotu dezakete.

Ondoren, odolean zehar garraiatu eta zelularen mintza zeharkatuz, zenbait organotan pila daiteke, arazo metaboliko [9] eta gaisotasun ugari eraginez: osteomalazia hezurretan [10], anemia odoleko globulu gorrietan, edota gaisotasun neurodegeneratiboak [11] burmuinean.

Eredu anitz izan dira proposatuak aluminioak zelularen mintza nola zeharkatzen duen azaltzeko [12]. Masa haundiko (hala nola transferrina eta albumina) eta txikiko (adibidez, zitratoa, fosfatoak, oligopeptidoak [13], aminoazidoak [6], etab.) espezieei lotuta dagoela aluminioa odolean, gauza jakina da, eta hauek, espezie hauek, metala garraiatzeko eta zelularen mintza zeharkatzeko ahalmen handikoak dira. Mintzen ezaugarri biofisikoetan, aluminioak aldaketa garrantzitsuak eragin ditzakeela ere ikusi da [9]. Gai honen inguruan oraindik argitu gabe dago zein den aluminioaren garraiatze modua eta zelula barnerako sarbidea, lan asko egin bada ere.

Aluminioaren jomuga garrantzitsuenetako bat burmuina da, han metatu egiten baita, eta are gehiago adinean aurrera egin ahala [14]. Oso da neurotoxikoa aluminioa, nerbio sisteman kalte handiak eragiten ditu [15] eta alboko esklerosi amiotrofikoa, Parkinson, Alzheimer eta beste gaisotasun neurodegeneratibo askorekin lotua dago. Odolaren eta burmuinaren artean muga bat dago, euren artean egon daitekeen espezie trukaketak zorrozki zaintzeko eta neuronak odolean aurki daitezkeen konposatu toxikoetatik babesteko [16]. Horrexegatik da beraz garrantzitsua jakitea, nola zeharkatzen duen aluminioak aipatutako muga hori, horrela, ondorio toxikoak sahiesteko bideak ezagutzeko.

1.3 Proteinekin zerikusia duten prozesu toxikoak: metalen eragina

Proteinak dira, peptido eta aminoazidoekin batera, sistema bizidunetan aurki daitezkeen konposatu garrantzitsuenetakoak. Konposatu organiko erreaktibo gisa, organo eta ehunak osatu eta prozesu biologikoak erregulatzen dituzte [8].

Metal ioiak dauzkate proteinen erdiak, eta ribozima gehienentzat, metalak beharrezkoak dira euren funtzioa beteko badute, entzima askoren parte baitira, eta erreakzio katalitiko askorentzat ezinbestekoak [17]. Proteinekin erlazionatutako funtzio anitz betetzen dituzte metalek, eta askotan, lagundu egiten dute proteinen estruktura egonkortu edo proteinaren konformazio aktibo konkretu bat mantentzen. Gerta liteke, hala ere, metal eta proteinen arteko interakzioek prozesu toxikoak ematea, adibidez, "egitura gaisotasunak" deritzona, edota entzimen funtzio biologikoaren aldaketa.

Proteina konkreturen baten egitura aldaketa eta metaketaren ondorioz gaisotasun neurodegeneratibo ugari sortzen da, "egitura-gaisotasunak" deritzaienak. Hauen artean aurki daitezke Alzheimer gaisotasuna, Parkinson gaisotasuna, prioi gaisotasunak (Creutzfeld-Jacob gaisotasuna, entzefalopatia espongiformea, adibidez), Huntington-en gaisotasuna, fibrosi kistikoa, etab. Gaisotasun hauetan, proteinaren ohiko egitura aldatu eta forma kaltegarri bat sortzen da, beste proteinei elkartzeko gai dena, eta ondorioz toxikoak diren plaka solidoak osatzen ditu garunean. Plaka hauek oso ondo antolatuak eta oso egonkorrak dira, eta eritasun neurologikoak sortzen dituzte [18]. Prozesu osoa oso konplexua da, proteinaren forma eta tarteko konposatu oligomeriko ugarik hartzen bait dute parte. Hainbat esperimentutan ikusi da metalek, batez ere, Cu(II), Fe(III), Zn(II) eta Al(III)-ak, solido hauen eraketa eragin eta azkartzen dutela [19–23]. Halere, metal hauek, prozesuan duten funtzio zehatza ezezaguna da, batez ere aluminioarena. Nahiz gaisotasun mota honen eragilea ez izan, zalantzarik gabe esan daiteke aluminioak, gaisotasuna garatzen lagundu egiten duela.

Bestalde, metalek entzima bidez katalizaturiko erreakzioak kontrolatu ditzakete, eta baita sustratoa lotu eta modu egokian orientatu ere. Metal egokirik gabe, metaloentzima batek katalizaturiko erreakzio biokimikoa oso poliki gertatuko litzateke, gertatzekotan. Entzima bakoitzak metal konkretu batentzat neurri egokia eta talde lotzaile egokiak dituen gune bat du, dagokion ingurune hidrofobiko edo hidrofilikoan. Metala proteinaren kate nagusiko amino eta karbonilo taldeei lotuko zaie, baina lotura espezifikoa aminoazidoen alboko taldeei esker lortuko du, batez ere, azido aspartiko eta glutamikoaren talde karboxilatoari eta histidinaren eraztun nitrogenodunari esker. [24]

1.4 Aluminioa eta proteinak

Aluminioa aminoazidoei, oligopeptidoei [25] eta proteinei lotu dakioke, azken hauekin oso lotura sendoa osatzen duelarik [8]. Aluminioa proteina desberdin askori lotuta aurkitu da, odolean zehar garraiatzeko edota zelulamintza zeharkatzean, baina baita ere entzimen funtzionamendua aldatu eta prozesu toxikoak eragin ditzaketen egitura aldaketak sortuz proteinan [26]. Aluminioak egitura aldaketak eragin ditzake zitoeskeletoko proteinetan (neurofilamentuak, tau proteinak), gaisotasunekin erlazionatutako proteinetan (amiloidea, α-sinukleina) eta beste proteina batzuetan (kalmodulina, transferrina, laktoalbumina...) [15].

Aluminioak eragin negatiboa du euren funtzioa betetzeko beste metal batzuk (adibidez magnesioa eta kaltzioa) beharrezkoak dituzten proteinengan. Aluminioa entzima askoren funtzioa aldatzeko gai da, adibidez, hexokinasa, fosfofruktokinasa, monoamina oxidasa, dihidropterina reduktasa, anidrasa karbonikoa, tripsina, kimotripsina, azetilkolinesterasa, etab. [26, 27]. Aluminioak energiaren produkzioan eragina du, Krebs-en zikloan aldaketak eragiten bait ditu, eta baita inositolaren zikloan ere, zeina memoriaren eraketarekin erlazionatua dagoen. Neurotransmisoreen aktibitatea areagotu dezakeela ere esan izan da [9]. Aluminioaren aurrean eragina jasaten duten beste entzima batzuk, berriz, Alzheimerren gaisotasunarekin erlazionatuta daudela ikusi da.

1.5 Aluminioaren eragina beste metal batzuen metabolismoan

Aluminioari, naturan, ez dagokio inolako proteinarik, beraz, beste metalen lekua hartzeko joera du. Ca(II), Mg(II) eta Fe(III) dira metalik kaltetuenak, euren antzekotasun fisikokimikoa dela medio. Propietate fisikokimiko hauen artean daude ligando berdinak lotzeko joera eta metalen karga eta neurri antzekotasuna [17, 28–33].

1.5.1 Burdina

Transferrina (Tf) da aluminioak (erradio ionikoa 0.535 Å) burdina (erradio ionikoa 0.645 Å) ordezkatzen duen adibide nagusiena. Al-Tf konplexua odolean aurki dezakegun aluminio espezierik ugariena da, odoleko beste edozein ligando baino sendoago lotzen baitu aluminioa trasferrinak.

Tf-a burdina lotzen duen proteina bat da, 700 aminoazido inguru dituen polipeptido bakarraz osatua. Metala lotu dezaketen bi gune ditu, bakoitzean lau proteina ligando dituelarik, bi tirosina, histidina bat eta aspartato bat. Pro-

teinari lotuta metalik ez denean aurkitzen, gune hauek konformazio irekia dute, eta metala lotuta badute berriz, konformazio itxia deritzona. Odolean aurki dezakegun aluminioaren % 90a Tf-ri lotuta aurki dezakegu, eta modu honetan, endozitosiaren bidez burmuinera iritsi daitekeela gauza jakina da. Halere, burmuinera iristeko duen bide nagusia hau den ala ez eztabaidagai da, ikerketa batzuen arabera [8, 34].

Tf-a odolean konzentrazio normaletan dugunean, metala lotu dezaketen guneetatik % 30a besterik ez dago Fe atomo bati lotuta [35]. Ikerketen arabera, aluminioa ez da burdinarekiko lehiakorra Tf lotzean, beraz, aluminioak libre dauden Tf-ren guneak beteko dituela onartzen da [36]. Oraindik zalantzan dago nola gertatzen diren metalaren lotzea eta askatzea. Orain dela gutxi, burdinaren askatzea eta guneen konformazio ireki eta itxiak ikertu dira [37, 38]. Hala eta guztiz ere, oso informazio gutxi dugu Al-Tf espeziaren egitura zehatzari buruz. Prozesuen zinetikari buruz ere oso gutxi dakigu, eta lortutako emaitzak, gainera, ez datoz bat [36, 39]. Tf-ak daraman metala zelulara sartu dadin lehenik transferrina hartzailea den molekulari lotu behar zaio. Lan batzuek diotenez, Al-Tf eta Fe-Tf konplexuak hartzaileari sendotasun antzekoarekin lotu dakizkioke [40], baina beste batzuen arabera, ez da elkarrekintzarik ikusten Al-Tf eta hartzailearen artean [36]. Bestalde, hartzailearen bidezko aluminioaren garraioa zelula barnera ez dela batere eraginkorra esan da. [8]

1.5.2 Kaltzioa

Aluminioak era anitzetan oztopatzen du kaltzioaren (erradio ionikoa 0.99 Å) metabolismoa.

Odolean aurki dezakegun proteina ugarienetakoa albumina da, eta Ca-rentzako lotura-gune espezifikoa du. Gune honi lotzeko aluminioa gai dela ikusi da [8, 41], eta, horrela, albumina beste garraiobide bat da odolean aluminioarentzat.

Kaltzioa lotzen duten proteina talde bat EF-familia deiturikoa da, non guztiek lotura-gune baliokideak dituzten. Aipatu taldean aurki ditzakegu, bakoitza bere funtzioarekin, kalmodulina, parbalbumina, C-troponina, adibidez. Metal tribalenteek, karga-karga interakzio indartsuagoa sortzen dutenez, kaltzioa bezain tinko hel diezaiokete EF proteinari [42, 43]. Hau da, hain zuzen, kalmodulinaren kasua; eta aluminioa lotzen zaionean egitura aldaketa garrantzitsuak jasaten ditu [8].

Halere, orokorrean, aluminioa eta kaltzioaren arteko lehia lotura-gune batekiko ez da litekeena. Izan ere, kaltzioa aluminioa baino dexente handiagoa da, eta gainera, lotura gune espezifikotan aurkitzen dugu orokorrean. Kaltzioaren bolumena, gogokoen duen koordinazioan (8 ligandori lo-

tuta), aluminioarena baino bederatzi aldiz haundiagoa da. Beraz, aluminioak ezingo luke kaltzioaren lekua hartu inguruko taldeen berrantolaketa sakon bat ematen ez bada, eta hala balitz, energia asko eskatuko luke. Beraz, aluminio eta kaltzioaren arteko lehia gerta liteke ligando txikietan, proteinetan, aldiz, ez [45].

1.5.3 Magnesioa

Bizitzarako beharrezkoa den elementua da magnesioa, erreakzio biokimiko askotan hartzen du parte eta proteina ezberdin ugari lotzen ditu, (gorputzean ematen diren 300 erreakzio entzimatiko baino gehiagotan parte hartzen du [46]), eta horretaz gain funtzio fisiologiko askotan berebiziko garrantzia duten funtzioak betetzen ditu. Zelula barneko eta zelulaz kanpoko funtzioetan parte hartzeaz gain, prozesu metabolikoetan, proteina sintesian, nerbio sisteman, hormonen jariapenean etab.etan ere parte hartzen du [46]. Neurona babeslea dela esaten da, izan ere, magnesio gabeziak gaisotasun neurodegeneratiboak dakartza nahiz eta eskasi honek bakarrik ezin duen gaisotasuna sortu [47].

Aluminioarekin lehia gehien duen metala da magnesioa (erradio ionikoa 0.72 Å) [8, 48, 49], biak neurriz antzekoak direlako. Neurri antzekotasuna karga antzekotasuna baino garrantzitsuagoa da metalen arteko lehiakortasunari dagokionez [45, 48, 50, 51]. Nahiz eta magnesioa aluminioa baino zertxobait haundiago den, ezaugarriak alderatuz gero aluminioak magnesioaren lotura guneak bilatuko lituzkeela pentsatzeak zentzuzkoa dirudi [45]. Euren funtzioa betetzeko magnesioa beharrezkoa duten entzima askok aluminioaren aurrean beren funtzioa galtzen dutela ikusi da [9], eta gehienetan, aluminioak magnesioaren lekua hartzen duela ikusi da edo onartu da, behintzat [8].

Eskuragarri diren datu kristalografiko gutxien artean, D-xylosa isomerasa deritzon entzima dugu. Entzima honek aldosa motako azukreak ketosa bihurtzen duen erreakzioa katalizatzen du. Mg (II), Co (II) edo Mn (II) beharrezkoak ditu aktibatua izango bada, aldiz, Ca(II), Ba(II) eta Al(III)-ak erreakzioa inhibitzen dute. Emaitzek adierazten dutenez, aluminioa lotzeak ez du gune aktiboan egitura aldaketa esanguratsurik eragiten, magnesioarekin alderatuz, baina, hala eta guztiz ere, aluminioa lotzea nahikoa da entzimari bere funtzioa betetzea galerazteko [48].

Proteinak metal bat edo beste aukeratzean, metalaren propietateak (estereokimika, karga, neurria), dagokion ingurune biologikoan metalak duen konzentrazioa, edota proteinaren propietateak (metal lotura gunean dituen ligandoak eta gunearen estereokimika) kontutan hartu behar dira.

Magnesio eta aluminioaren ezaugarri fisikokimikoek trukaketa baimentzen dute, biek sei ligandori lotuz koordinazio oktaedrikoa osatzeko joera dute,

eta ioi 'gogorrak' dira, hau da, ligando 'gogorrak' lotuko dituzte, batez ere oxigenodun eta nitrogenodun taldeak [48].

Aluminioak magnesioak baino ligando trukaketa abiadura txikiagoa du. Magnesioa oso katalizatzaile egokia da erreakzioaren aktibazio energia baxua duten kasutan. Aluminioaren karga altuagoa dela eta, magnesioak baino sendoago lotzen ditu ligandoak, eta beraz, ligando bat askatzean izango duen abiadura ere motelagoa izango da, horrela proteinaren funtzioa galeraziz [5].

Halere, kontutan izan behar dugu ohiko egoeran sistema biologikoetan aurki dezakegun magnesio (10^{-3} M) konzentrazio altuak horrelako trukaketa bat ekidingo duela, aluminioaren konzentrazio baxuaren aurrean (10^{-10} M pH=7.3-an) [52]. Badirudi, eboluzioan zehar proteina batzuek magnesioa aukeratu dutela kofaktore gisa bere konzentrazio altua dela eta. Magnesioa lotzen duten proteinak ez daude orokorrean babestuak kaltegarri izan daitezkeen beste metal batzuen lehiaren aurrean. Hau da, ez da proteina magnesioa lotzeko diseinatua izan dena, baizik eta zelula da magnesioren konzentrazio altua mantentzen duena [17].

Halere, baliteke aluminio eta magnesioaren konzentrazioak aldatzea, aluminio intoxikazio haundi bat dugunean, adibidez, edota magnesio gabezia ematen denean.

Magnesio falta adinekoen artean sarri ematen da, batez ere magnesioaren metabolismoa kontrolatzen duten faktoreen funtzionamendu txarraren ondorioz [46] eta, lehen esan bezela, gorputzean metatutako aluminioa gero eta gehiago da adinean aurrera goazen heinean. Ikerketa batzuk diotenez, nerbio sistema zentralean magnesioaren gabeziak aluminioaren xurgapena areagotu dezake, gaisotasun neurodegeneratiboak areagotuz [47, 53].

Metalen konzentrazio erlatiboan ematen diren aldaketa hauek proteinaren metal aukeraketa alda dezakete, horrela aluminioa proteinan sartu eta prozesu toxikoak eragin ditzakeelarik. Gaixotasun neurodegeneratiboak izandako burmuin ehunak aztertzean, kaltetuen izan diren burmuin zatietan magnesio konzentrazio baxua eta aluminio konzentrazio altua aurkitu dira [53–56]. Are gehiago, uste da Kii penintsula eta Guam-en ikusitako alboko esklerosi amiotrofiko eta Parkinsonen gaisotasuna aluminio konzentrazio altua eta kaltzio eta magnesio konzentrazio baxuaren ondorioz eman izan direla [15]. Halere, metalen konzentrazio aldaketak gaisotasun neurologikoetan izan dezakeen eragina ez dago oraindik argi [57].

Aluminioak magnesioaren lekua hartzea arazo hauek azaltzeko saiakera bat da [54], izan ere, oinarri molekularrak oraindik ezezagunak baitira. Ikerketa batzuek diotenez, proteina konkreturen batetan ematen den konformazio aldaketa baten ondorioz Alzheimerren gaisotasuna areagotzen da. Proteinaren egitura kaltegarri honek afinitate haundiagoa luke aluminioarenganako, magnesioarenganako ordez, proteina normalean gertatzen denaren alderantzizkoa [53] .

1.6
Ikerketa lan honen helburua

Ikusi dugunez, aluminioaren metabolismoan proteina ugarik hartzen du parte, eta bere eraginez proteina ugarik jasaten ditu egitura eta funtzio biokimiko aldaketak ere. Beraz, aluminioak proteinetan bilatzen dituen lotura guneen ezaugarriak zeintzuk diren jakitea oso erabilgarria da nola garraiatzen den, zelulara nola sartzen den ulertzeko, baita bere toxizitatean mekanismoak ulertzeko ere. Halere, aluminio-proteina egiturei buruz oso datu kristalografiko eta termodinamiko gutxi dago. Beraz, gure helburuetako bat datu hauek ematea izango da, metalaren lehen solbatazio geruzan oinarrituz, hori baita proteinari lotzen dena. Datu hauek, ondoren, aluminioak proteina konkretuekin osatu ditzakeen sistemen ikerketan lagundu dezakete.

Bestalde, aluminioaren toxikotasunaren oinarri izan daitekeen mekanismoetako bat magnesioa ordezkatzea da. Magnesioa proteina mota, lotura gune eta proteina ingurune desberdinetan aurki dezakegu. Ikerketa lan honetan, magnesio eta aluminioaren lotura energi erlatiboak neurtuko ditugu, sistematikoki, proteinen lotura gune desberdinetan, horrela, trukaketa hau baldintzatzen duten faktoreak zeintzuk diren jakiteko.

2
Introduction

2.1
The origin of the presence of aluminium in the biosphere

The biogeochemical cycle of aluminium, elaborated for the first time by C. Exley [1] (see Fig. 2.1), helps to understand the origin of the ubiquitous presence of aluminium in biota, despite its lack of essentiality. Al(III) is the third most abundant element in the earth crust, after oxygen and silicon, comprising about its 8% [2]. Its retention in the lithosphere is extremely efficient, with 99.999% of cycled aluminium being retained. It is cycled through a series of dissolution/precipitation events, going from primary and secondary minerals as feldspars, kaolinite, or aluminosilicates to colloidal phases and then returned to the Earth's crust via sedimentary processes. This involves a significant proportion of cycled aluminium being fully dissolved in the aqueous phase. Soluble aluminium can either form the precursors to the insoluble phases, or in the presence of competitive functional groups associated with organic molecules [3], can form soluble complexes with organic molecules, as free inorganic complexes or chelates with citric or humic acids, and in this way, enter the biotic cycle.

Al(III) is ubiquitous in the biosphere, being found in all forms of life on Earth. However, there is no evidence to support an essential function for aluminium in humans, and there is only limited information to suggest any essential role in any other form of life [1]. All trivalent ions are difficult for biological systems to handle, due to their small size and their slow exchange rates. Al(III) is extreme in both respects, and thus, has never found a use in living systems [4, 5]. The lack of any known biological essentiality of aluminium should also be interpreted as a testimony to the efficiency with which the lithospheric cycle has successfully excluded aluminium from the biotic cycle.

Nevertheless, its biospheric abundance is still high relative to a number of essential metals, which is hardly in accordance with the effective retention of

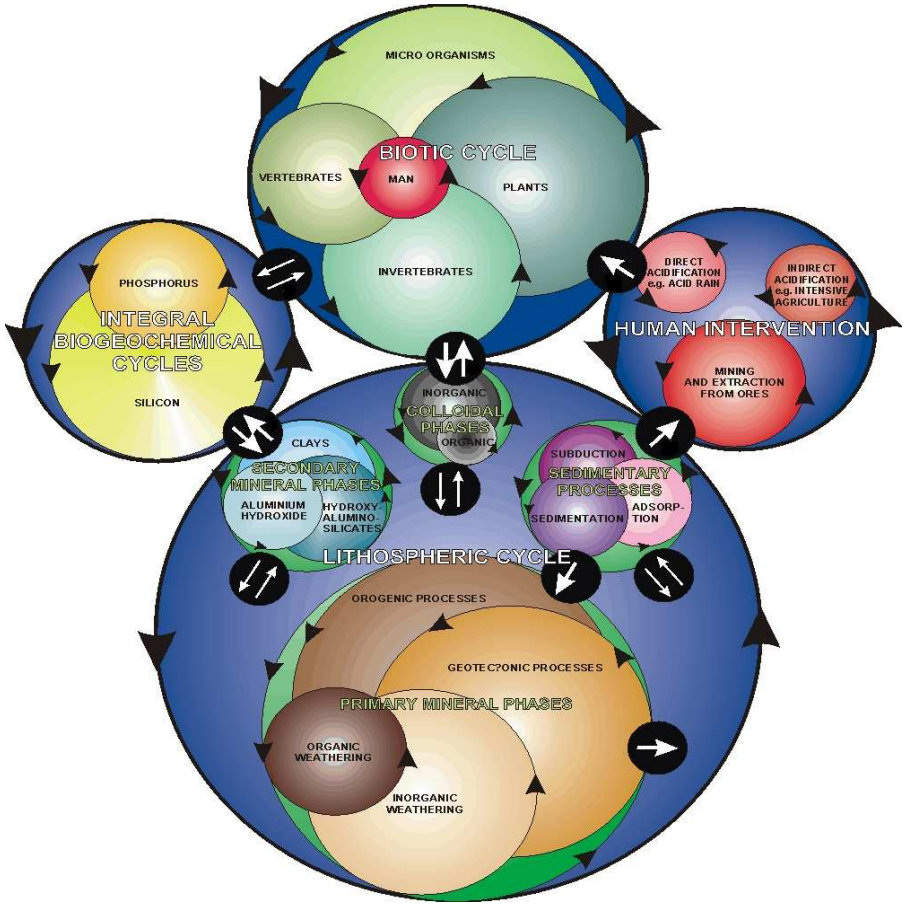

Fig. 2.1 Biogeochemical cycle for Al(III) [1]

Al(III) in the lithosphere and its lack of biological role. In fact, a significant contribution in increasing its bioavailability and thus, its presence in biota has resulted from human activities.

This contribution has happened in two different ways: On one hand, man made acidification of the environment has altered the patterns of weathering in the lithosphere, depleting the buffering capacity of vast areas of the World's agricultural land [3]. Solution Al(III) chemistry depends strongly on pH, as its solubility is significantly increased under acidic or alkaline conditions. Consequently, acid rain may substantially mobilize and release Al(III) into soil, underground and surface waters. This phenomenon is accentuated particu-

larly in poorly buffered soils [2], and has largely increased the bioavailability of the metal.

On the other hand, since the late 19th century, aluminium has been widely used in industry and has been given many different applications, arising in several sources of exposure, as drinking water, occupational exposure, aluminium containing products such as drugs, vaccines, parenteral nutrition [6] and cosmetics [7,8].

These anthropogenic sources of Al(III) represent an additional burden to the environment, and have resulted in our increased exposure to aluminium through our diet and specially through our everyday use of the metal [1].

2.2 Aluminium in the human body

The first barrier which excludes Al(III) from our body is the gut barrier. Al(III) (10-30 mg) is estimated to be ingested each day, but only a very small proportion of this Al(III) (5-10 μg) is absorbed. The amount absorbed from the gastrointestinal tract depends on the presence of other dietary agents, such as citrate, Ca, Mg, Si, Vitamin D, the status of the body iron stores and parathyroid hormone [9]. Other factors, such as an abnormally high Al(III) load, impaired renal function, age, etc, can promote its absorption to the blood.

This absorbed Al(III) can be transported to various target organs, where, once the cell membrane is crossed, it may accumulate and exert harmful effects, provoking a large number of metabolic errors [9] and several diseases, e.g. osteomalacia in the bones [10], microcytic anaemia in the red blood cells or neurodegenerative diseases in the brain [11].

Many models and transport mechanisms have already been proposed [12] in an attempt to explain the transport mechanism which allows the aluminum to permeate the cell. It is known that Al(III) in blood can be found bound to high molecular mass species (HMM), as transferrin and albumin, and low molecular mass species (LMM), such as citrate, phosphate, oligopeptides [13] or amino acids [6], which can transport the metal and also form species which may be able of crossing the cell membranes. Furthermore, it has been found that Al(III) significantly modifies the biophysical properties of membranes [9]. Despite the research carried out on the field, the transport of Al(III) and its uptake by the cell remains unclear, and is still a matter of debate.

As pointed out before, the brain is one of the main targets for Al(III) to get accumulated, where its concentration has been seen to be correlated with the age [14]. Al(III) is a known neurotoxicant, causes several damages in the nervous system [15] and it has been found involved in the etiology of the amyotrophic lateral sclerosis, parkinsonism dementia complex, Alzheimer's

disease (AD), and several other neurodegenerative diseases. The neurons are protected by the blood brain barrier (BBB) from potential toxic compounds in the bloodstream, by tightly regulating what gets in and out of the brain [16]. Consequently, how the Al(III) crosses the BBB is another crucial research area. Several theories have been put forward, but in essence, how does the Al(III) reach the brain is not fully understood yet.

2.3 Protein-related toxic processes: the role of metal ions

Proteins, and to a lesser extent their building blocks, peptides and amino acids, may be the most important materials of living systems. They are not only bulk constituents of organs and tissues, but as reactive organic compounds are important regulators of biological processes [8] .

Currently, about half of all proteins contain metal ions and most ribozymes cannot function without them, as they constitute an integral part of many enzymes and are indispensable in several catalytic reactions [17]. Metal ions perform a wide variety of specific functions associated with proteins and, in many cases, stabilize the structure of folded proteins or help to fix a particular physiologically active conformation of the protein. Toxicity can arise in different forms from metal interactions with proteins, e.g., enhancing the so called 'conformational diseases' or altering the biological activity of the enzymes.

The 'conformational diseases' are diverse human disorders which are considered to arise from the misfolding and aggregation of the underlying protein. Neurodegenerative diseases, such as Alzheimer's disease, Parkinson disease, prion diseases (including bovine spongiform encephalophathy and Creutzfeld-Jacob Disease) and triplet repeat diseases (including Huntington's disease), as well as cystic fibrosis, systemic amyloidosis are a few disorder of this kind. The common mechanism underlying these disorders implies an aberrant form of a protein with a tendency to aggregate and form toxic solid deposits in the brain, which can be highly organized and extremely stable, resulting in fatal neurological disorders [18]. This process is very complex, involving a variety of morphologies and different oligomeric intermediates. A large body of data has already demonstrated that the presence of metal ions, in particular Cu(II), Fe(III), Zn(II) and Al(III) modulates and fastens this aggregation and, consequently, the formation of solids [19–23].The exact role that the metals, and, in particular, Al(III) play is not clear yet, despite the large number of studies published. Even Al(III) is certainly not a causative factor of the conformational protein diseases, it might be a risk factor as it enhances conformational changes.

Metal ions can also effectively control an enzyme catalyzed reaction, and also bind and orient the substrate with respect to functional groups. Without the appropriate metal ion, a biochemical reaction catalyzed by a particular metalloenzyme would proceed very slowly, if at all. The enzyme provides an arrangement of side-chain functional groups having an appropriate sized hole with the preferred groups on enzyme side chains needed to bind the required metal ion. The optimal number of such binding groups is chosen for the particular metal ion, together with the appropriate hydrophobic or hydrophilic environment in the binding site. Metal ions may be bound by main-chain amino and carbonyl groups, but specific binding is achieved by the amino acid side chains, particularly the carboxylate groups of aspartic and glutamic acid, and the ring nitrogen atom of histidine [24].

2.4
Aluminium and the proteins

Al(III) can bind to amino acids, oligopeptides [25] and proteins, the latter being extremely strong binders [8]. Several different proteins have been found to be bound by Al(III), taking part in its transport and uptake by the cell, and also undergoing conformational changes that result on aggregation or toxic processes and alteration of enzymes [26]. For example, the strong binding of Al(III) promotes the self aggregation of highly phosphorylated cytoskeletal proteins such as neurofilament or microtubule-associated proteins. Al(III) induces conformational changes in cytoskeleton proteins (neurofilament, tau proteins), disease-related proteins (β amyloid, α-synuclein, hyperphosphorilated tau), and other proteins (calmodulin, transferrin, lactoalbumin) [15].

The metal has negative effects on several important biochemical reactions involving the binding of other metals, such as Mg(II) and Ca(II), with proteins. Al(III) has been seen to be able to alter a myriad of enzymes, as the hexokinase, phosphofructokinase, monoamine oxidase type B, dihydropterine reductase, α-chymotrypsin, carbonic anydrase, glutamate dehydrogenase, trypsin, chymotrypsin, monoamine oxidase type b, acetylcholinesterase, etc. [26,27]. Al(III) may also compromise energy production via the Krebs cycle by altering some enzyme's activity (as α ketoglutarate dehydrogenase, succinate dehydrogenase and aconitase), and also the inositol pathway, which has been found to be involved with long term potentiation, i.e., a mechanisms underlying memory formation. It has also been proposed that Al(III) may potentiate the activities of neurotransmitters through the action of Al(III)-ATP at ATP receptors in the brain [9].

Some of these enzymes have been seen to be altered in some neurological diseases, like AD.

2.5 Interference of Al(III) in the metabolism of other metals

Al(III), as it has no natural binding protein, tends to enter and permanently occupy binding sites which in normal conditions should be occupied by other metals. Metals like Ca(II), Mg(II) and Fe(II) are some of the most affected ones, due to the similar physicochemical characteristics of these metals as compared to Al(III), as the affinity for specific ligands (HSAB principle) and the charge and size of the metals [17,28–33].

2.5.1 Iron

The main example of Al(III) (ionic radius 0.535 Å) occupying a Fe(III) (ionic radius 0.645 Å) binding site occurs in transferrin (Tf). The predominant aluminum species in blood plasma is the Al(III)-transferrin complex, as it binds the aluminum stronger than any other known ligand commonly present in serum.

The human serum transferrin is an iron-binding protein that consists of a single polypeptide chain of about 700 amino acids organized in two lobes (-C and -N) linked by an interlobe chain. Each lobe consists of two domains containing four protein ligands to which metals can coordinate. The ligands engaged in complex formation between transferrin and the metal are 2Tyr, 1His, 1Asp and a bicarbonate ion. When the protein is in the metal-free state, the two lobes are mostly in an open conformation, whereas they are in a closed conformation when the protein is metal-loaded. Aluminum in serum is known to be bound by transferrin, such that the 90 percent of the total aluminum may be in this form. It is known that aluminum can enter the brain via the transferrin-receptor mediated endocytosis. Anyway, it is still a matter of debate whether this is the main transport pathway of aluminum into the brain, since some studies suggest a mechanism for brain aluminum uptake other than transferrin mediated [8,34].

At normal concentration of transferrin in plasma, only 30 per cent of the available metal ion binding sites are occupied by Fe(III) [35]. Several studies indicate that aluminum is not competitive with iron in binding to transferrin, and is considered that Al(III) serves only the available binding sites not occupied by iron [36]. There is still doubt about how the metal-binding and release mechanisms occurs. Recently, the mechanism of iron release and the open and closed forms of the N-lobe for the iron have been studied [37,38]. Nevertheless, for the case of aluminum, very little structural information about the aluminum-transferrin complex is available. Also, the kinetics of the process is not still largely understood, and contradictory results have been obtained in recent researches [36,39]. The metal-loaded transferrin transports the cation

to the transferrin receptor, where then it is released into the cell. Even some studies estimated that the affinity of the aluminum-loaded transferrin for the trasferrin receptor is of the same order of magnitude as that of the iron-loaded protein [40], other works claim that no interaction between the trasferrin receptor and aluminum-loaded trasferrin is seen [36]. Additionally, it has been hypothesized that the transferrin receptor mediated entry of aluminum in the cell is very ineffective [8].

2.5.2 Calcium

Al(III) interferes with the metabolism of Ca(II) (ionic radius 0.99 Å) in several ways. In particular, it has been seen to be able to bind albumin in the binding sites which are specific to Ca(II) [8], what pinpoints the albumin as another possible carrier for the Al(III) to be transported through the bloodstream [41].

The EF-hand family is a large class of Ca(II) binding proteins that contain homologous Ca(II) binding sites within a characteristic helix-loop-helix motif. This motif is widely used in nature, where its functions include Ca(II) signaling, buffering and structural stabilization. The EF-hand motif was discovered in calcium-binding proteins including calmodulin, parvalbumin, and troponin C, required for muscle contraction and calcium buffering in many organisms. Trivalent metals, due mainly to stronger charge-charge interactions, have affinities comparable to that of Ca(II) in the EF-hand proteins [42,43]. As an example, the enzyme-regulating small Ca(II) protein calmodulin interacts with Al(III), what generates considerable conformational changes [8].

Al(III) was found to reduce the vitamin D-dependent Ca(II) absorption, reducing the Ca(II) binding protein calbindin amount in the intestine [44]. Anyway, also in this case the competition of Al(III) with Ca(II) for the binding site was discarded.

In fact, this competition is hindered both by the much larger size of Ca(II) as compared to Al(III) and also by the specificity that natural Ca(II) protein binding sites present for this metal (as happens in the EF-hand family). In its favored eightfold coordination the volume of Ca(II) is nine times greater than in Al(III) sixfold coordination. Since making the cavity is energetically costly, Al(III) cannot replace Ca(II) in proteins without substantial readjustment of liganding groups. Thus competition between Al(III) and Ca(II) is less apt to be for protein binding sites than for small molecule ligands and phosphate, with which both form insoluble complexes. [45]

2.5.3 Magnesium

Mg(II) is an essential element, which takes part in a wide variety of biochemical reactions and binds several different proteins (it is involved in more than 300 enzymatic reactions in the body [46]), playing a crucial role in many physiological functions. It is one of the most versatile metal cofactors in cellular biochemistry, serving both intracellular and extracellular roles [17]. It is critical in energy-requiring metabolic processes, in protein synthesis, membrane integrity, nervous tissue conduction, neuromuscular excitability, muscle contraction, hormone secretion, and in intermediary metabolism [46]. Considered a neuron protector element, its deficient intake is related to neurodegenerative diseases [47], even though only magnesium deficiency cannot result in neurodegenerative diseases.

Mg(II) (ionic radius 0.72 Å) seems to be one of the most affected by Al(III) competition [8, 48, 49], since the two cations are of similar size, a factor that dominates over the charge identity towards metal competition [45, 48, 50, 51]. Though Mg(II) is somewhat larger than Al(III), displacement of the ubiquitous Mg(II) in biological systems by Al(III) appears likely, and comparison suggests that Al(III) should seek the sites normally used by Mg(II) [45]. Numerous examples of Al(III) inhibition of Mg(II) dependent metalloenzymes have been reported [9]. Hexokinase, adenylate cyclase, 3,5-cyclic nucleotid phosphodiesterase, acid and alkaline phosphatases, acetylcholinesterase, etc., are some cases where the enzymatic activity is seen to be altered by Al(III), and in which substitution of Mg(II) by Al(III) is documented or at least assumed [8].

D-xylose isomerase is one of the few enzymes for which crystallographic results are available. This enzyme catalyses the reversible conversion of D-xylose to D-xylulose and that of other sugars from aldose to ketose, and is well known to require certain divalent metal cations (Mg(II), Co(II) or Mn(II)) for activation, whereas Ca(II), Ba(II) and Al(III), among others, inhibit the reaction. Results show that the binding of the Al(III) instead of Mg(II) does not alter the overall structure significantly (see Fig. 2.2), even if there are local rearrangements in the octahedral coordination sphere of the Al(III) [48].

The selectivity of a protein for a metal can be due to the properties of the metal (its stereochemical and charge to size requirements) or the natural abundance of the metal in the biological locality, or the properties of the protein (its unique set of amino acid residues forming the metal binding pocket and the stereochemistry of this pocket).

The physicochemical characteristics of the metals favour the substitution of Mg(II) by Al(III), as both Mg(II) and Al(III) favor sixfold, octahedral coordination [51], and are 'hard' ions (HSAB principle), so they prefer 'hard' ligands of

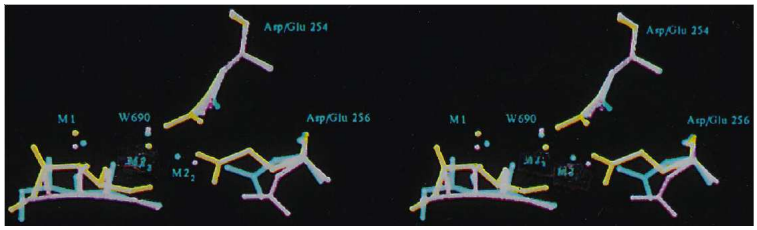

Fig. 2.2 Superposition of the inhibited wild-type xylose isomerase structure in complex with Al(III) and Mg(II) (cyan) and Mg(II) (magenta) onto the double mutant structure in complex with Al(III) (yellow) [48]

low polarizability, with oxygen being the most preferred coordination atom, followed by nitrogen [17].

Al(III) displays a relatively slow ligand exchange rate as compared to Mg(II), which is an ideal catalyst for controlling reaction steps where the activation energy is low. Due to its higher charge, the binding of the Al(III) is much stronger than that of Mg(II), and the slow rate at which Al(III) leaves any ligand is much slower. Once in a system, Al(III) can inhibit the proteins because of this large rate constant, and it would block the binding of other metals such as magnesium because it has higher binding constants [5].

Nevertheless, we have to consider that in normal conditions, the abundance of Mg(II) in biological environments prevents it to be easily substituted. It is reasonable to assume that Al(III) (with a concentration of 10^{-10} M at pH 7.3) will meet competition from Mg(II) with a concentration larger than 10^{-3} M [52]. It seems likely that during evolution some proteins have chosen Mg as a natural cofactor based mainly on its natural abundance in living cells. Mg binding sites appear to be weakly protected against other metals, which can replace Mg and, in some cases, inhibit enzymatic activity. Therefore, it seems that it is not the protein that has evolved to select Mg from other cations. Instead, it is the cell machinery that regulates the process of metal binding by regulating appropriate concentrations of Mg and other cations in various biological compartments [17].

This means that in normal conditions the protein will select the magnesium over other metals due to its abundance. However, this relative concentration of Al(III) to Mg(II) may change in acute Al(III) intoxication or in case of high concentration of Al(III) in damaged areas of the brain, and even in cases of Mg depletion.

Mg(II) depletion, attributed to deregulation of factors controlling magnesium metabolism [46], and the high Al(III) body burden, due to its chronic accumulation are both common physiological features in the aged. It is also speculated that magnesium depletion in various structures of the central ner-

vous system (CNS) may further accelerate the uptake of Al(III) into the CNS, promoting the neurodegenerative processes [47, 53].

This variation in the metal concentration may alter the selection of the protein, allowing Al(III) to enter the protein and trigger toxic processes. In fact, post-mortem analysis of brain tissues of patients suffering from neurodegenerative diseases reveals a substantial magnesium depletion in some of the most affected areas of the brain, where a high concentration of aluminum has been found [53–56]. Furthermore, an increased level of Al(III) and decreased levels of Ca and Mg are suspected to underlie the pathogenesis of amyotrophic lateral sclerosis (ALS) and Parkinsonism dementia (PD) in the Kii Peninsula and Guam [15]. The consequences of this metal disregulation in neurological diseases have yet not been clarified [57].

The substitution of Mg(II) by Al(III) is a possible explanation of this interference [54], for which no molecular mechanisms has been proved, even if it has been proposed that an altered serum protein contributes to the progression of AD by having a greater affinity for Al(III) than for Mg(II), in contrast to the normal protein, which binds Mg(II) preferentially over Al(III) [53].

2.6 Aims of the work

Several different proteins participate in aluminum metabolism and are altered in its presence. Thus, identifying the characteristics of the preferred binding sites of Al(III) in proteins is a crucial step towards the understanding of its transport and uptake into the cell. This will shed light on its toxicity and the mechanisms underlying it.

Very little experimental or theoretical data regarding structure and thermodynamics of aluminium-protein complexes is available. Therefore, one of the aims of this work is to report this kind of data, focusing in the first hydration shell of the metal in a protein environment. This information can be useful for the research on more specific aluminium systems.

On the other hand, substitution of Mg(II) may be one of the main mechanisms by which Al(III) is toxic. As already said, Mg(II) can be found in several different binding sites and environments, and is clear that aluminium interferes in the activity of a large variety of proteins. Some of these interferences have been suggested to occur upon Mg(II)/Al(III) substitution, but have not been yet proved. Therefore, we will systematically study the relative affinity of aluminium and magnesium for different binding sites, in order to identify the factors that govern this substitution.

Quantum mechanical methods give us the possibility of building different binding sites, so that we can know which is the most thermodynamically

preferable set of inner-sphere ligands for each metal cation and calculating the relative affinity of the metals for each binding site.

In Part 2, a brief explanation about the computational methods account and the molecular models used for simulating the metal binding site will be given. In Part 3, first, we will study the affinity of the metals for a broad variety of possible bioligands, in order to choose the preferred side chains for binding aluminium and magnesium, and also for comparison with other theoretical and experimental works found in literature. Afterwards, binding sites with two and three of these preferred bioligands will be studied, and, finally, a deeper discussion about Mg/Al exchange in different binding sites will be presented.

References

1 C. Exley, J. Inorg. Biochem. 97 (2003) 1–7.

2 J. Scancar, R. Milacic, Anal. Bioanal. Chem. 386 (2006) 999–1012.

3 R. W. Smith, Coord. Chem. Rev. 149 (1996) 81–93.

4 R. Williams, J. Inorg. Biochem. 76 (1999) 81–88.

5 R. J. P. Williams, Coor. Chem. Rev. 149 (1996) 1.

6 D. Bohrer, P. C. do Nascimento, J. K. A. Mendonca, V. G. Polli, L. M. de Carvalho, Amino Acids 27 (2004) 75–83.

7 P. D. Darbre, J. Inorg. Biochem. 99 (2005) 1912–1919.

8 C.Exley (Ed.), Aluminium and Alzheimer's disease, Elsevier, Amsterdam, 2001.

9 P. Zatta, R. Lucchini, S. van Resburg, A.Taylor, Brain Research Bulletin 62 (2003) 15–28.

10 E. Rowatt, E. S. Sorensen, J. Triffit, A. Viess, R. J. P. Williams, J. Inorg. Biochem. 68 (1997) 235–238.

11 T. Dudev, Y. Lin, M. Dudev, C. Lim, J.Am. Chem. Soc. 125 (2003) 3168–3180.

12 M. Bragadin, S. Manente, G. Scutari, M. P. Rigobello, A. Bindoli, J. of Inorg. Biochem. 98 (2004) 1169–1173.

13 A. Sanz-Medel, A. S. Cabezuelo, R. Milacic, R. B. Polak, Coord. Chem. Rev. 228 (2002) 373–383.

14 R. A. Yokel, Neurotoxicology 21 (2000) 813–828.

15 M. Kawahara, J. of Alzheimer's disease 8 (2005) 171–182.

16 S. Everts, Chem. Eng. News June (2007) 33–36.

17 T.Dudev, C. Lim, Chem. Rev. 103 (2003) 773–787.

18 E. Gaggelli, H. Kozlowsky, D. Valensin, G. Valensin, Chem. Rev 106 (2006) 1995–2044.

19 F. Ricchelli, R. Buggio, D. Drago, M. Salmona, G.Forloni, A. Negro, G. Tognon, P. Zatta, Biochemistry 45 (2006) 6724–6732.

20 J. Shearer, P. Soh, Inorg. Chem. 46 (2007) 710–719.

21 A. Khan, A. E. Ashcroft, V. Higenell, O. Korchazhkina, C. Exley, J. Inorg. Biochem. 99 (2005) 1920–1927.

22 L. Wilkinson-White, S. Easterbrook-Smith, Biochemistry 46 (2007) 9123-9132.

23 F. Ricchelli, D. Drago, B. Filippi, G. Tognon, P. Zatta, Cell. Mol. Life Sci. 62 (2005) 1724.

24 J. Glusker, A. Katz, C. Bock, The Rigaku Journal 16 (1999) 8–16.

25 T.Kiss, M. Kilyen, A. Lakatos, F. Evanics, T. Kortvelyesi, G. Dombi, Z. Majer, M. Hollosi, Coord. Chem. Rev. 228 (2002) 227–236.

26 S. J. Yang, J. W. Huh, J. E. Lee, S. Y. Choi, T. U. Kim, S. W. Cho, Cell. Mol. Life Sci. 60 (2003) 2538–2546.

27 K. R. Dave, A. R. Syal, S. S. Katyare, Brain Research Bulletin 58 (2002) 225–233.

28 C. S. Babu, T. Dudev, R. Casareno, J. Cowan, C. Lim, J. Am. Chem. Soc. 125 (2003) 9318–9328.

29 C. W. Bock, A. K. Katz, G. D. Markham, J. P. Glusker, J. Am. Chem. Soc. 121 (1999) 7360–7372.

30 L. Rulisek, Z. Havlas, J. Phys. Chem. A 106 (2002) 3855–3866.

31 N. Gresh, D. R. Garmer, J. Comp. Chem. 17 (1996) 1481–1495.

32 T. Ozawa, M. Fukuda, M. Nara, A. Nakamura, Y. Komine, K. Kohama, Y. Umezawa, Biochemistry 39 (2000) 14495–14503.

33 M. S. Cates, M. L. Teodoro, G. N. Phillips, Biophysical J. 82 (2002) 1133–1146.

34 C. Exley, J. Beardmore, G. Rugg, Int. J. Quantum Chem. 107 (2007) 275–278.

35 M. Nagaoka, T. Maitani, The Analyst 125 (2000) 1962–1965.

36 M. Hemadi, G. Miquel, P.H.Kahn, J. E. H. Chahine, Biochemistry 42 (2003) 3120–3130.

37 D. Rinaldo, M. Field, Biophysical J. 85 (2003) 3485.

38 D. Rinaldo, M. Field, Austr. J. Chem. 57 (2004) 1219.

39 M. H. Nagaoka, R. Maitani, Analyst 125 (2000) 1962–1965.

40 A. Roskams, J. Connor, PNAS 87 (1990) 9024–9027.

41 S. J. A. Fatemi, F. Kadir, G. Moore, Biochemical J. 280 (1991) 527–532.

42 S. Drake, M. Zimmer, C. L. Miller, J. Falke, J. Biochemistry 36 (1997) 9917.

43 S. Drake, M. Zimmer, C. Kundrot, J. Falke, J. Gen. Physiol. 110 (1997) 173.

44 K. Cox, M. Dunn, J. Nutr. 131 (2001) 2007–2013.

45 R. B. Martin, Clin. Chem. 32 (1986) 1797.

46 M. Laires, C. Monteiro, M. Bicho, Frontiers in Bioscience 9 (2004) 262–276.

47 J. Durlach, Magnesium Research 10 (1997) 339–353.

48 T. Gerczei, Z. Bocskei, E. Szabo, B. Asboth, G. Naray-Szabo, Int. J. Biol. Macro. 25 (1999) 329.

49 A. Sigel, H. Sigel, R. Sigel (Eds.), Neurodegenerative diseases and metal ions, Wiley, England, 2006.

50 P. O. Ganrot, Env. Hth. Period. 65 (1986) 363.

51 V. Lunin, E. Dobrovetsky, G. Khutoreskaya, R. Zhang, A. Joachimiak, D. Doyle, A. Bochkarev, M.E.Maguire, A. Edwards, C. Koth, Nature 440 (2006) 833.

52 R. Williams, Coord. Chem. Rev. 228 (2002) 93–96.

53 J. L. Glick, Med. Hypotheses 31 (1990) 211–225.

54 J. Durlach, Magnesium Research 3 (1990) 217–218.

55 P. Collery, L. Pirer, M. Manfait, J. Etienne (Eds.), Alzheimer's disease and dementia syndromes consecutie to imbalanced mineral metabolisms subsequent to blood brain barrier alteration., Metal ions in biology and medicine, John Libbey-Eurotext, London-Paris, 1990.

56 M. R. Lemke, Biol. Psychiatry 37 (1995) 341–343.

57 E. Andrasi, N. Pali, Z. Molnar, S. Kosel, J. of Alzheimer's disease 7 (2005) 273–284.

Part 2 Methods

3
Computational methods used

3.1
Density Functional Theory

In the field of applied computational chemistry, density functional normally stands for the Kohn-Sham implementation of the theory. In essence, the Kohn-Sham formulation of density functional theory relies on the fact that the electron density of the ground state of a system, can be computed as the density of a system of independent particles, moving in an effective one-particle potential. Once this effective potential has been determined, the Kohn-Sham method solves self consistently the nonlinear Kohn-Sham equations which contain an unknown *exchange-correlation* functional [1–3].

The theoretical foundations for the Kohn-Sham method are the Hohenberg-Kohn theorems [4]. The first theorem demonstrates that the nondegenerate ground state energy of the exact Hamiltonian can be expressed in terms of a unique, universal functional of the electron density. The second theorem establishes the variational principle for this ground state energy functional.

3.1.1
The Hohenberg–Kohn theorems

Modern Density Functional Theory was put on firm ground through the two groundbreaking theorems of Hohenberg and Kohn [1]. The first Hohenberg and Kohn theorem legitimizes the use of the ground state electron density $\rho(\mathbf{r})$ as a basic variable. It states that external potential $v(\mathbf{r})$ and the electron density hold a one-to-one relationship. Namely,

$$\rho(\mathbf{r}) \leftrightarrow v(\mathbf{r}) \tag{3.1}$$

Therefore, since the external potential determines univocally the external potential operator through,

$$\hat{V}_{ext} = \sum_{i=1}^{N} \int \delta(\mathbf{r} - \mathbf{r}_i) \left[\sum_{A=1}^{M} \frac{-Z_A}{\mid \mathbf{r} - \mathbf{R}_A \mid} \right] d\mathbf{r} = \sum_{i=1}^{N} v(\mathbf{r}_i) \tag{3.2}$$

the halmiltonian operator of the system,

$$\begin{aligned} \hat{H} &= \sum_{i=1}^{N} \frac{-\nabla^2}{2} + \sum_{i<j} \frac{1}{\mid \mathbf{r}_i - \mathbf{r}_j \mid} + \hat{V}_{ext} \\ &= \hat{T} + \hat{U} + \hat{V}_{ext} \end{aligned} \tag{3.3}$$

is also univocally determined by the electron density. Provided that the Schrödinger equation corresponding to the hamiltonian of Eq.(3.3) is solved, every observable of every stationary state, either ground or excited, of our system of N given electrons can be calculated, in principle exactly, from the ground state electron density alone. In particular, the ground state energy can be written as functional of the ground state density: $E[\rho(\mathbf{r})]$, although this theorem provides no clue about the precise form of the functional.

The second Hohenberg and Kohn theorem establishes the energy variational principle for the ground state energy functional. Namely, it reads: For a trial non-negative electron density $\rho(\mathbf{r})$ normalized to N electrons,

$$E[\rho(\mathbf{r})] \geq E\left[\rho_{g.s.}(\mathbf{r})\right] = E_{g.s.} \tag{3.4}$$

where $\rho_{g.s.}(\mathbf{r})$ is the ground state electron density and $E_{g.s.}$ is the ground state energy.

The original formulation of Hohenberg and Kohn requires a non degenerate ground state having a v-representable electron density. An electron density is v-representable if it is associated with an antisymmetric wave function of *some* hamiltonian $\hat{H}'$ formed from $\hat{H}$ by replacing $v(\mathbf{r})$ by $v'(\mathbf{r})$, which may or may not equal $v(\mathbf{r})$.

However, Levy [5] reformulated DFT is such a way that neither the non degeneracy of the ground state nor the v-representability of its electron density are necessary. He considered the following universal functional

$$Q[\rho] = \min_{\Psi \to \rho} \left\langle \Psi \left| \hat{T} + \hat{U} \right| \Psi \right\rangle \tag{3.5}$$

defined for the domain of N-representable electron densities, namely: $\rho(\mathbf{r})$ must be non-negative, $\int \rho(\mathbf{r}) d\mathbf{r} = N$ and $\int \mid \nabla \rho^{1/2}(\mathbf{r}) \mid^2 d\mathbf{r} < \infty$. Recall that $Q[\rho]$ is universal in the sense that the same value is delivered for a given trial N-representable electron density ρ no matter what external potential is actually under consideration.

The search in Eq. (3.5) is *constrained* to the subspace of all antisymmetric Ψ that yield the same electron density $\rho(\mathbf{r})$. Using DFT one can determine the ground state energy exactly provided that the functional $Q[\rho]$ is known.

3.1.2 The Kohn-Sham formulation

Let us consider the variational principle stated in Eq.(3.4). Hence, we wish to minimize the functional $E[\rho]$ under the constrain of normalized densities. Namely, we have to minimize the following functional,

$$L[\rho] = E[\rho] - \mu\left[\int d\mathbf{r}\rho(\mathbf{r}) - N\right] \tag{3.6}$$

which imposes the constrain of normalized electron density, and obtain the Euler equation:

$$\frac{\delta E[\rho]}{\delta\rho(\mathbf{r})} - \mu = 0 \tag{3.7}$$

Since,

$$E[\rho] = T[\rho] + U[\rho] + \int d\mathbf{r}\rho(\mathbf{r})v(\mathbf{r}) \tag{3.8}$$

where $T[\rho]$ is the kinetic energy and $U[\rho]$ the electron-electron repulsion term, the Euler equation can be cast as

$$v(\mathbf{r}) + \frac{\delta T[\rho]}{\delta\rho(\mathbf{r})} + \frac{\delta U[\rho]}{\delta\rho(\mathbf{r})} = \mu \tag{3.9}$$

which requires explicit functional expressions for $T[\rho]$ and $U[\rho]$.

Let us begin by considering the kinetic energy. Gilbert demonstrated that for every N-representable electron density $\rho(\mathbf{r})$ there exist a set of N *orbitals*, $(\psi_i)_{i=1}^N$, such that

$$\rho(\mathbf{r}) = \sum_{i=1}^{N} \psi_i^*(\mathbf{r})\psi_i(\mathbf{r}) \tag{3.10}$$

Our electronic density is N-representable, thus, we can obtain these orbitals $\psi_i(\mathbf{r})$, and then, write a sort of *kinetic energy*

$$T_s = \sum_{i=1}^{N}\langle\psi_i \mid -\frac{1}{2}\nabla^2 \mid \psi_i\rangle \tag{3.11}$$

Beware that this kinetic energy is not the kinetic energy of the real system, T. This allows us to write the energy as

$$E[\rho] \quad = \quad T_s[\rho] + U[\rho] + (T[\rho] - T_s[\rho]) + \int \rho(\mathbf{r})v(\mathbf{r})d\mathbf{r} \tag{3.12}$$

whose Euler equation can now be cast as

$$\frac{\delta T_s\left[\rho\right]}{\delta\rho(\mathbf{r})} + v_{eff}(\mathbf{r}) = \mu \tag{3.13}$$

with

$$v_{eff}(\mathbf{r}) = v(\mathbf{r}) + \frac{\delta U\left[\rho\right]}{\delta\rho(\mathbf{r})} + \frac{\delta(T\left[\rho\right] - T_s\left[\rho\right])}{\delta\rho(\mathbf{r})} \tag{3.14}$$

The $U\left[\rho\right]$ term can be divided in classical and non-classical electron repulsion terms:

$$U\left[\rho\right] = J\left[\rho\right] + E_{nc}\left[\rho\right] = \frac{1}{2}\int \frac{\rho(\mathbf{r})\rho(\mathbf{r}')}{|\mathbf{r}-\mathbf{r}'|} d\mathbf{r}d\mathbf{r}' + E_{nc}\left[\rho\right] \tag{3.15}$$

and then, the exchange-correlation functional is defined as

$$E_{xc}\left[\rho\right] = E_{nc}\left[\rho\right] + T\left[\rho\right] - T_s\left[\rho\right] \tag{3.16}$$

Therefore, the expression for the effective potential can be written as follows:

$$v_{eff}(\mathbf{r}) = v(\mathbf{r}) + \frac{\delta J\left[\rho\right]}{\delta\rho(\mathbf{r})} + \frac{\delta E_{xc}\left[\rho\right]}{\delta\rho(\mathbf{r})} \tag{3.17}$$

From Eq. (3.13) we can express the energy functional as

$$E\left[\rho\right] \quad = \quad T_s\left[\rho\right] + \int \rho(\mathbf{r}) v_{eff}(\mathbf{r}) d\mathbf{r} = \langle \Phi \mid \hat{T}_s + \hat{V}_{eff} \mid \Phi \rangle \tag{3.18}$$

where Φ is a single determinant eigenfunction of a non-interacting system with the following hamiltonian

$$\hat{H}_s = \sum_{i=1}^{N} \left[-\frac{1}{2}\nabla^2 + v_{eff}(\mathbf{r}) \right] \tag{3.19}$$

and which delivers by construction the electron-density of the real system. Observe that within this scheme T_s is the kinetic energy of a *fictitious system of noninteracting N particles* . Consequently, the orbitals ψ_i are the eigenvalues of

$$\left(-\frac{1}{2}\nabla^2 + v_{eff}(\mathbf{r}) \right) \psi_i(\mathbf{r}) = \epsilon_i \psi_i(\mathbf{r}) \tag{3.20}$$

These are the so called Kohn-Sham orbitals. Consequently, the Kohn-Sham operational procedure can be outlined as follows,

1. Devise an explicit function for $E_{xc}\left[\rho\right]$ and obtain

$$v_{xc}\left[\rho\right] = \frac{\delta E_{xc}\left[\rho\right]}{\delta\rho(\mathbf{r})} \tag{3.21}$$

2. Make a guess for the orbitals $(\psi_i)_{i=1}^N$ and estimate the electronic density ρ (from Eq.(3.10))

3. Set up the effective potential

$$v_{eff}(\mathbf{r}) = v(\mathbf{r}) + \int \frac{\rho(\mathbf{r}')}{|\mathbf{r} - \mathbf{r}'|} d\mathbf{r}' + v_{xc}[\rho] \tag{3.22}$$

4. Solve the following one-electron eigenvalue equations

$$\left[-\frac{1}{2}\nabla^2 + v_{eff}(\mathbf{r})\psi_i'(\mathbf{r})\right] = \epsilon_i \psi_i'(\mathbf{r}); i = 1, \cdots, N \tag{3.23}$$

   until consistency between the sets ψ_i and ψ_i'

5. Set up the electron density as in Eq.(3.10) and the kinetic energy T_s (from Eq.(3.11)). Evaluate the energy from

$$\begin{aligned} E[\rho] &= T_s[\rho] + \int \rho(\mathbf{r}) v_{eff}(\mathbf{r}) d\mathbf{r} \\ &= T_s[\rho] + J[\rho] + E_{xc}[\rho] + \int \rho(\mathbf{r}) v(\mathbf{r}) d\mathbf{r} \end{aligned} \tag{3.24}$$

The difficult part of the procedure is to devise an explicit functional expression for $E_{xc}[\rho]$.

3.1.3 The adiabatic connection

Recall that the exchange-correlation functional can be expressed like

$$E_{xc}[\rho] = E_{nc}[\rho] + (T[\rho] - T_s[\rho]) \tag{3.25}$$

Consider a group of systems $\hat{H}_\lambda$ with the same density $\rho(\mathbf{r})$ for all λ.

$$\hat{H}_\lambda = \hat{T} + \hat{V}_{ext}^\lambda + \lambda \hat{U}, \text{ with } \lambda \in (0, 1) \tag{3.26}$$

for each λ, V_{ext}^λ is adapted such that the density always equals the density of the fully interacting system ($\lambda = 1$). Hence $\rho(\mathbf{r})$ is independent of λ. When λ is zero, the system will be a non-interacting system of N electrons with density $\rho(\mathbf{r})$.

The average of the energy along the values of λ can therefore, be expressed as

$$\int_{E_{\lambda=0}}^{E_{\lambda=1}} \delta E_\lambda = E_{\lambda=1} - E_{\lambda=0} \tag{3.27}$$

Therefore the energy of the fully interacting system is

$$E_{\lambda=1} = \int_0^1 \frac{\delta E_\lambda}{\delta\lambda}\delta\lambda + E_{\lambda=0} \tag{3.28}$$

Consider the evaluation of δE_λ

$$\delta E_\lambda = \int \rho(\mathbf{r})\delta v_{ext}^{\lambda}(\mathbf{r})d\mathbf{r} + \frac{1}{2}\delta\lambda \int \frac{\rho(\mathbf{r})\rho(\mathbf{r}')}{|\mathbf{r}-\mathbf{r}'|} + \int_0^1 \frac{\delta E_{nc}^{\lambda}}{\delta\lambda}\delta\lambda \tag{3.29}$$

Observe that the kinetic energy does not appear in this equation because $\hat{T}$ does not depend on λ. Hence,

$$E_{\lambda=1} - E_{\lambda=0} = \int \rho(\mathbf{r})(v_{ext}^{\lambda=1} - v_{ext}^{\lambda=0})d\mathbf{r} + \frac{1}{2}\int \frac{\rho(\mathbf{r})\rho(\mathbf{r}')}{|\mathbf{r}-\mathbf{r}'|} + \overline{E}_{nc}[\rho] \tag{3.30}$$

Now, since

$$E_{\lambda=0} = T_s + \int \rho(\mathbf{r})v_{ext}^{\lambda=0}(\mathbf{r})d\mathbf{r} \tag{3.31}$$

we arrive at

$$E_{\lambda=1} = T_s[\rho] + \int \rho(\mathbf{r})v_{ext}^{\lambda=1}(\mathbf{r})\delta\mathbf{r} + \frac{1}{2}\int \frac{\rho(\mathbf{r})\rho(\mathbf{r}')}{|\mathbf{r}-\mathbf{r}'|}d(\mathbf{r})d(\mathbf{r}') + \overline{E}_{nc}[\rho] \tag{3.32}$$

we have subsumed the excess kinetic energy $T[\rho] - T_s[\rho]$ into the coupling parameter averaged exchange-correlation functional $\overline{E}_{nc}[\rho]$, which shall be denoted hereafter as $\overline{E}_{xc}[\rho]$.Observe that at this stage all the ignorance about our N-electron system has been displaced to the $E_{xc}[\rho]$ term, while the remaining terms in the ground state energy are well known. Naturally, the success of the Kohn-Sham method hinges largely on finding reliable approximations for this functional.

3.1.4
The local (spin) density approximation

The original approach of Kohn and Sham for the exchange–correlation energy functional was a gradient expansion like:

$$E_{xc}[\rho] = \int \rho(\mathbf{r})\,\varepsilon_{xc}[\rho(\mathbf{r})]\,d\mathbf{r} + O\left(|\nabla\rho(\mathbf{r})|^2\right) \tag{3.33}$$

Keeping only the leading term of Eq. (3.33), renders the so–called *local density approximation* (LDA). The functional $\varepsilon_{xc}[\rho(\mathbf{r})]$ is the exchange–correlation energy density of a *uniform electron gas*, except that the constant electron gas density has been replaced by the local of the inhomogeneous interacting system $\rho(\mathbf{r})$.

In spite of its simplicity the local density approximation has been extremely successful, even addressing systems with highly inhomogeneous electron density [6] like atoms and molecules.

For systems with larger and smoother density, the local density approximation works increasingly better. However, for systems with substantial electron density gradients, its simple form is often not accurate enough,and fails for the simplest case of one electron.

3.1.5
Generalized Gradient Approximations.

Generalized Gradient Approximations (GGA), a term coined by Perdew and Wang [7], and that refers to exchange–correlation functionals which incorporate information about not only the electron density itself but also their local gradients:

$$E_{xc}^{GGA}[\rho] = \int d\mathbf{r} f^{GGA}\left(\rho_\sigma, \vec{\nabla}\rho_\sigma\right);\ \sigma = \alpha, \beta \tag{3.34}$$

Two remarkably successful strategies to design suitable approximations for the function f^{GGA} have flourished during that last fifteen years. On the one hand, Becke has led a pragmatic *empirical* approach, while Perdew has championed a non-empirical approach.

The resulting exchange–correlation density functional of the former is known under the BLYP acronym and is very popular in quantum chemistry.

The PW91 of the latter is also a widely used exchange–correlation density functional in modern quantum chemistry. This functional has its roots in an earlier proposal of Perdew and Wang [7], known under the acronym PW86.

3.1.6
Meta Generalized Gradient Approximations (mGGA)

These functionals constitute a step beyond the generalized gradient approximation. Indeed, these functionals take the more general form

$$E_{xc}^{mGGA}[\rho] = \int d\mathbf{r} f^{mGGA}\left(\rho_\sigma, \vec{\nabla}\rho_\sigma, \nabla^2\rho_\sigma, \tau_\sigma\right) \tag{3.35}$$

with $\sigma = \alpha, \beta$ and

$$\tau_\sigma(\mathbf{r}) = \sum_{i=1} \left|\vec{\nabla}\psi_i(\mathbf{r})\right|^2 \tag{3.36}$$

is the Kohn-Sham orbital kinetic energy density for electron of spin σ.

3.1.6.1 Hybrid Functionals

Imagine that E_{xc}^{λ} is a linear function of λ. Hence, since

$$E_{xc} = \int_0^1 \frac{\delta E_{xc}^{\lambda}}{\delta \lambda} \delta\lambda \tag{3.37}$$

Consequently,

$$E_{xc} \equiv E_{xc}^{\lambda=1} = E_{xc}^{\lambda=0} - \frac{1}{2}(E_{xc}^{\lambda=0} - E_{xc}^{\lambda=1}) \tag{3.38}$$

When λ is 0, there is no correlation, and thus, we only have HF exchange. The E_{xc} simply corresponds to the exact exchange of the Slater determinant built up with the Kohn-Sham orbitals. Thus,

$$\begin{aligned} E_{xc} &= E_x^{\lambda=0} - \frac{1}{2}\left(E_x^{\lambda=0} - (E_x^{\lambda=1} + E_c^{\lambda=1})\right) \\ E_{xc} &= \frac{1}{2}E_x^{\lambda=0} + \frac{1}{2}E_x^{\lambda=1} + \frac{1}{2}E_c \end{aligned} \tag{3.39}$$

Thus, Eq.(3.39) tell us that the exact expression for the exchange correlation functional can be written as a hybrid of the exchange functional for the non-interacting system ($\lambda = 0$) and the fully interacting system ($\lambda = 1$). The former corresponds to the Hartree-Fock exchange functional and is normally referred to as *exact* exchange. Since the exchange-correlation energy functional does not depend linearly on λ, as assumed above, a generalized hybridization scheme can be used to devise improved functionals. The simplest such hybrid functional can be cast as

$$\begin{aligned} E_{xc}^{hyb}[\rho] &= E_x^{exact}[\rho] + (1-a)\left(E_x^{GGA}[\rho] - E_x^{exact}[\rho]\right) \\ &+ E_c^{GGA}[\rho] \end{aligned} \tag{3.40}$$

The most popular of the hybrid functionals, namely the B3LYP:

$$\begin{aligned} E_{xc}^{BLYP}[\rho] &= E_{xc}^{LSD}[\rho] + 0.20 \cdot \left(E_x^{exact}[\rho] - E_x^{LSD}[\rho]\right) \\ &+ 072 \cdot \Delta E_x^{B88}[\rho] + 0.81 \cdot E_c^{LYP}[\rho] \end{aligned} \tag{3.41}$$

is probably the most used density functional in chemistry, and the reason for the growing popularity of DFT in calculations of molecules. Indeed, B3LYP has been found to give surprisingly accurate results in many cases, and will be used in the present work.

3.2 Basis Sets

The choice of an appropriate basis set is an essential requirement for the success of the calculations [8]. However, we have to balance the precision of the

basis set and its size, since by increasing the size of the basis set the calculation cost becomes more expensive. The Contracted Gaussian Functions (CGF) are the most used in quantum chemistry calculations. They consist of linear combinations (contractions) of cartesian Gaussian functions (primitives),

$$\varphi_{\mu}^{CGF}(|\vec{r}-\vec{R}_A|) = \sum_{p=1}^{L} d_{p\mu} g(\alpha_{p\mu}, |\vec{r}-\vec{R}_A|) \tag{3.42}$$

with

$$g(\alpha_{p\mu}, |\vec{r}-\vec{R}_A|) = N(x-X_A)^l (y-Y_A)^m (z-Z_A)^n e^{-\alpha_{p\mu}|\vec{r}-\vec{R}_A|^2} \tag{3.43}$$

N is the normalization constant and l, m, and n are positive integer numbers. The exponent of the primitives $\alpha_{p\mu}$ and the contraction coefficients $d_{p\mu}$ have been optimized for the different elements. In this thesis Pople's standard 6-31++G** [9–11] double zeta basis set was chosen for the metal cations. This basis set treats the core electrons with 6 contracted primitives for each core orbital, and two CGF for the valence orbitals, where the former constitutes a contraction of three primitives and the latter consists of only one primitive Gaussian function. The symbols ++ and ** stand for diffuse and polarization functions respectively. Diffuse functions have large spatial extent, and are designed to describe loosely bound electrons, and polarization functions have higher angular momentum, *d*-type primitives for aluminum and magnesium and *p*-type primitives for hydrogen, which are designed to provide additional flexibility to the basis set as to handle properly the chemical bonding directionality of the electron density in molecules relative to the isotropic atomic environment.

For the non-metal atoms, we have chosen to replace the chemically inert core electrons by a suitably chosen function, the so called *pseudopotentials*. The effective core pseudopotentials developed by Stevens *et al.* [12] were selected, with their corresponding -31 split valence basis sets for all atoms but aluminum and magnesium (see references [13] and [14] for more details). The valence basis set accompanying the effective core pseudopotentials for each atom was augmented with a diffuse *sp*-set of functions and a polarization set of *p*- and *d*-functions. The pseudopotentials have been chosen due to the computational efficiency gained and to the fact that they include more functions than a double zeta basis set for describing the chemically sensible valence electrons. Gresh et al. [15–17] found that this pseudopotentials/all-electron basis set combination for the ligand and the metal cation respectively, represents a nicely balanced compromise between accuracy and computational efficiency. This method has been widely used and has shown to be adequate for this type

of calculations [18–22]. In the present work, the results presented have been compared to all electron basis set results found in literature, with satisfactory agreement. This basis set will hereafter be referred as SBKJ/*+.

The 6-311++G(2df,2p) triple-zeta basis set, 2 sets of d-functions and one set of f-functions on heavy atoms, and 2 sets of p-functions on hydrogens, was chosen for the single point calculations, for all the elements.

3.3
Representation of the solvent. The polarizable continuum model.

Most chemical processes take place in a solvent and consequently, it is important to consider how the solvent affects the behaviour of a system. Placing a solute molecule into a solvent can be thought of as a process in which first a cavity is dug into the solvent to place the solute in. Then, we consider the polarization of the cavity due to the electric field created by the solvent. This cavity's polarization, in turn, generates an electric field at the solvent molecule. The latter can be modeled as a perturbation operator which is added to the hamiltonian operator of the unsolvated solute molecule. Hence, it is this perturbation operator the one that contains all the information about the solvent effects.

When we embed a molecule (the solute) in a polarizable continuum of dielectric constant ε (the solvent), first, a cavity to accommodate the solute into the solvent is created. The free energy variation during this stage is called the *cavitation energy*, and depends only on the solvent and the geometric features of the cavity which resemble those of the solvent molecule. This quantity is always positive. When the molecule, with the same geometry and electronic structure as in the gas phase, is placed into the cavity, the electric field created by the molecule in its surroundings polarizes the continuum, and an electrostatic potential arises in the cavity. This electrostatic potential, named *reaction potential* interacts with the molecule, and generates a total free energy change. The free energy change arising from the solute-solvent, solvent-solvent and internal solute electrostatic interactions is called the *electrostatic* contribution, and will always be negative. The electrostatic component is considered to be the main contribution to the free energy change. Finally, the solute-solvent dispersion energy gives rise to another negative contribution to the free energy variation, the *dispersion* term [23].

Therefore, the solvation free energy ΔG_{sol}, the free energy change to transfer a molecule from vacuum to solvent, can be splitted into three components:

$$\Delta G_{sol} = \Delta G_{elec} + \Delta G_{disp} + \Delta G_{cav} \tag{3.44}$$

The key reason for choosing to characterize the solvent continuum by its dielectric constant is that it allows one to use the power of classical electrostatics machinery. When the solute is represented explicitly, and the solvent is treated as a continuum, the Laplacian of the reaction potential, $\phi(\mathbf{r})$ is related to the free charge density (i.e. the charge density due exclusively to the solute) ρ ($\mathbf{r}$) by Poisson's equation: [24]

$$\nabla^2\phi = -\frac{4\pi\rho(\mathbf{r})}{\varepsilon} \tag{3.45}$$

where ε is the homogeneous dielectric constant, and $\mathbf{r}$ denotes the position in space. That is, the Poisson equation connects the electron density to the electrostatic potential.

The polarizable continuum model (PCM) introduced by Tomasi and coworkers [25, 26] solves the electrostatic problem of the evaluation of the interaction energy between solute and solvent by introducing an apparent charge distribution spread on the cavity surface. The cavity volume is obtained by adding up the van der Waals spheres of the atoms of the solute. The surfaces of these resulting volumes are rather irregular and in general no analytical functions can fit them.

Due to the non analytical nature of the cavity shapes, within the PCM approach, the ΔG_{elec} will be calculated numerically. The cavity surface is divided into a large number of small surface elements (tesserae) and there is a point charge associated with each surface element. An initial value of the point charge for each surface element is then estimated from the electric field gradient due to the solute alone.

The reaction potential is then added to the solute Hamiltonian and the SCF calculation is initiated.

$$\hat{H} = \hat{H}_0 + \phi(\mathbf{r}) \tag{3.46}$$

After each SCF iteration new values of the surface charges are calculated from the current wavefunction to update the reactive potential, which is used in the next iteration until the solute wavefunction and the surface charges are self-consistent [27].

To calculate ΔG_{elec} we must take into account of the work done in creating the charge distribution within the cavity in the dielectric medium. This is equal to one-half of the electrostatic interaction energy between the solute charge distribution and the polarized dielectric. Consequently,

$$\Delta G_{elec} = \int \psi\hat{H}\psi d\tau - \int \psi_0\hat{H}_0\psi_0 d\tau - \frac{1}{2}\int \phi(\mathbf{r})\rho(\mathbf{r})d(\mathbf{r}) \tag{3.47}$$

The dispersion and cavitation components are usually considered proportional to the surface area of the cavity. For the cavitation contribution, PCM considers the surface defined by the van der Waals spheres, and the solvent accessible surface is used to calculate the dispersion contribution. The United Atom for Hartree-Fock (UAHF) model will be used to build the cavity. In this model the van der Waals surface is constructed from spheres located on heavy (non-hydrogen) elements only, where the van der Waals radius of each atoms is a function of atom type, connectivity, overall charge of the molecule, and the number of attached hydrogen atoms.

In this work both PCM and the integral equation formalism PCM (IEFPCM) will be used. The latter is a more recent formulation where the standard Poisson operator formalism is replaced by the use of equivalent operators derived from the theory of integral equations [28].

4
Geometric and electronic structure methods

All calculations presented in this work were carried out with the GAUSSIAN98 [29] and GAUSSIAN03 [30] packages. It has already been established that density functional methods give excellent results in most chemical systems [8, 31–34].

Geometry optimization of the complexes studied was performed in the B3LYP/6-31++G** level for the metal cations and the B3LYP/SBKJ/*+ level for the rest of the atoms. Frequencies, thermal corrections (E_{TRV}) and entropies were calculated at this level of theory and the corresponding zero-point vibrational energy (ZPVE) corrections made to the total energy, using standard statistical mechanical methods [35] at 298 K. The enthalpy, and free energy changes were evaluated at 298 K as follows:

$$\Delta H = \Delta E_{elec} + \Delta E_{TRV} + \Delta ZPVE + \Delta nPV \quad (4.1)$$

$$\Delta G = \Delta H - T\Delta S_{TRV} \quad (4.2)$$

where ΔE_{elec}, ΔE_{TRV} and $\Delta ZPVE$ are the electronic energy, thermal corrections to the vibrational, rotational and translational energies, and zero-point vibrational energies, respectively. n stands for the change of the number of molecules from reactants to products. The gas phase energies were recalculated on the optimized geometries at the B3LYP/6-311++G(2df,2p) level of theory, and corrected with the ZPVE and thermodynamical corrections calculated at the B3LYP/SBK*+ level of theory.

Aqueous phase optimizations where carried out using the IEFPCM [28, 36, 37] procedure at the B3LYP(IEFPCM)/SBKJ/*+ level of theory, with default solvation parameter values, excepting the tessera number which was set to TSNUM=100 for a finer partition of the cavity's surface. Solvation free energies were also recalculated on the B3LYP(IEFPCM)/SBKJ/*+ geometries at the B3LYP/6-311++G(2df,2p) level of theory.

4.1 Dielectric effects

This work regards the metal complexes being inside the protein, where the environment differs both from gas and aqueous phases. The protein surrounding the metal cavity induces a long range polarization on the active site, which will be simulated with the PCM.

The metal binding site can be found at different parts of the protein (see Fig. 4.1), more or less solvent accessible. Therefore, the continuum that surrounds our molecular model at the binding site will have different polarizability depending on which part of the protein are we considering. The polarizability of each zone will be characterized by a dielectric constant.

Gas phase calculations do not require consideration of environmental effects. Thus, the dielectric constant for this case is one. Notice that gas phase data reflects the intrinsic thermodynamic propensity of the reaction. The dielectric constant in a buried zone of the protein will be that defined by the protein environment. The polarizability inside a protein is low, what favours the electrostatic interactions between the metal and the ligands, and in the present study, dielectric constant values 2 and 4 will be considered for this protein area (see ε_1 in Fig. 4.1). If the binding site is in a more solvent-exposed area of the protein, we will have a middle-way situation, the effect of the solution around the protein increases its polarizability, and ε_2 will be set to 20 in our work. A higher polarizability in the cavity will favor the interaction of the metal with water. Finally, we can consider a totally solvent exposed area of the protein, where the dielectric will be that of water, thus, 78. This will be the highest polarizability area, and is represented by the data optimized in aqueous phase. Recall that our dielectric constants are relative to the dielectric constant of vacuum, ε_0= 8.85418742 * 10^{-12} C^2/Jm

The ΔG of the complexes modelling the metal in the binding site will be calculated as follows,

$$\Delta G = \Delta G_{gas} + \Delta G_{solv} \tag{4.3}$$

where the ΔG_{gas} is the free energy of the molecular model in the gas phase and ΔG_{solv} is the free energy of solvation in each dielectric environment. The latter will be calculated by carrying out PCM single point calculations at the HF/6-31+G* level of theory.

4.1.1 Calibration of the Solvation Effects.

The dielectric environment around a cavity can be modulated by changing the parameters of the solvent. This can be made imposing a solvent with

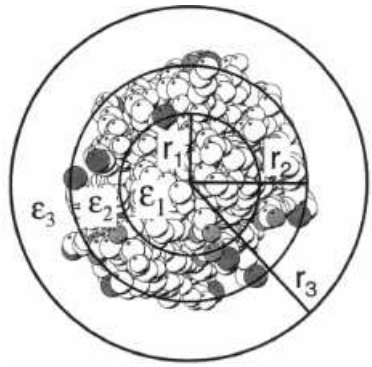

Fig. 4.1 Different dielectric environments inside a protein

the adequate dielectric environment [18] or otherwise, imposing water to be the solvent in all cases and changing only the dielectric constant value. Both strategies are available for PCM and IEFPCM. In this section, we will carry out a comparison of the different models.

Values obtained with the different methods for some of the structures studied are presented in Fig. 4.2 and 4.3.

Initially, the structures with two monodentate acetate ligands were chosen, for both magnesium and aluminum. The magnesium-containing complex is neutral and the analogous aluminum complex, has one positive charge. For the magnesium complex, no remarkable differences are observed between IEFPCM and PCM calculations (see Figure 4.2), when using different solvents or when imposing a dielectric constant. However, analyzing the aluminum solvation plots, anomalous behaviour of the IEFPCM results can be observed at low dielectric constant values.

Analogous data analysis was carried out for aluminum and magnesium complexes with one monodentate acetate and one methylimidazole (Fig. 4.3). This time, both complexes are positively charged,and disagreement between IEFPCM and PCM is seen in both cases, with some artifacts again at small IEFPCM dielectric constant values.

The results obtained using different dielectric values and solvents disagree specially at dielectric constant values around 20 and 40, that is, acetone and DMSO solvents, for both methods PCM and IEFPCM, due to the influence of the other solvent parameters. Solvation energies when using acetone and DMSO are around 7 and 10 kcal/mol higher, respectively, while for ether and

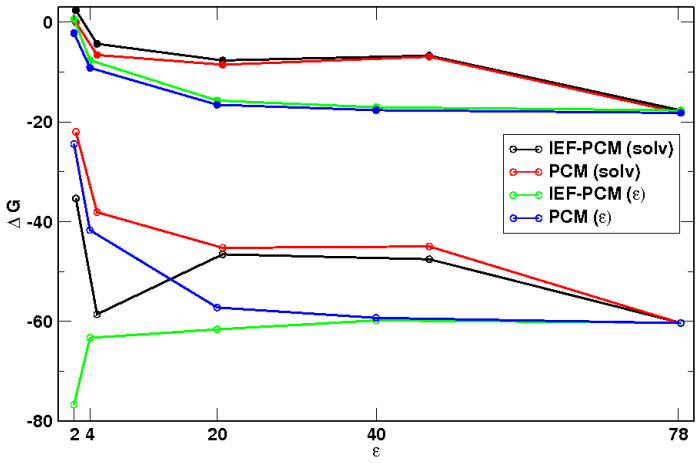

Fig. 4.2 Solvation free energies calculated at different dielectric and different solvents for the X-2M structures. The colour corresponds the different approaches, *i.e.*, solv stands for the ΔG obtained with the full parameters of the CCl4, Ether, Acetone, DMSO and water solvents. While (ε) corresponds to the values obtained only changing the (ε) of the media and keeping constant the rest of the parameters. Empty symbols correspond to aluminum complexes and filled to the magnesium ones.

CCl_4 are around 2 kcal/mol. This affects to the tendency of increasing the solvation energy, as we get closer to the water. When changing only the ε parameter, we see that the curve follows the tendency that we expected.

For the positively charged aluminum complexes same behaviour is reported, solvation energies in acetone and DMSO do not agree with those for 20 and 40 dielectric values. IEFPCM and PCM values do not agree for low dielectric values, either, differences going up to more than 60 kcal/mol in some cases.

In calculations using dielectric constant values, the bigger the dielectric constant, the bigger the solvation energy, despite this solvation energy changes much less from dielectric 20 to 78.34 than it does from 2 to 20. When using specific solvents for each dielectric, usually the solvation energy is smaller in DMSO than in acetone, and sometimes even smaller than for ether. From dielectric 46.7 to 78.34, there is a substantial increase of the solvation energy.

In the present work only dielectric constants will be varied when simulating different protein environments, since the results in this case reproduce the behaviour expected *a priori* in a protein binding site. Altering all the solvent parameters for each environment has seen to change remarkably this tendency.

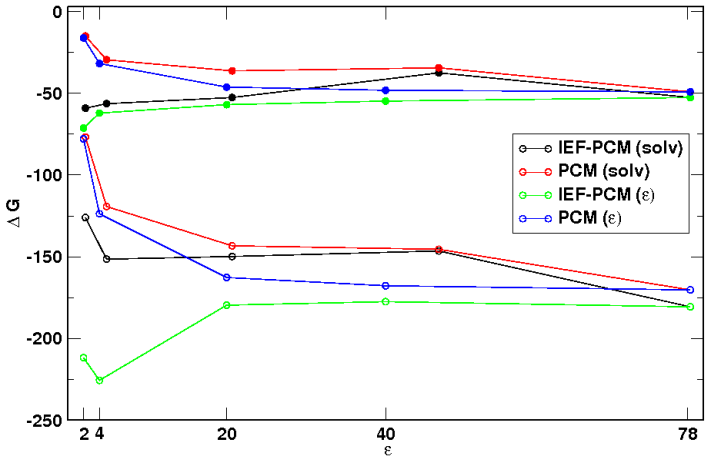

Fig. 4.3 Solvation values calculated at different dielectric and different solvents for the X-MI structures. The colour corresponds the different approaches, *i.e.*, solv stands for the ΔG obtained with the full parameters of the CCl4, Ether, Acetone, DMSO and water solvents. While (ε) corresponds to the values obtained only changing the (ε) of the media and keeping constant the rest of the parameters. Empty symbols correspond to aluminum complexes and filled to the magnesium ones.

In fact, inside a protein, the polarizability is the only parameter that differs the possible environments.

PCM at the HF/6-31+G* level will be used to calculate the solvation free energies in the different dielectrics. Anyway, optimization of the aqueous phase geometries will be carried out by IEFPCM, as it was seen to give similar results in water and is computationally less expensive.

4.2 Molecular models

Selected molecular models will be used to simulate the metal bound to the binding site of the protein. In protein active sites, the metal is bound to the side chains of the amino acids. This immediate environment will dictate the biological activity of the metalloprotein, since the first shell ligands play crucial roles in contributing to the metal complex stability and in determining the selectivity of the binding site [38,39]. Considering that the geometry of metal sites in proteins are very close to those obtained in vacuum, we will model the active sites with molecular complexes formed by the metal and its first co-

ordination shell, which will be composed by some bioligands (side chains of the amino acids most frequently found in proteins) and water molecules. X-ray studies suggest that the metals are usually coordinated to water molecules even in buried sites of the protein; consequently, we will add up to the metal the required water molecules as to fill up the first solvation shell of the metals. Recall that both Al(III) and Mg(II) are normally found octahedrally coordinated in biological environments [40,41].

The metal binding affinity will be evaluated by calculating the energy of the following reaction:

$$L_m^q + X(H_2O)_6^{ch} \longrightarrow X - L_m - (H_2O)_{6-m-n}^{ch+q} + (m+n)H_2O \tag{4.4}$$

where ch and q are the charge of the metal cation and the sum of the charges of the m ligands, respectively. n corresponds to the number of acetates bound bidentately, and X stands either for the Al (III) or the Mg (II) cation.

The reaction defines the metal binding affinity as the water/ligand substitution from the first hydration shell of the metal, where all the exchanges occur simultaneously.

The metal exchange reaction will be defined as follows:

$$\begin{aligned} Mg - L_m - (H_2O)_{6-m-n}^{2+q} + Al(H_2O)_6^{+3} \longrightarrow \\ Al - L_m - (H_2O)_{6-m-n}^{3+q} + Mg(H_2O)_6^{+2} \end{aligned} \tag{4.5}$$

The energy balance of this reaction, the exchange energy, will indicate the likelihood for the hydrated Al(III) to substitute a Mg(II) already attached to a binding site in a protein.

References

1 W. Kohn, L. Sham, Phys. Rev. A. 140 (1965) 1133.

2 R. G. Parr, W. Yang, Density Functional Theory of Atoms and Molecules, Oxford University Press, New York, 1989.

3 E. S. Kryachko, E. V. Ludeña, Energy Density Functional Theory of Atoms and Molecules, Kluwer Academic Publishres, Dordrecht, The Netherlands, 1990.

4 P. Hohenberg, W. Kohn, Phys. Rev. B. 136 (1964) 864.

5 M. Levy, Proc. Natl. Acad. Sci. USA 76 (12) (1979) 6062–6065.

6 J. P. Dahl, J. Avery, Local Density Approximations in Quantum Chemistry and Solid State Physics, Plenum Press, New York, 1984.

7 J. P. Perdew, W. Yang, Phys. Rev. B. 33 (1986) 8800.

8 W. Koch, M. C. Holthausen, A Chemist's Guide to Density Functional Theory, Wiley-VCH, Weinheim, Germany, 2001.

9 R. Ditchfield, W. J. Hehre, J. A. Pople, J. Chem. Phys. 54 (1971) 724.

10 W. J. Hehre, R. Ditchfield, J. A. Pople, J. Chem. Phys. 56 (1972) 2257.

11 P. C. Hariharan, J. A. Pople, Mol. Phys. 27 (1974) 209.

12 W. J. Stevens, M. Krauss, H. Basch, P. G. Jasien, Can. J. Chem. 70 (1992) 612.

13 L. Szasz, Pseudopotential Theory of Atoms and Molecules, Wiley, New York, 1985.

14 M. Krauss, W. J. Stevens, Annu. Rev. Phys. Chem. 35 (1984) 357.

15 D. R. Garmer, N. Gresh, J. Am. Chem. Soc. 116 (1994) 3556–3567.

16 N. Gresh, W. J. Stevens, M. Krauss, J. Comp. Chem. 16 (1995) 843–855.

17 N. Gresh, D. R. Garmer, J. Comp. Chem. 17 (1996) 1481–1495.

18 E. San Sebastian, J. M. Mercero, R. H. Stote, A. Dejaegere, F. P. Cossío, X. Lopez, J. Am. Chem. Soc. 128 (2006) 3554–3563.

19 J. M. Mercero, J. E. Fowler, J. M. Ugalde, J. Phys. Chem. A 102 (35) (1998) 7006–7012.

20 J. M. Mercero, J. E. Fowler, J. M. Ugalde, J. Phys. Chem. A 104 (2000) 7053–7060.

21 L. Rulised, J. Vondrasek, J. Inorg. Biochem. 71 (1998) 115–127.

22 J. M. Mercero, J. I. Mujika, J. M. Matxain, X. Lopez, J. M. Ugalde, Chem. Phys. 295 (2003) 175.

23 J. Rivail, D. Rinaldi, in: J. Leszczynski (Ed.), Computational Chemistry, Review of Current Trends, World Scientific Publishing, 1996, pp 139-174.

24 C. Cramer, D. Truhlar, in: P. Politzer, J. Murray (Eds.), Solute/solvent interactions (Theoretical and computationa chemistry, vol. 1), Elsevier, Amsterdam, 1994, pp 9-54.

25 S. Miertus, E. Scrocco, J. Tomasi, Chem. Phys. 55 (1981) 117.

26 S. Miertus, J. Tomasi, Chem. Phys. 65 (1982) 239.

27 A. R. Leach (Ed.), Molecular modelling. Principles and applications, Pearson, Essex, 2001.

28 M. T. Cances, V. Mennucci, J. Tomasi, J. Chem. Phys. 107 (1997) 3032.

29 M. J. Frisch, G. W. Trucks, H. B. Schlegel, G. E. Scuseria, M. A. Robb, J. R. Cheeseman, V. G. Zakrzewski, J. A. Montgomery, R. E. Stratmann, J. C. Burant, S. Dapprich, J. M. Millam, A. D. Daniels, K. N. Kudin, M. C. Strain, O. Farkas, J. Tomasi, V. Barone, M. Cossi, R. Cammi, B. Mennucci, C. Pomelli, C. Adamo, S. Clifford, J. Ochterski, G. A. Petersson, P. Y. Ayala, Q. Cui, K. Morokuma, D. K. Malick, A. D. Rabuck, K. Raghavachari, J. B. Foresman, J. Cioslowski, J. V. Ortiz, B. B. Stefanov, G. Liu, A. Liashenko, P. Piskorz, I. Komaromi, R. Gomperts, R. L. Martin, D. J. Fox, T. Keith, M. A. Al-Laham, C. Y. Peng, A. Nanayakkara, C. Gonzalez, M. Challacombe, P. M. W. Gill, B. G. Johnson, W. Chen, M. W. Wong, J. L. Andres, M. Head-Gordon, E. S. Replogle, J. A. Pople, Gaussian 98, a.11, Gaussian, Inc., Pittsburgh PA (2001).

30 M. J. Frisch, G. W. Trucks, H. B. Schlegel, G. E. Scuseria, M. A. Robb, J. R. Cheeseman, J. A. Montgomery, Jr., T. Vreven,

K. N. Kudin, J. C. Burant, J. M. Millam, S. S. Iyengar, J. Tomasi, V. Barone, B. Mennucci, M. Cossi, G. Scalmani, N. Rega, G. A. Petersson, H. Nakatsuji, M. Hada, M. Ehara, K. Toyota, R. Fukuda, J. Hasegawa, M. Ishida, T. Nakajima, Y. Honda, O. Kitao, H. Nakai, M. Klene, X. Li, J. E. Knox, H. P. Hratchian, J. B. Cross, V. Bakken, C. Adamo, J. Jaramillo, R. Gomperts, R. E. Stratmann, O. Yazyev, A. J. Austin, R. Cammi, C. Pomelli, J. W. Ochterski, P. Y. Ayala, K. Morokuma, G. A. Voth, P. Salvador, J. J. Dannenberg, V. G. Zakrzewski, S. Dapprich, A. D. Daniels, M. C. Strain, O. Farkas, D. K. Malick, A. D. Rabuck, K. Raghavachari, J. B. Foresman, J. V. Ortiz, Q. Cui, A. G. Baboul, S. Clifford, J. Cioslowski, B. B. Stefanov, G. Liu, A. Liashenko, P. Piskorz, I. Komaromi, R. L. Martin, D. J. Fox, T. Keith, M. A. Al-Laham, C. Y. Peng, A. Nanayakkara, M. Challacombe, P. M. W. Gill, B. Johnson, W. Chen, M. W. Wong, C. Gonzalez, J. A. Pople, Gaussian 03, Revision C.02, Gaussian, Inc., Wallingford, CT, 2004.

31 J. Labanowsky, J. Andelzelm, Density Functional Methods in Chemistry, Springer-Verlag, New York, 1991.

32 M. Alcamí, O. Mo, M. Yañez, Mass. Spectr. Rev. 20 (2001) 195.

33 J. M. Mercero, J. M. Matxain, X. Lopez, D. M. York, A. Largo, L. A. Eriksson, J. M. Ugalde, Int. J. Mass Spectr. 240 (2005) 37–93.

34 S. F. Sousa, P. A. Fernandes, M. J. Ramos, J. Phys. Chem. A. (2007)

35 D. A. McQuarrie, Statistical Mechanics, Harper and Row, New York, 1976.

36 M. Cossi, V. Barone, B. Mennucci, J. Tomasi, Chem. Phys. Lett. 286 (1998) 253.

37 E. Cances, B. Mennucci, J. Tomasi, J. Chem. Phys. 109 (1998) 260.

38 F. Himo, Theor. Chem. Acc. 116 (2006) 232–240.

39 U. Ryde, Dalton Trans. (2007) 607.

40 G. D. Markham, J. P. Glusker, C. W. Bock, J. Phys. Chem. B. 106 (2002) 5118.

41 C. W. Bock, G. D. Markham, A. K. Katz, J. P. Glusker, Inorg. Chem. 42 (2003) 1538.

Part 3 Results

5
Selection of a set of preferred ligands

5.1
Introduction

Here, we report a systematic study concerning complexes formed by the aluminum (III) and different ligands including the water of hydration sphere around the cation. Analogous magnesium (II) complexes have also been calculated and compared to the aluminum ones. The formation energetics, structural parameters of the different ligands around the metal and the thermodynamic stability of the complexes, along with the possibilities of occurring the magnesium/aluminum exchange in the proposed models, in different protein environments, will be estimated and discussed.

We have studied the systems where a single ligand substitutes a water molecule from the first hydration shell of the metal cation. The amino acid side chain functional groups have been used as ligands, e.g., acetate as a representative model for glutamate and aspartate, methyl-thiol/thiolate for cysteine, methylthioethane for methionine, acetamide for asparagine and glutamine, methanol for serine and threonine, methylimidazole for histidine, and toluene and methylbenzenol for phenylalanine and tyrosine respectively.

A broad variety of side chains was chosen in order to represent a wide range of amino acids that may be present in a protein, and study the affinity aluminium presents for each of them. Generally, the charge, electron density distribution, polarizability, size and rigidity of the ligand govern the competitiveness of the ligand relative to water for binding the cation [1]. The aim is to select a set of preferred ligands for Al(III) to be in its first hydration sphere in the protein, and to compare the results obtained with the data found in the literature, so that we can validate our method for future studies.

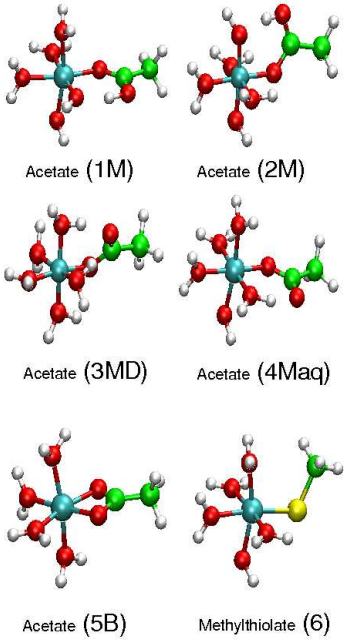

Fig. 5.1 The metal complexes described along this report formed by the aluminum/magnesium and the negative (acetate and methylthiolate) ligands, and the corresponding water molecules to complete the first coordination shell of the metal cation are shown. The letter M, MD and B stand for Monodentate, Monodentate-Diagonal and Bidentate respectively.

5.2 Results

The number of isomers (rotomers and ortho, meta and para depending on the position at which the metal interacts with the aromatic rings) is very large in these systems, and the relative energies between the rotomers are very small (around 2 kcal/mol). The difference between the ortho, meta and para isomers of the aromatic compounds are larger in some cases (around 15 kcal/mol since the isomer may involve some additional stabilization interactions). For the sake of brevity, the most stable complex will be considered in each case. The most relevant structures are shown in Fig. 5.1 (negatively charged ligand containing complexes) and 5.2 (neutral ligand containing complexes).

5.2.1 Negatively Charged Ligands Containing Complexes.

The negatively charged ligands studied are the acetate and the methylthiolate. The former represents the glutamate and aspartate aminoacids side chains, and dehydrogenated cysteine the latter. The acetate can bind in a monodentate and bidentate mode to the metal cation, oriented in different positions. The carboxylate group of the monodentate acetate may lie either in the equatorial plane, or out of it, in a diagonal conformation (1M and 2M in Fig. 5.1 for the former and 3MD for the latter).

1M and 2M complexes were characterized for aluminum. However, the diagonally oriented complex (3MD) was not found. Attempts to find such a structure collapsed to complexes 1M and 2M, where the only difference is the water molecule rotation, which energetically contributes a tiny amount (the energy difference between 1M and 2M is 3.6 kcal/mol). Similar calculations were performed by Tunega et al. [2]. After an extensive investigation using different density functionals and basis set combinations, they report the results with the BLYP/SVP+sp level of theory and optimized the complexes in aqueous phase at the BLYP(PCM)/SVP+sp level of theory. They only report the structure 2M, and do not mention 1M, which is found slightly more stable by us. Nevertheless, the only difference between these two structures is one apical water molecule rotation, and this contributes a very little either in the geometries (i.e. X-L or X-O_w bond lengths) or energetics, as it can be seen in Table 5.1. Comparing the gas phase and aqueous phase geometries (figures in *italics* and in parenthesis for aluminum in Table 5.1), a good agreement between their work and ours is observed, for both 1M and 5B structures.

Three different monodentate acetate complexes were located to be a minimum for the magnesium (II) cation, which are shown in Fig. 5.1 (1M, 2M, 3MD). Only one structure for bidentate acetate was characterized, namely, 5B in Fig. 5.1. The electronic and solvation energies, and the main geometrical features are shown in Table 5.1, where values obtained with different levels of theory for a number of properties found in the literature are also collected.

Tab. 5.1 Electronic and free energies of the negative ligand containing metal complexes. Energies (E^g, in hartrees) correspond to the B3LYP/6-311++G(2dp,2d)//B3LYP/SBKJ+* level of theory. ΔG_{Hyd} is the solvation energy of the complex (in kcal/mol). The bond lengths are given in Å. X-L is the bond length between the ligand and the metal cation, while X-O_w is the average of the bonds formed between the metal cation and the water molecules of the complex. Values in parenthesis were obtained after PCM optimization at the B3LYP/6-311++G(2df,2p) level of theory, and figures in *italics* have been taken from the literature.

	Aluminum (III)				Magnesium (II)			
	E^g	ΔG_{Hyd}	X-L	X-O_w	E^g	ΔG_{Hyd}	X-L	X-O_w
Acetate (1M)	-852.80467	-193.96	1.867	1.988*	-810.82139	-62.57	2.013	2.11
	(-853.11842)		(1.896)	(1.930)	(-810.92811)		(2.013)	(2.086)
							1.980[a]	*2.123*[a]
Acetate (2M)	-852.79890	-195.94	1.865	1.993*	-810.81814	-64.50	2.003	2.141
			1.881[b]*(g)*	*2.022*[b]*(g)*				
			1.913[b]*(aq)*	*1.966*[b]*(aq)*				
Acetate (3MD)					-810.81930	-59.50	2.020	2.117
					(-810.92345)		(2.031)	(2.092)
							1.992[a]	*2.126*
Acetate (4M)	(-853.11887)		(1.830)	(1.911)				
Acetate (5B)	-776.32259	-203.32	1.871	1.960	-734.35921	-64.50	2.065	2.120
			1.900[b]*(g)*	*1.980*[b]*(g)*			*2.118*[a]	*2.118*[a]
			(1.910)	(1.904)			(2.082)	(2.085)
			1.935[b]*(aq)*	*1.931*[b]*(aq)*				
Methylthiolate (6)	-1062.3761	-208.08	2.227	2.004	-1020.37039	-66.47	2.468	2.133

* The Al-O corresponding to the OH was not included in the average.

[a] reference [3]

[b] reference [2]. (g) and (aq) stand for gas and aqueous phases respectively.

Deerfield et al. [3] found for the Mg-HCOO$(H_2O)_5^{+1}$ complex the diagonal orientation to be the global minimum of the potential energy surface (3MD) at the HF level of theory with a 6-31++G** basis set. The energy difference is only 0.8 kcal/mol with respect to 1M. Our calculations at the B3LYP/SBKJ+*//B3LYP/6-311++G(2df,2p) report very small electronic energy differences among these three complexes, as it is shown in Table 5.1. 1M is the global minimum, and 3MD and 2M are 1.3 and 2.0 kcal/mol higher in electronic energy.

The bond lengths calculated by Deerfield et al. (values in *italics* for magnesium in Table 5.1) are slightly shorter for the X-L and larger for X-O_w than the ones calculated by us for the monodentate acetate complexes, while the bidentate bond lengths are very similar. We also include the values of the structures optimized in aqueous phase at the B3LYP(PCM)/6-311++G(2df,2p) level of theory (in parenthesis) and we observe that the only difference with respect to the gas phase geometries are the X-O_w bonds, which are larger in gas phase (2.086 vs. 2.112 Å). For the bidentate complex (5B), a similar trend is observed upon comparison of ours and Deerfield et al. geometries (see Table 5.1).

Comparison between both aluminum and magnesium reveals a remarkable difference at the monodentate complexes. While for the magnesium complex the five water molecules retain their molecular identity, for the aluminum complex there is a proton transfer from one of the water molecules to the carboxylate, and thus, an OH is now bound to the aluminum cation (see 1M in Fig. 5.1). The Al-OH bond length is 1.77 Å and the hydrogen which is now at the carboxylate interacts with the oxygen of the OH forming an hydrogen bond with a bond length of 1.57 Å (1.56 Åis the value reported by Tunega et al.). For the magnesium complex we observe that the hydrogen of the water molecule is oriented towards the oxygen of the acetate. The Mg-O bond length corresponding to this oxygen is the shortest M-O bond (2.0 while the average is 2.14 Å) but this effect is not as dramatic as the one described for the aluminum complex. This proton transfer was also reported by Tunega et al. They tried to locate a structure without the proton transfer on the aqueous phase, but they did not succeed. On the contrary, our aqueous phase calculations at the B3LYP(PCM)/6-311++G(2df,2p) level of theory, located a structure where the proton remains in the water molecule forming a hydrogen bond with the oxygen of the acetate ($4M^{aq}$ in Fig. 5.1). The geometrical parameters of this complex are very similar to the other monodentate structures (slightly shorter Al-O and Al-O_w bonds) with the main difference being the Al-O of the water and the Al-O of the OH. Energetically, 1M and $4M^{aq}$ are nearly degenerated as it can be observed in Table 5.1 (recall that it should be compared with the number obtained after aqueous phase optimization), with a difference smaller than 0.5 kcal/mol.

The methylthiolate ligand only presents one interacting mode, where the metal cation binds to the sulfur atom. We have also located rotomers corresponding to water and/or methyl rotations, but, as for the acetate anion complexes, the differences among these rotomers are negligible. The distances between the metal cation and the ligand (sulfur atom in this case) are larger than the O-X bond lengths as it can be seen in Table 5.1.

The binding energies of these complexes will be calculated according to the following reaction 5.1,

$$X^q + L^y + (5-n)H_2O \longrightarrow X - L(H_2O)_{5-n}^{q+y} \tag{5.1}$$

where q and y are the charges of the metal cation and ligand respectively, and n is 2 when the ligand binds with a bidentate coordination, and 1 when it is monodentate. X stands either for the aluminum or the magnesium cation.

The results are shown in Table 5.2, for the sake of comparison with the data found in the literature.

Tab. 5.2 Binding energies and free energies (in kcal/mol), as described by reaction 5.1, of the anionic ligand complexes (see Fig. 5.1). Values in parenthesis were obtained after PCM optimization at the B3LYP/6-311++G(2df,2p) level of theory, and figures in *italics* have been taken from the literature.

	Aluminum (III)			Magnesium (II)		
	ΔE_B^g	ΔG_B^g	ΔG_B^{aq}	ΔE_B^g	ΔG_B^g	ΔG_B^{aq}
Acetate (1M)	-1022.20	-966.64	-56.63	-508.02	-455.34	-4.03
			(-70.87)	*0.8*[a]		(-19.55)
Acetate (2M)	-1018.61	-963.47	-55.44	-505.79	-454.05	-4.66
	-1028.5[b]					(-20.1)
Acetate (3MD)				-506.79	-453.11	-0.15
				0.0[a]		(-15.8)
Acetate (5B)	-996.6	-950.44	-57.22	-494.81	-451.63	-9.67
	-1001.9[b]	*-940.7*[b]	(-69.89)	*15.0*[a]		(-22.08)
Methylthiolate (6)	-995.41	-941.81	-48.72	-493.03	-443.22	1.4

[a] reference [3]. They did not report the E_B defined, but they did report the relative energies between the different complexes.
[b] reference [2].

There are big differences between the gas phase and aqueous phase binding energies. While these energies are around -1000 kcal/mol for aluminum in the gas phase, in aqueous phase the energies are reduced to -55 kcal/mol. The gas phase ΔE_B^g is larger for the monodentate binding orientation by 22 and 12 kcal/mol as compared to the bidentate orientation, for aluminum and mag-

nesium complexes respectively, which agrees well with the values of Tunega et al. for aluminum (27 kcal/mol) and Deerfield et al. for magnesium (14 kcal/mol). After the solvent effects (PCM single points) are taken into account, the difference between the monodentate and bidentate complexes, is very small. Our results predict that both (mono- and bidentate complexes) have almost identical binding free energies, while for magnesium, the bidentate complex binding free energy is 4.5 kcal/mol stronger than the monodentate one.

The B3LYP(PCM)/6-311++G(2df,2p) optimizations predict larger ΔG_B^{aq} than single point PCM calculations as it can be observed in Table 5.2. Nevertheless, note that the relative energies between the complexes remain unchanged. Thus, both methods predict a nearly identical ΔG_B^{aq} for the aluminum mono- and bidentate complexes, while for magnesium, bidentate is 3 kcal/mol more stable. Tunega predicted the monodentate aluminum complex to be 4 kcal/mol more stable than the bidentate.

The binding energies and binding free energies of the X-methylthiolate complexes, in gas phase, are similar to the acetate bidentate complexes, as shown in Table 5.2. The ΔG_B^{aq} decreases as a consequence of solvation. Observe that the magnesium (II) complex results in a positive ΔG_B^{aq}, which is indicative of the instability of this complex in water.

A water molecule substitution of the hexahydrated cation (the $\Delta E_f^{aq/g}$ formation energy) by an anionic ligand (see formation reaction 4.4) will give us an idea of the metal affinity towards the different side chains. As can be observed in Table 5.3 these formation energies are highly favorable in the gas phase.

The ΔG_f^g are -337, -321 and -312 kcal/mol for the acetate 1M, 5B and methylthiolate 6 complexes. For magnesium a similar trend with smaller ΔG_f^g is observed (-203, -199 and -190 kcal/mol respectively). As described for the binding energy, the formation of the monodentate complexes is favored over the bidentate ones, by 16 kcal/mol aluminum and 4 kcal/mol for magnesium.

The ΔG_f^{aq} in aqueous phase, however, shows a very different picture. The formation of the ligand-metal complexes is unfavorable for the aluminum cation, i.e., it prefers to be hexahydrated than forming a complex with either the acetate or the methylthiolate ligands, while the ΔG_f^{aq} 's for the magnesium-carboxylate complexes are negative (-2 and -7 kcal/mol for the mono and bidentate carboxylates respectively). The free energies obtained optimizing the complexes in aqueous phase give similar results. Our optimizations at the B3LYP(PCM)/6-311++G(2df,2p) yield ΔG_f^{aq} 3.47 and 4.45 kcal/mol for the mono- and bidentate aluminum complexes respectively. Tunega et al. obtained 3.5 and 8.1 kcal/mol respectively. The values obtained by Tunega and

Tab. 5.3 Formation energies and free energies (in kcal/mol) corresponding to the water/ligand exchange . Values in parenthesis were obtained after PCM optimization at the B3LYP/6-311++G(2df,2p) level of theory, and figures in *italics* have been taken from the literature.

	Aluminum (III)			Magnesium (II)		
	ΔE_f^g	ΔG_f^g	ΔG_f^{aq}	ΔE_f^g	ΔG_f^g	ΔG_f^{aq}
Acetate (1M)	-337.56	-336.86	6.17	-203.73	-202.70	-1.81
			(3.47)			(-8.11)
			3.5[b]			
Acetate (2M)	-333.96	-333.69	7.36	-201.69	-201.42	-2.46
	-326.9[b]	*-328.8*[b]				
Acetate (3MD)				-202.42	-200.41	2.12
Acetate (5B)	-311.85	-320.67	5.57	-190.52	-199.00	-7.47
			(4.45)			(-11.88)
	-300.3[b]	*-311.6*[b]	*8.1*[b]			
Methylhiolate (6)	-310.80	-312.08	14.03	-188.74	-190.59	3.6

[b] taken from ref [2].

ours agree very well for the monodentate complexes, while our value for the bidentate is half of their value.

Palmer and Bell [4] measured the experimental ΔG and ΔH for the aluminum-acetate formation, the values being -3.8$\pm$0.2 and 4$\pm$1.4 kcal/mol for the ΔG and ΔH respectively. We have also evaluated the ΔH, (using the gas phase corrections) and, obtained 3.68 and 15.34 kcal/mol for the mono and bidentate complexes respectively. The monodentate enthalpy agrees with the experimental value, not however the ΔG. Palmer and Bell experiments were questioned by Öman [5], and Tunega (which obtained very similar results to ours) attributed these discrepancies not only to the inaccuracies of the computational procedures, but also to the fact that the thermodynamical models used by the experimentalist to estimate the ΔG and ΔH were not flexible enough.

Dudev and Lim [6] performed similar theoretical calculations for magnesium and formate-monodentate complexes. Despite that we have focused on acetate, we have also some data for the magnesium formate complexes, obtained at the B3LYP/SBKJ+* and solvent effects by single point PCM calculations over the gas phase geometries. The ΔG_f^g for the magnesium formate complex is -189.9 kcal/mol as calculated by Dudev et al., and our value is -191.29. Thus, there is a good agreement for the gas phase. Some discrepancies arise when the solvent effects are considered. Dudev et al. optimize the formate parameters to obtain the experimental value of -82 kcal/mol, while PCM is parameterized to obtain an experimental value of -75 kcal/mol [7]. This discrepancy in the experimental reference value of 7 kcal/mol, yields to

a discrepancy between their and our results. We report a ΔG_f^{aq} of -2.5 kcal/mol while they give a value of 7.6 kcal/mol.

According to the metal exchange reaction energies and free energies shown in Table 5.4 the substitution of the magnesium complexed with acetate or methylthiolate by an aluminum (as described in the exchange reaction 4.6), seems to be quite favorable in gas phase, but not in solution, where the $\Delta G_{Mg/Al}^{aq}$ are unfavorable for all the complexes considered.

Tab. 5.4 Metal exchange energies and free energies (in kcal/mol).

	$\Delta E_{Mg/Al}^{g}$	$\Delta G_{Mg/Al}^{g}$	$\Delta G_{Mg/Al}^{aq}$
Acetate (1M)	-135.14	-136.46	7.98 (12.83)
Acetate (5B)	-121.33	-121.67	13.04 (16.33)
Methylthiolate (6)	-122.02	-121.45	10.47

In summary, we can say that the evaluation of the solvent effects over the gas phase geometries gives reasonably good results, and the obtained relative energies, enthalpies and free energies agree very well with the values obtained by optimization of the complexes in aqueous media. However, we have found structures in the aqueous phase, that were not stable in the gas phase, e.g., the aluminum monodentate acetate complex with no proton transfer from the water to the acetate. We have also observed that the monodentate and bidentate acetate complexes are nearly energetically degenerated for aluminum, while for the magnesium this difference is slightly larger in favor of the bidentate complex.

5.2.2 Neutral Ligand Containing Complexes

In this section we describe the complexes formed between aluminum (III) and magnesium (II) cations and the following neutral ligands: acetamide, methanol, methylimidazole, toluene, methylphenol, methylthiol, and methylthioethane which are the side chains of the asparagine/glutamine, serine/threonine, histidine, phenylalanine, tyrosine, cysteine (neutral) and methionine respectively.

As discussed in the previous section, there is a large number of possible isomers due to the water and/or methyl rotations, and present different interaction modes of the aromatic groups with the cation, i.e., the metal may interact in the ortho, meta or para position of the substituent in the aromatic

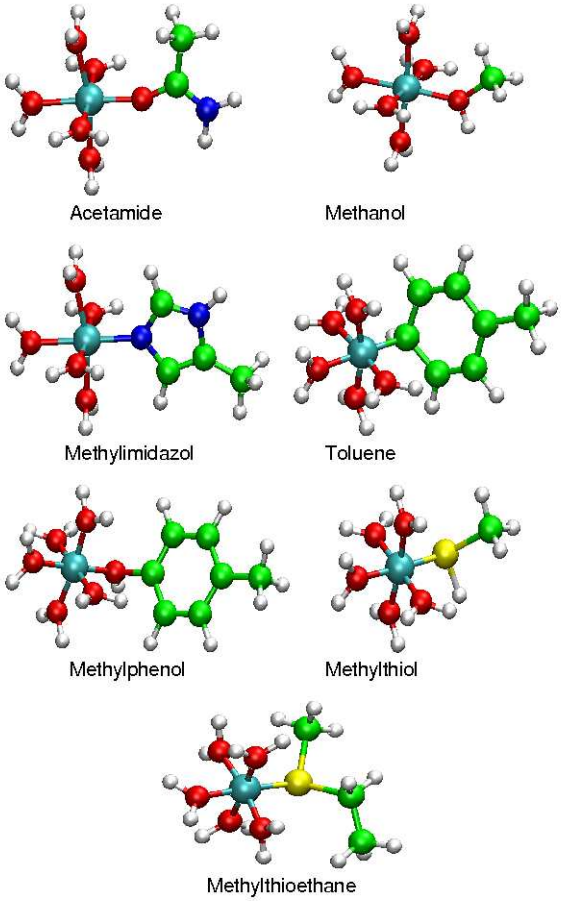

Fig. 5.2 The metal complexes described along this report formed by either the aluminum or the magnesium and the neutral ligands, and the corresponding water molecules to complete the first coordination shell of the metal cation are shown.

ring. The differences among these complexes are energetically very small. Thus for the sake of brevity, we are going to focus on the global minima of the corresponding potential energy surface, whose structures are shown in Fig. 5.2.

The electronic energy, solvation free energy and X-L, X-O_w bond lengths are shown in Table 5.5.

The shortest Al-L bond occurs in the acetamide complex while the largest corresponds to the sulfur containing ligands. This trend is repeated for the Mg-L distances, with the exception of the magnesium toluene complex, where

Tab. 5.5 Electronic and free energies of the neutral ligand containing metal complexes. Energies (E^g in hartrees) correspond to the B3LYP/6-311++G(2dp,2d)//B3LYP/SBKJ+* level of theory. ΔG_{Hyd} is the solvation energy of the complex (in kcal/mol). The bond lengths are given in Å. The X-L is the bond length between the ligand and the metal cation, while X-O_w is the average of the bonds formed between the metal cation and the water molecules of the complex.

	Aluminum (III)				Magnesium (II)			
	E^g	ΔG_{Hyd}	X-L	X-O_w	E^g	ΔG_{Hyd}	X-L	X-O_w
Acetamide	-833.00616	-397.88	1.798	1.960	-791.19145	-175.27	2.002	2.128
Methanol	-739.43988	-422.25	1.899	1.950	-697.65758	-185.38	2.086	2.116
Methylimidazole	-889.32520	-394.69	1.927	1.971	-847.50234	-173.11	2.123	2.135
Toluene	-895.24377	-391.70	2.218	1.976	-853.44649	-176.64	2.869	2.095
Methylphenol	-970.52315	-398.18	1.905	1.943	-928.71683	-176.76	2.114	2.109
Methylthiol	-1062.41013	-410.18	2.443	1.959	-1020.62804	-179.66	2.679	2.112
Methylthioethane	-1141.03030	-393.02	2.404	1.968	-1099.23224	-172.15	2.649	2.119

the Mg-L is very large, 2.869 Å, and the Mg-O_w distances shorter, indicative of the weak magnesium-toluene interactions.

The Al-O_w distances are similar in all the complexes, the shortest value for aluminum corresponds to the methylphenol complex, 1.943 Å and to toluene the largest (1.976 Å). The magnesium Mg-O_w distances are larger, around 2.1 Å, the largest occurring for the methylimidazole complex, and the shortest for the complex with toluene (see Table 5.5 for more details). The X-O_w bond lengths in the $Al/Mg(H_2O)_6^{+3/+2}$ complex are 1.940 and 2.110 Å for aluminum and magnesium respectively. Once the ligand is included the metal-oxygen bond length increases slightly for aluminum and even less for the magnesium. Recall that at the magnesium-toluene complex the Mg-O_w distance shrinks slightly (0.01 Å), due to the lengthening of the Mg-L distance. This lengthening renders a more visible magnesium (II) for the water ligands to approach closer, i.e, the interaction with the toluene is very small, and being the number of water molecules around the magnesium only *five*, the interactions are on average stronger than the ones in the *hexa*-hydrated magnesium complex.

The binding energies of these complexes (as described in reaction 5.1), summarized in Table 5.6, will help us to rationalize their stabilities.

The methylimidazole binding free energies are the largest, -688.34 and -277.67 kcal/mol for aluminum and magnesium respectively, and that of toluene and methylthiol the smallest for magnesium (-245.07 kcal/mol) and aluminium (-632.16 kcal/mol), respectively. Once the solvent effects are considered, these energies change substantially and their relative difference is reduced. The magnesium complexes binding free energies are all positive except for acetamide and methylimidazole complexes. As in the gas phase, the aluminum complex binding energies are negative but significantly smaller, and

Tab. 5.6 Binding energies and free energies (in kcal/mol), as described by reaction 5.1, of the different neutral ligand complexes (see Fig. 5.2).

	Aluminum (III)			Magnesium (II)		
	ΔE_B^g	ΔG_B^g	ΔG_B^{aq}	ΔE_B^g	ΔG_B^g	ΔG_B^{aq}
Acetamide	-733.83	-678.47	-39.45	-325.36	-272.47	-0.87
Methanol	-696.01	-641.22	-31.36	-306.93	-255.45	1.20
Methylimidazole	-743.73	-688.34	-46.06	-330.18	-277.67	-3.89
Toluene	-694.92	-639.57	-1.17	-297.42	-245.07	18.31
Methylphenol	-715.03	-660.17	-22.11	-312.21	-259.94	9.09
Methylthiol	-686.77	-632.16	-15.24	-298.81	-247.64	9.76
Methylthioethane	-702.63	-647.37	-12.93	-304.64	-252.48	12.75

as for magnesium, methylimidazole and acetamide have the largest binding free energies.

The formation energies (ΔE_f) and formation free energies (ΔG_f), given by the water/ligand exchange, as described previously, are collected in Table 5.7.

Tab. 5.7 Formation energies and free energies (in kcal/mol) corresponding to the water/ligand exchange (for the neutral ligand complexes) as described in reaction 4.4 . Figures in *italics* have been taken from the literature.

	Aluminum (III)			Magnesium (II)		
	ΔE_f^g	ΔG_f^g	ΔG_f^{aq}	ΔE_f^g	ΔG_f^g	ΔG_f^{aq}
Acetamide	-49.18	-48.70	23.39	-21.10	-19.84	1.33
						4.2[a]
Methanol	-11.36	-11.45	31.43	-3.62	-3.63	2.59
Methylimidazole	-59.08	-58.56	16.74	-25.88	-25.04	-1.69
						-1.3[a]
Toluene	-10.27	-9.79	61.63	6.87	7.56	20.51
Methylphenol	-30.73	-30.39	40.32	-7.92	-7.31	11.29
Methylthiol	-2.12	-2.39	47.55	5.49	5.03	11.96
Methylthioethane	-17.98	-17.60	49.86	-0.35	0.15	14.95

[a] taken from ref [6]. Note that this values are calculated for the non-methylated ligands, i.e., acetamide, and methylimidazole.

In the gas phase, all the formation energies and free energies for aluminum have negative values. For magnesium positive ΔG_f^g 's are found for toluene, and methylthiol, for the aqueous phase only the methylimidazole containing magnesium complex formation is favorable in water. Dudev et al. obtained similar results for the magnesium formate and methylimidazole, despite that

their ligands are smaller (they lack the terminal CH_3) the ΔG_f^{aq} 's are similar [6] (4.2 and -1.3 kcal/mol respectively).

Apart from methylimidazole, acetamide and methanol show small positive formation free energy values in aqueous phase. These results are in accordance with the fact that, beside the negatively charged ligands, methylimidazole (histidine) and acetamide (asparagine or glutamine) are the most frequent ligands at the magnesium-protein binding sites [9]. Thus, special consideration should be given to these ligands in future chapters.

We have seen that the aluminum/magnesium exchange is unfavorable for the negatively charged ligands (see Table 5.4) in the aqueous phase, and, on the contrary, favorable in the gas phase. A similar trend, with larger positive $\Delta G_{Mg/Al}^{aq}$ and smaller negative $\Delta G_{Mg/Al}^{g}$ energies is estimated for the neutral ligand containing complexes (see Table 5.8).

Tab. 5.8 Metal exchange energies and free energies (in kcal/mol) in gas and aqueous phase (for the neutral ligand complexes)

	$\Delta E_{Mg/Al}^{g}$	$\Delta G_{Mg/Al}^{g}$	$\Delta G_{Mg/Al}^{aq}$
Acetamide	-28.08	-28.86	22.06
Methanol	-7.74	-7.82	28.84
Methylimidazole	-33.2	-33.52	18.43
Toluene	-17.14	-17.36	41.11
Methylphenol	-22.81	-23.08	29.03
Methylthiol	-7.61	-7.42	35.59
Methylthioethane	-17.63	-17.75	34.91

5.2.3 Dielectric Effects

Based on our data, aluminum/magnesium exchange is unfavorable even for negatively charged ligands when aqueous phase (where the dielectric value ε is 80) is considered. However, it is highly favorable in the gas phase (ε=1). This suggests that the calculated aluminum/magnesium exchange and formation energies are strongly dependent on the dielectric medium. We investigate this behavior in the present section.

Recently, T. Dudev and C. Lim have reported that the formation reaction free energy is sensitive to the dielectric constant of the environment [6]. We obtained similar results for the formation reactions which are summarized in Table 5.9.

We have also calculated the effect of the dielectric in the metal exchange reaction. The free energy changes at the different dielectric environment are collected in Table 5.10.

Tab. 5.9 Formation free energies (in kcal/mol) for selected values of the dielectric constant ε.

	Aluminum (III)					Magnesium (II)				
	ε=1	ε=2	ε=4	ε=20	ε=80	ε=1	ε=2	ε=4	ε=20	ε=80
1M	-336.86	-163.55	-76.51	-6.15	6.17	-202.70	-100.23	-49.72	-9.38	-1.81
5B	-320.67	-154.47	-72.1	-6.18	5.57	-199.00	-100.18	-52.35	-14.62	-7.47
6	-312.08	-145.83	-63.47	2.48	14.03	-190.59	-90.63	-42.17	-3.56	3.60
Acetamide	-48.70	-11.78	6.38	21.29	23.39	-19.84	-8.09	-3.24	0.62	1.33
Metanol	-11.45	10.7	21.6	30.47	31.43	-3.63	0.51	1.69	2.48	2.59
Methylimidazole	-58.56	-19.32	-0.51	14.63	16.74	-25.04	-11.79	-6.66	-2.47	-1.69
Toluene	-9.79	30.34	47.63	60.2	61.63	7.56	12.86	17.32	20.25	20.51
Methylphenol	-30.39	9.05	26.24	22.26	40.32	-7.31	4.43	8.27	10.87	11.29
Methylthiol	-2.39	26.33	38.46	46.92	47.55	5.03	11.43	12.29	12.13	11.96
Methylthioethane	-17.60	21.94	37.93	48.84	49.86	0.15	11.91	14.22	14.97	14.95

Tab. 5.10 Metal exchange free energies (in kcal/mol) for selected values of the dielectric constant ε.

	ε=1	ε=2	ε=4	ε=20	ε=80
1M	-136.46	-63.32	-26.79	3.23	7.98
5B	-121.67	-54.29	-19.75	8.44	13.04
6	-121.45	-55.16	-21.26	6.08	10.47
Acetamide	-28.86	-3.69	9.62	20.67	22.06
Metanol	-7.82	10.19	19.91	27.99	28.84
Methylimidazole	-33.52	-7.53	6.15	17.1	18.43
Toluene	-17.36	12.43	27.56	39.61	41.11
Methylphenol	-23.08	4.62	11.39	17.97	29.03
Methylthiol	-7.42	14.9	26.17	34.79	35.59
Methylthioethane	-17.75	10.03	23.71	33.87	34.91

The formation free energies are affected significantly by the dielectric constant, becoming more positive as ε increases. The acetate aluminum complex formation presents negative free energies in a buried and partial buried (ε=2, 4 and 20) environment, while it is positive in fully solvent accessible environment. For the magnesium acetate complexes, the formation free energy is negative in the entire ε range. Finally, among the negative ligands, the methylthiolate, only has negative free energy values for both metals for small ε, 2 and 4, and for magnesium, ε=20 also has a negative free energy of -3.56 kcal/mol. Another important trend is that aluminum has largest affinity for the acetate and the methylthiol for the smaller ε values, but when ε=20, the affinity is changed, and the formation free energies are smaller for the magnesium complexes.

For the neutral ligands, only acetamide and methylimidazole will replace a water molecule from the inner shell at small dielectric values, in ε=2 acetamide, and in ε=2 and 4 methylimidazole forming a complex with aluminum. The dielectric range in which magnesium-ligand complexes are formed is wider. Acetamide-magnesium complexes are formed in the 1-4 range, while methylimidazole-magnesium complex formation occurs in the entire dielectric range. The neutral ligands have larger affinity for aluminum only in the gas phase (ε=1). All the ligands (with the exception of acetamide and methylimidazole at ε=2) have larger affinity for magnesium when $\varepsilon > 1$.

The metal exchange ΔG over the dielectric range is summarized in Table 5.10. Also in this case, as we increase the dielectric constant value ε, the metal reaction exchange ΔG is more positive. The negative ligand complexes have negative free energies only at very small dielectric values (2 and 4), while for the neutral-ligand-X complexes, acetamide and methylimidazole complexes, at ε=2, may exchange the magnesium by aluminum. These results suggest that aluminum will only substitute magnesium in quite low polarizability sites around acetate, acetamide and methylimidazole ligands.

5.3 Conclusions

Formation and metal exchange free energies are very favorable in the gas phase, however, they are small and unfavorable in all aluminum (III) complexes and most of the magnesium (II) ones in aqueous phase.

Among the different coordination ways of the acetate, monodentate is preferred in the gas phase either for aluminum and magnesium complexes. In aqueous phase, there is a very small difference for the aluminum between the monodentate and the bidentate binding possibilities while bidentate magnesium complexes are around 6 kcal/mol more stable than monodentate ones.

Our results compared well with similar theoretical calculations found in the literature, and furthermore, are indicative of the good agreement between theory and *real systems* in the sense that the ligands that show the smallest ΔG_f^{aq} with magnesium are those that appear more frequently in proteins at magnesium binding sites.

The dielectric constant of the media plays an important role in the complex formation and in the metal exchange reaction free energies. Our calculations predict that no aluminum complexes will be formed in fully solvent accessible areas, i.e., ε=80, however, they may be formed in regions with smaller ε. Magnesium complexes, however, may bind acetate and methylimidazole in the full ε range.

The metal exchange is thermodynamically favored only if a negatively charged ligand is bound to magnesium, in a buried or partially buried protein region ($\varepsilon \approx 4$). If no negative ligands are present, then, the metal exchange may only occur in solvent inaccessible protein regions.

Overall, the affinity of the metals for the negative ligands is stronger than for the neutral ligands, since the metal-ligand interaction energy is most favorable for complexes with negatively charged ligands. Between the latter, acetamide and methylimidazole have been seen to be preferred, as expected, and in accordance to the ligands present in the natural binding sites of Mg(II). This will be taken into account for the next chapters, where systems that include a larger number of ligands will be studied. Together with the negatively charged acetate and methylthiolate, and the neutral methylimidazole and acetamide, methanol will be included in this group. Methanol is a very common ligand in natural protein binding sites, and it also represents the methylphenol, which has presented very favourable energetical properties in this first chapter.

References

1 T. Dudev, J. A. Cowan, C. Lim, J. Am. Chem. Soc. 121 (1999) 7665.

2 D. Tunega, Haberhauer, M. Gerzabek, H. Lischka, J. Phys. Chem A 104 (2000) 6824-6833.

3 D. W. Deerfield, D. J. Fox, M. Head Gordon, R. G. Hiskey, L. G. Pedersen, Proteins Structure Function and Genetics 21 (1995) 244–255.

4 D. A. Palmer, J. L. S. Bell, Geochim. Cosmochim. Acta 58 (1994) 651.

5 L. Öhman, Geochim. Cosmochim. Acta 59 (1995) 4775.

6 T. Dudev, C. Lim,J. Phys. Chem. B 104 (2000) 3692–3694.

7 M. Cossi, V. Barone, R. Cammi, J. Tomasi, Chem. Phys. Lett. 255 (1996) 327.

8 T. Dudev, C. Lim, Chem. Rev. 103 (2003) 773.

9 T. Dudev, Y. Lin, M. Dudev, C. Lim, J.Am. Chem. Soc. 125 (2003) 3168–3180.

6
Metal binding sites with two ligands

6.1
Introduction

In this chapter a systematic study concerning the different complexes formed by the Al (III) and selected ligands which presented the highest affinity for Al (III) in the previous chapter, together with the water of hydration molecules around the cation will be presented. Analogous magnesium complexes have also been studied and compared to the aluminum ones. We have evaluated the formation reaction energies, structural parameters of the different ligands and the possibilities of Mg/Al exchange to occur in the different models proposed.

In the previous section we concluded the low probability for the aluminum complexes formation in a system with only one protein side chain ligand, and as it is usual for other metal-natural ligand interactions [1, 2], more than one ligand seems to be involved in a hypothetical Al (III) protein binding site.

In the present chapter, we have considered a model with two non-water ligands interacting with the metal cation, and the rest of the first solvation shell is complemented by water molecules. As it has previously been reported in the literature [3], and was also confirmed by our previous results (see chapter 5), the acetate anion presents highly favorable energetical properties towards both, aluminum and magnesium cations. Due to this affinity, and also to the ubiquity of acetate in protein binding sites, in this study an acetate will be maintained as one of the ligands in all the studied complexes. The second ligand has been selected based on the previous chapter which showed that methylthiolate, methylimidazole and acetamide have the strongest affinity towards Al (III). Methanol will be included in this set, since, even its energetical contribution is not as large as other ligand's, is a very common ligand in protein binding sites [1], and also represents the methylphenol, which presented very favourable energetical properties in the previous chapter.

The aim of this chapter is to study different possible binding sites of Al by modeling its interactions with several ligands on one side and identify those coordinations where the Mg (II) might be replaced by Al (III), which can be

relevant to understand the mechanism of aluminum toxicity. By maintaining an acetate in all the complexes we will be able to study how does the acetate influence the stability of the complexes, so that we can define the most thermodynamically preferable, first-coordination shell for aluminium.

We have divided this chapter into (i) complexes formed by two negative ligands, and (ii) complexes formed by one negative and one neutral ligands. Finally, the effect of the dielectric media in the formation and metal exchange reactions described in chapter 2 will be discussed.

6.2 Results

6.2.1 Two Negatively Charged Ligands: Acetate + Acetate / Thiolate

All the complexes were optimized in gas phase and in aqueous phase, with inclusion of solvation effects based on the IEFPCM, as described in the methodology (part II).

The negatively charged ligands studied were the acetate and the methylthiolate. Recall that the former represents the glutamate and aspartate amino acid side chains and the deprotonated cysteine, the latter.

The acetate can bind either in a monodentate or in a bidentate mode to the metal cation, in properly oriented positions. Therefore, acetates may bound bidentately, monodentately or one monodentately and the second bidentately. Stable structures of these three isomers are shown in Fig. 6.1, labeled as **2B**, **MB** and **2M** respectively (see Fig. 6.1 for nomenclature explanation).

The main geometrical features of these complexes are plotted in Fig. 6.2 for both gas phase and aqueous phase. This data is also presented in more detail in the appendix (see Table 9.1).

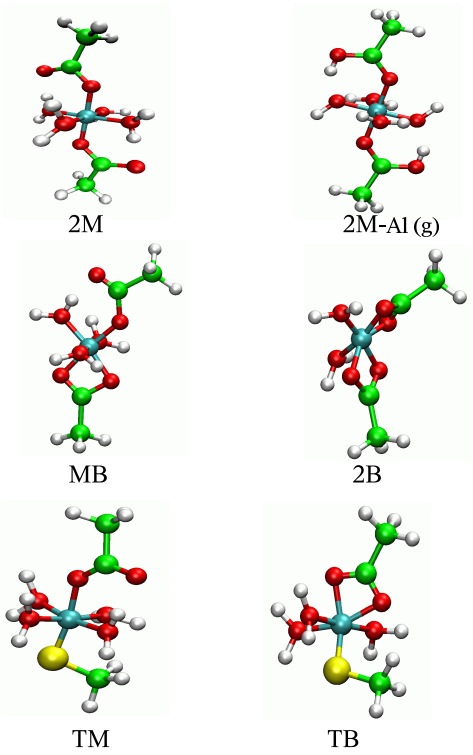

Fig. 6.1 Complexes formed between the metal cation and two negative ligands. Figures correspond to the aluminum aqueous phase geometries, where magnesium complexes are analogous either in aqueous and gas phase. Aluminum monodentate complexes in gas phase are slightly different since a proton is transfered from the water molecules to the adjacent acetate, as shown in **2M-Al(g)**, which is the analogous aluminum complex of **2M** in gas phase. **M** corresponds to a monodentate acetate, **B** is a bidentate acetate and **T** to methylthiolate.

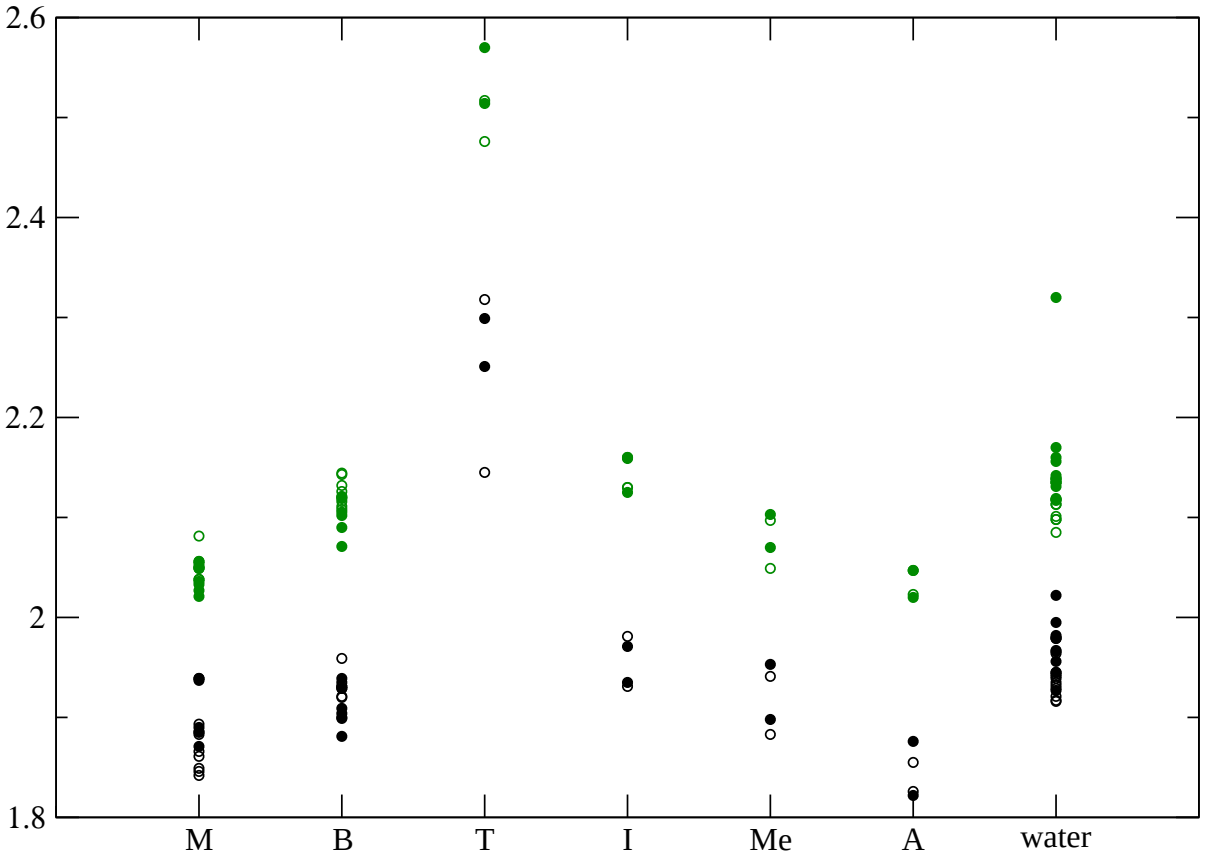

Fig. 6.2 Gas phase (filled symbols) and aqueous phase (empty symbols) metal-ligand bond lengths (in Å) of the complexes described along the text. The ligands are depicted in the X axis, green symbols stand for Mg(II) complexes and the black ones for Al(III).

Analogous Al (III) bi-acetate complexes have previously been reported in the literature, Kubicki et al. [5] studied gas phase structures at HF/3-21G** level of theory and Tunega et al. performed a gas and liquid phase study at the BLYP/SVP+sp level of theory [6]. Our data agrees well with the literature values; the global minima for the complex with two bidentate acetates corresponds to the conformation with the acetates in *ae* position, thus, in axial and equatorial position one respect to the other (2 kcal/mol energy difference in gas phase and 4 kcal/mol in solution respect the *aa* conformation, thus, axial-axial position one respect to the other). Within the **2M** structures, in gas phase, each acetate receives a proton from one water molecule. The lowest energy structure with two monodentate acetate ligands corresponds to the *aa* $Al(OH)_2(CH_3COOH_2)(H_2O)_2$, in agreement with Tunega et al. The *ea* isomer lays within 1 kcal/mol (2 kcal/mol reported by Tunega et al. [6]). We have also found a structure with only one proton transfer 2 kcal/mol higher in energy and a structure with no proton transfer, this one 7 kcal/mol higher in energy.

For magnesium, the *aa* and *ea* bidentate isomers are energetically degenerate at the level of theory described above, for the monodentate, *aa* structure is only 1 kcal/mol lower in energy than the *ea* isomer. Other structures, rotomers within 5 kcal/mol, are omitted for the sake of brevity. Finally, with respect to the **MB** structures, *aa* and *ea* isomers are nearly energetically degenerate either for aluminum and magnesium.

In aqueous phase the difference between the aluminum **2M** *aa* and *ea* structures is larger than in gas phase (around 7 kcal/mol), while for magnesium is very small. For **2B** and **MB** structures, *aa* are around 2 kcal/mol more stable than *ea*. Once solvent effects are considered, a structure with a single proton transfer is also found 8 kcal/mol higher in energy than the **2M**-*aa*.

The gas phase geometries calculated at the level of theory described above are closer to Tunega's values but still in good agreement with the structures obtained by Kubicki et al. despite of their lower level of theory (see Table 9.1 in appendix). These two authors only reported the **2B** and **2M** structures, but not **MB** (see Fig. 6.1). The aluminum-ligand (X-O_l, will hereafter correspond to the X-$O_{acetate}$ bond, while X-L_2 will be used for the non-acetate ligand) bond lengths are similar in all the complexes, slightly shorter when the acetate is bidentate (1.94 *vs.* 1.90 Å). The spontaneous proton transfer occurring from one water molecule to the free oxygen of the monodentate acetate in aluminum complexes results on an enlargement of the Al-$O_{acetate}$ bond and a shortening of the Al-O_{water} (which is now the distance between Al and $^{-}$OH) to 1.812 Å *vs.* 2.026 Å for the rest of Al-O_w. As expected, bonds in magnesium complexes are longer (around 0.2 Å) than in aluminum complexes, due to the bigger radius of the Mg (II) cation (effective ionic radius for hexacoordinated magnesium is 0.72 Å and for aluminum 0.535 Å) and the charge difference.

Mg complexes, on the other hand, present larger bidentate bonds than monodentate ones (2.10 Å vs. 2.05 Å, respectively), monodentate acetates bind more tightly to the metal.

The solvent effect is reflected in several geometrical changes. There is no proton transfer in the monodentately bound acetate aluminum structures. M-O_w bond distances are shortened with solvation, as found by Sánchez-Marcos et al. for similar systems [7], while M-O_{ac} remain similar, excepting those cases where a proton transfer occurred in gas phase (monodentate acetate aluminum complexes). This time, monodentate Al-O_l bonds are shorter than the bidentates ones (1.87 *vs.* 1.93 Å) since there are acetates instead of carboxylic acid ligands . As previously described in the literature, we have also observed that, structural changes due to the solvent effect decrease with decreasing the charge of the complexes [6].

In order to estimate the stabilities, the formation reaction 4.4 has been used, and the formation enthalpies and free energies for diacetate complexes are collected in Table 6.1 for gas and aqueous phases (the same data for the rest of the complexes described in the present manuscript are detailed in Table 9.2 of the appendix). Gas phase ΔEf^g are very large, around -550 kcal/mol for aluminum and -310 kcal/mol for magnesium. **2M** structures are favored over the **MB** and **2B** in 16, and 34 kcal/mol ΔHf^g for aluminum and 12 and 26 kcal/mol for magnesium. For ΔGf^g, these differences are smaller. This reduction is provoked by the entropic effects after two water molecules are released when an acetate binds bidentately the cation.

Tab. 6.1 Formation enthalpies and free energies (in kcal/mol) corresponding to the water/ligand exchange . ^{g} superscript stands for gas phase and ^{aq} for aqueous phase properties. Figures in *italics* have been taken from the literature.

	Al (III)				Mg (II)			
	ΔH_f^g	ΔG_f^g	ΔH_f^{aq}	ΔG_f^{aq}	ΔH_f^g	ΔG_f^g	ΔH_f^{aq}	ΔG_f^{aq}
2M	-561.9	-559.64	-19.26	-15.63	-324.43	-320.04	-14.24	-10.75
2M	*-552.5*[a]	*-551.7*[a]	*-16.3*[a]	*-14.7*[a]				
MB	-545.75	-554.62	-7.00	-15.87	-312.61	-318.88	-9.87	-16.14
2B	-527.3	-546.38	1.27	-17.79	-298.47	-316.71	-4.04	-22.28
2B	*-510.4*[a]	*-531.8*[a]	*6.8*[a]	*-11.7*[a]				

[a] taken from ref [6].

In aqueous phase, these formation energies are significantly reduced. Aluminum formation enthalpies are only favorable for **2M** and **MB**, while **2B** has a positive enthalpy (-19.26, -7.00, and 1.27 kcal/mol respectively). Analogously, for magnesium the same trend is observed, but all ΔHf^{aq} are negative, -14.24, -9.87 and -4.04 kcal/mol (see Table 6.1). The entropic effects, as noted above, alter these sequence and **2B** structure presents an smaller ΔGf^{aq} than

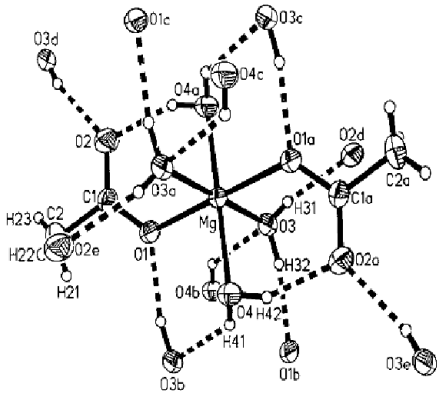

Fig. 6.3 X-ray analysis on crystalline magnesium diacetate, by D.Irish et al, in Acta Cryst. C47, 2322-2324 (see reference [8])

2M. The favorable entropic contribution of **2B** stems from the fact that the formation of two bonds by each acetate leads to the departure of a total of four water molecules instead of two as in **2M**, and therefore a much higher translation and rotational entropy of the system is obtained in the products. These entropic contributions could be however overestimated because our entropy calculation with infinitely separate molecules will lead to much higher translational and rotational contributions to the entropy than in a bulk solvent. In fact, X-ray [8] data support the idea of a monodentate complexation of the magnesium in line with the enthalpic formation energies (see Fig.6.3).

Overall, these figures are in good agreement with the values found for aluminum in the literature. Tunega et al. [6] found that the $\Delta G f^{aq}$ of **2M** is favored by 3 kcal/mol over the **2B**, while our calculations report the opposite. Nevertheless, the formation enthalpies agree reasonably well with our values, favoring both **2M** formation (see Table 6.1 for more details). It also fits well with the experimental data. X-ray analysis on crystalline magnesium acetate tetrahydrate confirms the monodentate binding of the two acetates [8], in *aa* position, and predicts a Mg-$O_{acetate}$ bond length of 2.07 Å , which is in agreement with our values.

Experimental values obtained by Palmer and Bell [9] for the diacetate complexes formation reaction give an enthalpy value of ΔH=7.2±7.2 kcal/mol and a free energy of ΔG=-6.2±0.7 kcal/mol. The larger enthalpy error gives a difference between enthalpy and free energy values ranging from -21.3 to -5.5 kcal/mol, where our formation energies for both **2B** and **MB** structures fit. Tunega et al also found the experimental values in better agreement with the formation energy values of the bidentate acetate than the monodentate ones.

Nevertheless, as remarked in the previous chapter, Palmer and Bell experiments have been questioned in literature [10].

Summarizing, in gas phase, where differences between monodentate and bidentate complexes energies are bigger than in aqueous phase, ($\Delta\Delta H$=-34.06 and $\Delta\Delta G$=-13.26 for Al and -25.96 and -3.33 for Mg, respectively), both the enthalpy and the free energy values favor the monodentate complex, for both metals. However, in aqueous phase, while the enthalpy favors monodentate complex formation, smaller (more negative) formation free energies are obtained for the bidentate complexes.

As regards to methylthiolate, it has only one binding mode, so two structures have been studied: a monodentately bound acetate and a methylthiolate and another with a bidentately bound acetate. The different orientations (*aa, ea*) were also considered; and the global minima for both types of structures was found to be the one with the ligands in *aa* position (see Fig. 6.1), the **TB** complex being 4 kcal/mol more stable than the other isomers and 1 kcal/mol the **TM**.

In gas phase complexes, X-S bond lengths are 0.3-0.4 Å larger than X-O bond, due to the larger atomic radius of the S. Al-S bond length is around 0.2 Å shorter than Mg-S. While for aluminum mono- and bidentate acetate complexes have both an Al-O_l of 1.94 Å, in the magnesium complex the monodentate Mg-O_l distance is shorter (see Fig. 6.2). As in the diacetate complexes this behavior is due to the proton transfer which changes the monodentate acetate ligand into an acetic acid, and lengthens the Al-O_l bond.

In aqueous phase, X-S bond is larger when the acetate is monodentate for both metals (2.32 Å vs 2.14 Å for aluminum), while the X-O_l bonds are shorter for the monodentate complexes (1.88 Å vs 1.96 Å for aluminum). In gas phase, X-O_l bonds are larger when acetate is bidentately bound (2.02 Å for bidentate acetate vs 1.98 Å for monodentate), while in aqueous phase a shortening of X-O_w bond is again observed and distances are almost identical (1.97 Å vs 1.96 Å).

Formation enthalpies of all the complexes are represented in Fig. 6.5 (the values are tabulated in the appendix 9.2), where energy values are represented on the *Y* axis and different ligands studied on the *X* axis (see circles for gas phase and diamonds for aqueous phase).

Comparing methylthiolate ligand complexes and acetate ligand complexes, a preference for the acetate is observed, formation energies are less negative than those found for the two acetate complexes. The $\Delta H f^{aq}$ for **TM** and **TB** are -7.66 and 1.22 kcal/mol for aluminum respectively, while these values for the **2M** and **2B** are -19.26 and 1.27 kcal/mol. This trend is repeated for magnesium as shown in Fig. 6.5.

In the previous chapter, the substitution of a water molecule by an acetate ligand was found strongly favored in the gas phase for both Al(III) and Mg (II)

coordination shells; but in aqueous phase this substitution is favored only in the Mg (II) coordination shell. The addition of one acetate for the first coordination shell of these cations yields more negative $\Delta H/Gf^g$ (up to 200 kcal/mol for aluminum complexes and 100 kcal/mol for magnesium complexes). In aqueous phase the gap is much smaller, since the stabilization due to the extra acetate ligand is not so remarked in solution but, still, two negative ligand aluminium complex formation is thermodynamically favored, and the magnesium complexes formations are favored.

Mg/Al exchange energies are presented in Fig. 6.6 (all metal exchange enthalpy energies ($\Delta H_{Mg/Al}$) and free energies ($\Delta G_{Mg/Al}$) are summarized in Table 9.3 of the appendix).

The metal exchange reaction defined previously (reaction 4.6) has the same number of reactants and products, hence, there is no added entropy that influences the free energy. The Mg (II) exchange by the Al (III) is strongly favorable in the gas phase (around 230 kcal/mol), but not in the aqueous phase; only **2M** and **TM** complex formations have negative $\Delta H_{Mg/Al}$'s (-5.02 and -2.14 kcal/mol respectively). The inclusion of an acetate in the Al (III) first coordination shell has enhanced strongly metal exchange reaction values in gas phase and in less extent in solution as is clearly seen in Fig. 6.6.

6.2.2
One Negatively Charged Ligand: Acetate + One Neutral ligand: Methanol, Methylimidazole and Acetamide

Complexes formed by Al(III) and Mg (II) cations, one acetate ligand and a neutral ligand were also studied. The neutral ligands chosen were methanol, methylimidazole and acetamide, a model for the side chains of the serine and threonine, histidine, and the backbone, asparagine and glutamine, respectively. These ligands were found to have the strongest affinity towards the aluminum and magnesium [11] cations and they are common in magnesium binding sites [12]. We have considered, as in the previous section, a monodentate or a bidentate coordination of the acetate. The located minima structures are shown in Fig. 6.4.

In both phases, methylimidazole presents the largest X-L_2 bond, and acetamide the shortest. X-L_2 bonds are slightly longer when the acetate is bound monodentately. X-L_2 obtained for the magnesium and methylimidazole complex agrees with that found by Deerfield et al, at the HF/6-31++G** level of theory (2.16 Å *vs.* 2.17 Å for the IM complex and 2.13 Å *vs.* 2.13 Å for BM). It is noted that, as reported by Mayaan et al [13], the X-O_w bond is elongated with the negatively charged ligand number. The geometries are very similar in both phases (see Fig. 6.2 and X-O_l, X-L_2 and X-O_w bond lengths shown in Table 9.1 for more details).

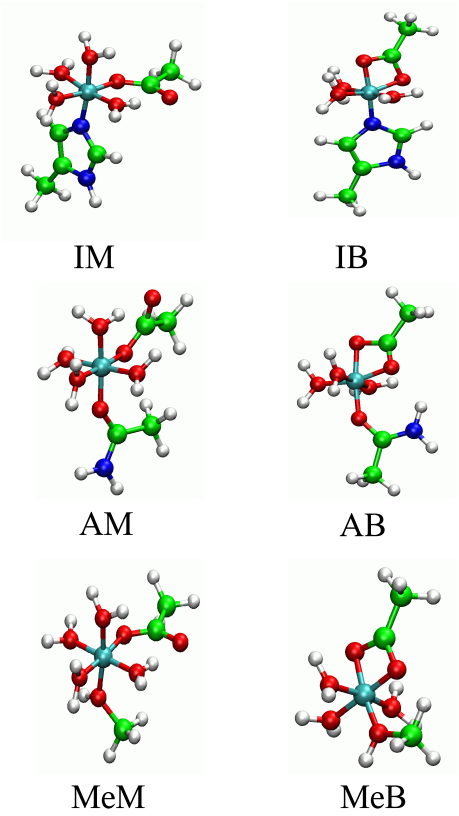

Fig. 6.4 Complexes formed between the metal cation an acetate and an neutral ligand. Figures correspond to the aluminum aqueous phase geometries, where Magnesium complexes are analogous either in aqueous and gas phase. Aluminum monodentate complexes in gas phase are slightly different since a proton is transfered from a water molecule to the adjacent acetate. The nomenclature is analogous to Fig. 6.1, and **Me** stands for methanol, **A** for acetamide and **I** for the methylated imidazole.

The global minima found for the bidentate acetate complexes are similar for all the complexes. Bidentate acetate and the second ligand are in the same plane, although in the case of methylimidazole the neutral ligand forms a 26^o dihedral angle with the bidentate acetate. The minimum for the monodentate acetate complexes is found to be the equatorial-axial conformation (see Fig. 6.4).

Formation enthalpies of these complexes are collected in Fig. 6.5. (Gas and aqueous phase formation enthalpies and free energies are reported in the appendix Table 9.2). Formation energy values are not as favorable as those for two negative ligand complexes, in agreement with Mayaan et al [13], since the metal-neutral ligand interaction results in a smaller energy gain than the

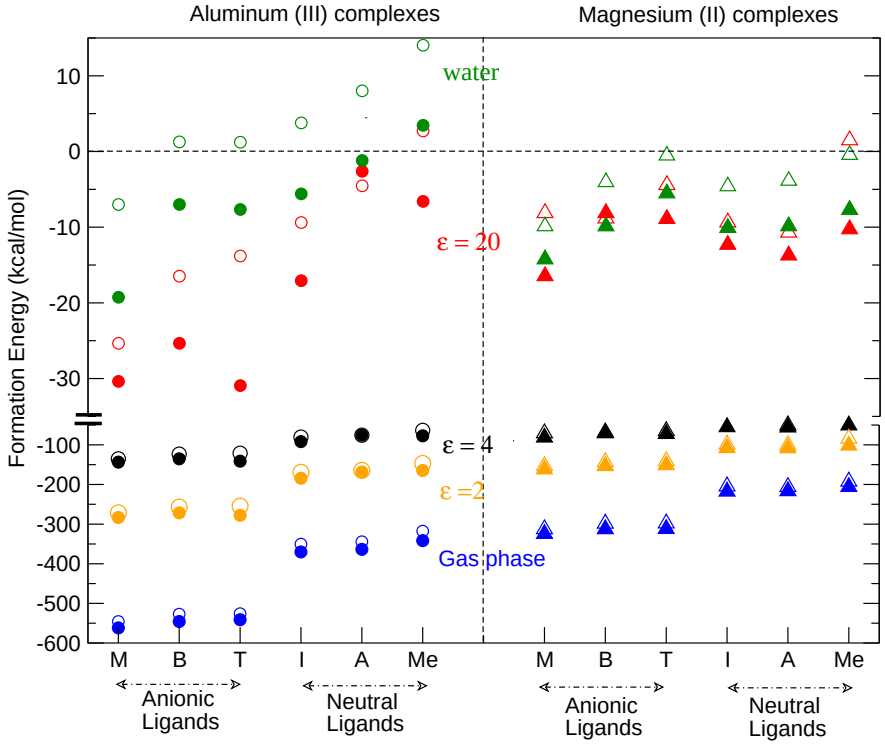

Fig. 6.5 Formation enthalpies of the complexes at the different dielectric values. The triangles represent the magnesium complexes and the circles the aluminum. Filled symbols stand for the complexes containing a monodentate acetate complexes and empty symbols for the bidentate acetate complexes. The second ligand is denoted by the X-axis. Note that the energy scale changes at -40 kcal/mol.

metal-negative ligand interaction. Methylimidazole is the preferred neutral ligand to substitute a water molecule in the present environment either for Al (III) (as it was in the previous chapter) and magnesium (in agreement with Deerfield et al. [11]) and the less favored the methanol as observed in Fig. 6.5.

In gas phase, aluminum complex formation is favored over magnesium; ΔH_f^g are around -350 kcal/mol for aluminum complexes and -210 kcal/mol for magnesium as it is clearly depicted in Fig. 6.5. However, in aqueous phase magnesium complex formations are favored, with formation energies more negative than for aluminum. Indeed, only the methylimidazole and for-

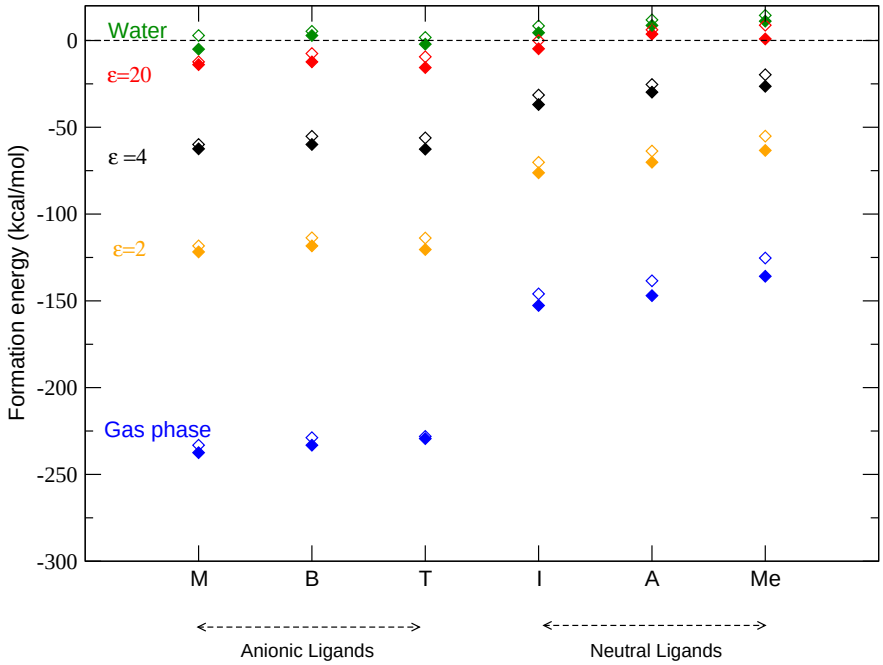

Fig. 6.6 Metal exchange reaction enthalpies of the complexes. Filled symbols stand for the complexes containing a monodentate acetate complexes and empty symbols for the bidentate acetate complexes. The second ligand is denoted by the X-axis. Note that the energy scale changes at -40 kcal/mol.

mamide monodentate acetate complexes show a negative formation enthalpy for aluminum while all magnesium ΔH_f^{aq} are negative.

Comparing mono/bi-dentate acetate binding modes, ΔH_f favors monodentate complex formation, as in the previous section.

The metal exchange is favored in gas phase, around -140 kcal/mol, (see Fig. 6.6), the most favored being when the methylimidazole is present.

In aqueous phase, free energies (around 10 kcal/mol) have positive values and suggest that an exchange of Mg (II) for Al (III) would not be favorable in aqueous media (all the values plotted in Fig. 6.6 are available in the appendix).

As concluded previously, the substitution of a water molecule by any of the studied neutral ligands was favorable in gas phase, and only the substitution of water by methylimidazole for Mg (II) in aqueous phase . When an acetate is already present in the first coordination shell the substitution of a water molecule in aqueous phase is now favorable for all the studied ligands with Mg (II) and for acetamide and methylimidazole with Al (III).

6.2.3 Dielectric Effects

The formation reaction (see Fig. 6.5 and Table 9.4 in the appendix) enthalpies and free energies are all favorable in dielectrics 2, 4 and 20, except for the **AB** formation in dielectric constant 20 for both metals (2.71 kcal/mol for Al and 1.49 for Mg). Ligand preference is maintained in all dielectrics.

The exchange reaction energies (collected in Fig. 6.6 and detailed in the appendix, Table 9.5), for all the complexes formed by two negative ligands, are negative and the metal exchange is probable to occur. On the other hand, in the presence of just one negative ligand, the exchange would occur only in the lowest dielectric values (2 and 4). In dielectric 20, excepting the complex formed by a methylimidazole and a monodentate acetate, the exchange energies are all positive (between 9 and 1.2 kcal/mol) or thermo-neutral (between -0.03, 0.87 kcal/mol).

Therefore, we can conclude that in a protein buried environment the formation of all the complexes is favorable in general, and that Al (III) may replace Mg(II) in the modeled binding sites, when the dielectric is around 2 and 4 which is the typical range in protein buried sites [14–18].

6.3 Conclusions

Formation enthalpies and free energies are very favorable in gas phase for all the complexes. Negative ligands give more favorable formation energies, specially acetate, the preferred binding mode being monodentate. This last conclusion may have its uncertainties due to the possible entropic effects which might be overestimated on our formation reaction model. Among the neutral ligands, methylimidazole is the one which presents the strongest affinity towards both cations. The metal-negative ligand interaction is much stronger than metal-neutral ligand interaction, thus the energy gained when displace a water molecule is higher. In solution, these energies are much smaller, and for some of the Al(III) complexes, even unfavorable. The aqueous environment stabilizes the hydrated cation, and therefore the displacement of a water molecule demands a higher energy than in gas phase. However, the solvation

does not change the relative stability of the complexes, the preferred coordination pattern is the same as in gas phase. We previously observed that the formation of Al(III) and one ligand complexes was unlikely to occur. Only acetate, acetamide and methylimidazole complex formation were favorable at low dielectric values (ε=2). We conclude now that with one acetate present in the coordination shell of the Al(III) the complexation to other ligands is highly enhanced. For instance, acetamide and imidazole present negative formation enthalpies at ε=78, and when the dielectric is decreased to ε=20 all complexes show negative formation enthalpies. Therefore, our data is very suggestive that at least one acetate ligand should be present in the Al(III) protein interaction sites. The affinity gained by Al(III) with the presence of the acetate in the binding site is much larger than that gained by Mg(II), since the metal-negative ligand interaction is much larger for aluminum due to its higher positive charge.

The Mg/Al metal exchange was also found difficult to occur when considering one single ligand in the binding site (see previous chapter), although we can not rule out this possibility at small ε values. When an acetate is present, the exchange probability is larger. All the complexes have negative exchange energies at ε=4, and besides the two negative ligand complexes, IM and 2B show favored metal exchange values at ε=20. Thus, the presence of two acetates in the coordination shell enhances the Mg/Al exchange. A combination of an acetate with an imidazole, also fulfills the thermodynamic properties of an Mg/Al exchange to occur.

We have characterized a wide range of likely binding sites with enhanced affinity towards aluminum as compared to magnesium for protein sites having at least one acetate ligand and one more non-aqueous ligand.

This pinpoints to the possibility of thermodynamically favored Mg/Al exchange reactions to occur at this metal binding sites.

References

1 E. San Sebastian, J. M. Mercero, R. H. Stote, A. Dejaegere, F. P. Cossío, X. Lopez, J. Am. Chem. Soc. 128 (2006) 3554–3563.

2 T. Dudev, C. Lim, Chem. Rev. 103 (2003) 773.

3 T.Dudev, C. Lim, Chem. Rev. 103 (2003) 773–787.

4 J. M. Mercero, J. I. Mujika, J. M. Matxain, X. Lopez, J. M. Ugalde, Chem. Phys. 295 (2003) 175.

5 J. Kubicki, G. Blake, S. Apitz, Geochimica et Cosmochimica acta 60 (1996) 4897–4911.

6 D. Tunega, Haberhauer, M. Gerzabek, H. Lischka, J. Phys. Chem A 104 (2000) 6824–6833.

7 E. Sánchez-Marcos, R. R. Pappalardo, J. Martinez, B. Mennucci, J. Tomasi, J. Phys. Chem. B 106 (2002) 1118–1123.

8 D. Irish, J. Semmler, N. Taylor, G. Toogood, Acta Cryst. C47 (1991) 2322–2324.

9 D. A. Palmer, J. L. S. Bell, Geochim. Cosmochim. Acta 58 (1994) 651.

10 L. Öhman, Geochim. Cosmochim. Acta 59 (1995) 4775.

11 D. W. Deerfield, D. J. Fox, M. Head Gordon, R. G. Hiskey, L. G. Pedersen, Proteins Structure Function and Genetics 21 (1995) 244–255.

12 T. Dudev, Y. Lin, M. Dudev, C. Lim, J. Am. Chem. Soc. 125 (2003) 3168–3180.

13 E.Mayaan, K. Range, D. York, J. Biol. Inorg. Chem. 9 (2004) 807–817.

14 L. Rulised, Z. Havlas, J. Am. Chem. Soc.

15 T. Dudev, C. Lim, J. Phys. Chem. B 108 (2004) 4546–4557.

16 T. Simonson, J. Am. Chem. Soc. 20 (1998) 4875–4876.

17 T. Simonson, C. L. Brooks, J. Am. Chem. Soc. 118 (1995) 8452–8458.

18 T. Simonson, D. Perahia, Proc. Natl. Acad. Sci. U.S.A. 4 (1992) 1082–1086.

7
Metal binding sites with three ligands

7.1
Introduction

We have now included a third ligand in the binding site. In the present chapter we report on the affinity of Al(III) and Mg(II) for these binding sites (most frequent binding sites for Mg(II) [1]), focusing on the evaluation of the structural and energetical parameters of their binding to the proteins. The role of the carboxylate binding mode and the neutral ligands will be carefully analyzed.

Five different ligands, which have shown the highest affinity for both Mg(II) and Al(III) in previous chapters have been considered: negatively charged acetate (to simulate Aspartate and Glutamate) and methylthiolate (for deprotonated Cysteine), and the neutral methylimidazole (for Hystidine), acetamide (for Asparagine, Glutamine and the backbone carbonyl groups) and methanol (for Serine and Threonine). PDB surveys found in literature [1] and the results obtained in previous chapters reveal the low probability of finding binding sites not containing at least one acetate, and highlight the abundance of three ligand containing Mg(II) binding sites in nature. Hence, in the present work, we will always include at least one acetate in the binding site, bound either in a monodentate or a bidentate way. Different combinations of the remaining two ligands will be studied, forming binding sites with charge -3, -2 and -1.

7.2
Results

Due to the big number of the structures and in order to present the data in a clear and comprehensible way, in this chapter the results have been divided in three sections: evaluation of structural parameters, the metal binding affinity, and the metal exchange reaction. In each section, all the complexes characterized will be discussed at the same time.

7.2.1 Evaluation of the structural parameters

Several isomers were studied for each combination of ligands, and the most stable conformations are shown in Fig. 7.1. Overall, very similar structures were obtained for both metals.

Binding sites with charge -3 can be formed by either three acetates, two acetates and one methylthiolate or one acetate and two methylthiolates. Both monodentate and bidentate ways of binding were considered for the acetate.

Thus, we have four different ligand combinations when considering three acetates in the binding site (3B, M-2B, 2M-B and 3M, see Fig. 7.1 for the complex labeling). Several isomers were found for each of them, up to 16 kcal/mol less stable than the absolute minimum in the case of Al(III) and 9 kcal/mol for Mg(II). The highest stability was achieved by interaction of the free oxygen of the monodentate acetate with one hydrogen of the water molecule bound to the metal (for example, see 3M in Fig. 7.1). This motif is very commonly found in metalloprotein crystal structures [2].

Only two complexes formed by two acetates and one methylthiolate were found (2M-T and MB-T). As a consequence of the steric hindrance arising from S atom's big size, it was not possible to characterize any complex with two bidentate acetates and one methylthiolate, for any of the studied metals. For the same reason, the binding site presenting one monodentate acetate, a bidentate acetate and a methylthiolate ligand did not form any kind of stable hexacoordinated structure with the Mg(II). Al(III) can accommodate the bidentate acetate and the sulfur atom in the first hydration shell, and due to its higher charge as compared to Mg(II) presents a higher affinity for the binding site with charge -3. Therefore, several MB-T structures were found for Al(III), falling in a range of 13 kcal/mol. The most stable isomer for 2M-T complex presents both acetates in axial-axial orientation with respect to each other; other orientations presented 14 kcal/mol less stable formation energies for Al(III) and 6 kcal/mol for Mg(II).

Complexes consisting of two methylthiolates and one acetate showed a smaller range of energies, (2 kcal/mol for Al(III) and 1.8 kcal/mol for Mg(II), and in both cases the preferred orientation of the ligands was equatorial-axial one respect to the other (M-2T and B-2T).

Nine different complexes were optimized for dianionic cavities (binding sites with one neutral ligand and two acetates). The absolute minima found for each coordination fashion of the acetate (2B-L, 2M-L and MB-L) was very similar for the three neutral ligands studied, as can be seen in Fig. 7.1. Equatorial-axial arrangement is favoured in 2M-L and MB-L complexes, instead, in 2B-L structures, the neutral ligand is preferred to be in axial orientation as respect to the acetate.

Finally, when two neutral ligands are found in the binding site, monoanionic cavities are formed. The most stable conformation presents both neutral ligands in axial-axial position one respect to another, when the acetate is monodentate, and all the ligands in axial-equatorial position when is bidentate. The isomers found fall in a range of 1.4 kcal/mol for Al(III) and 3.2 kcal/mol for Mg(II).

Related to the metal-ligand bond lengths, overall, three tendencies are observed in all the complexes, regardless the ligands considered: First, Mg(II)-ligand bond lengths are around 0.2 Å larger than the Al(III)-ligand ones (see Fig. 7.2), due to the weaker electrostatic interaction between the lower-charged Mg(II) and the ligands as compared with the Al(III), and also to the larger ionic radius of the former (0.72 Å vs. 0.54 Å). Second, no remarkable variation was seen between gas phase and solution bond distances [3]. Anyway, a subtle difference is noted, which increases when increasing the charge of the complex, namely, that bonds in solution are equal or slightly larger for negative ligands but not for the neutral ligands, in this case, bong lengths decrease in solution as compared to gas phase. And last, all bond lengths become smaller as the charge of the cavity increases, even this variation is very subtle.

Concerning the acetates, bidentate acetate presents a metal-$O_{acetate}$ bond larger than the monodentate acetates, for both metals (2.14 Å vs 2.06 Å for Mg(II) and 1.95 Å vs 1.88 Å for Al(III)) (see Fig. 7.2). This feature is widely known, and was also reported in previous chapters. When the acetate binds monodentately, more charge is transferred to the metal along the bond, and the metal-oxygen distance becomes shorter. An exception: binding sites containing neutral ligands, thus, dianionic and monoanionic cavities, presented in gas phase spontaneous proton transfers from a water molecule of the hydration shell to the free oxygen of the monodentate acetates, when bound to Al(III). This feature has also been observed in previously (see chapters 5 and 6), as a consequence of the strong acidity of the water molecules, caused by the high charge in Al(III). The proton transfer elongates the Al-$O_{acetate}$ distance, and the difference with the Al-$O_{acetate}$ distance in bidentate acetates is reduced to about 0.02 Å (see Table 10 in the appendix). The larger charge transfer to Al(III) in binding sites with charge -3 prevents this proton transfer to occur [2].

Tunega et al. [3] studied Al-acetate complexes, and reported one structure with three bidentate acetates. The Al-$O_{acetate}$ distances they reported were slightly longer than ours, 1.966 Å vs. 1.940 Å in gas phase and 1.958 Å vs. 1.937 Å in aqueous phase, but are in general in good agreement considering the different computational level used.

The other negatively charged ligand considered, methylthiolate, presents bond lengths 0.5 Å larger than the rest of the ligands, due to the larger radius of the S atom as compared to the others. The lower affinity of Mg(II)

for methylthiolate ligand, as compared to Al(III) can also be seen in the long bonds formed by Mg(II) in the structures containing methylthiolates, where in some cases the ligands are almost taken away from the first hydration shell (see Fig. 7.2).

The neutral ligands presented little geometrical variation in the different ligand combinations considered, as can be seen in Fig. 7.2. Al(III) presented bond lengths of 1.98 Å , 1.96 Å and 1.87 Å for methylimidazole, methanol and formamide, respectively, and in Mg(II) complexes the distances were 2.18 Å , 2.13 Å and 2.09 Å, in the same order.

Metal-O_{water} distances, in gas phase, fall in a range of 2.03-2.01 Å for Al(III) in gas phase and 2.23-2.14 Å for Mg(II). The largest bonds are found for binding sites with charge -3, and the shortest in monoanionic cavities. When proton transfer occurs the bond is shortened around 0.2 Å, since the metal is now bound to a hydroxile instead of a water molecule (see Table 10 in the appendix). In solution, the bond lengths decrease about 0.06 Å for Al(III) and 0.03 Å for Mg(II), as compared to gas phase.

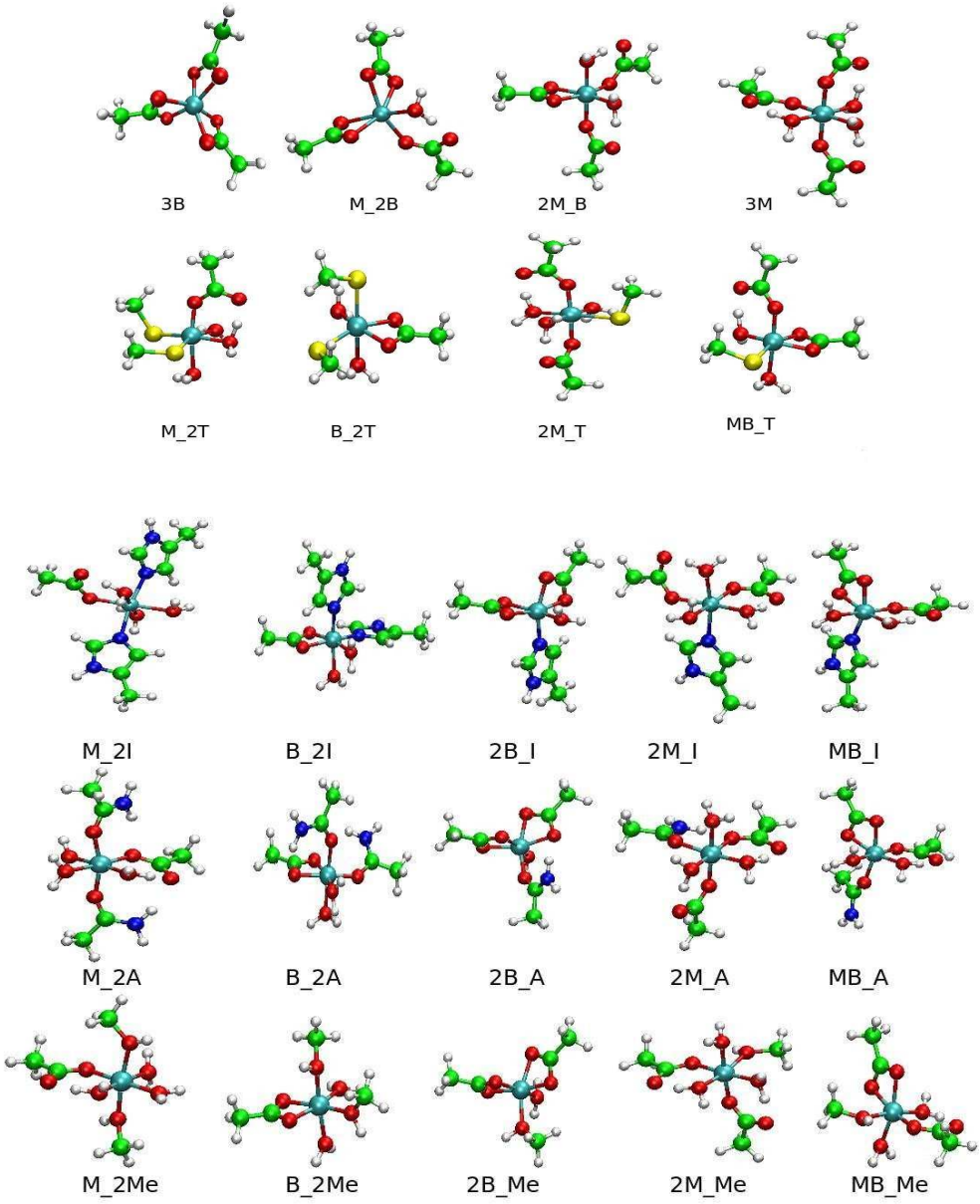

Fig. 7.1 Complexes studied. Figures correspond to the aluminum aqueous phase geometries, where magnesium complexes are analogous either in aqueous and gas phase. **M** corresponds to a monodentate acetate, **B** is a bidentate acetate, **T** stands for the methylthiolate, **I** for the methylated imidazole, **A** for the acetamide and **Me** for the methanol.

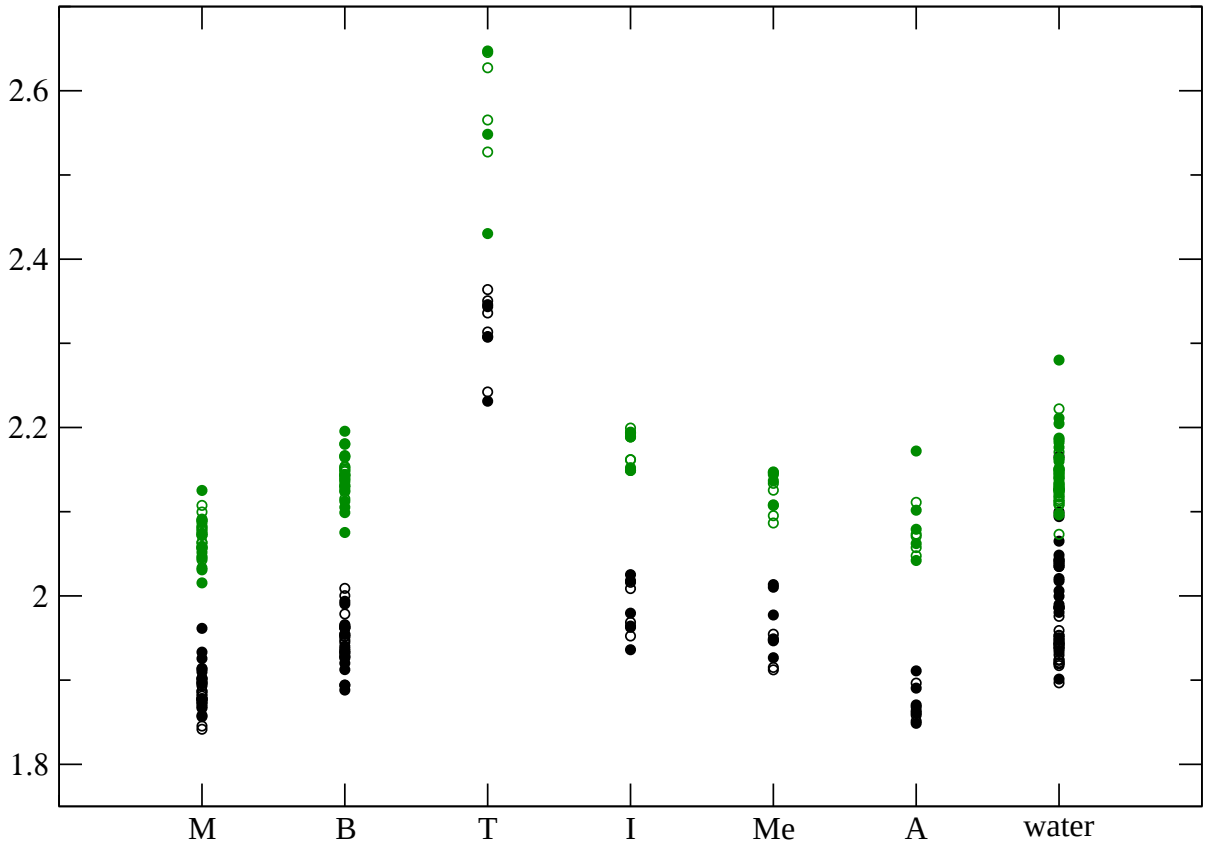

Fig. 7.2 Gas phase (filled symbols) and aqueous phase (empty symbols) metal-ligand bond lengths (in Å) of the complexes described along the text. The ligands are depicted in the X axis, red symbols stand for Mg(II) complexes and the black ones for Al(III).

7.2.2
Metal binding affinity

The formation (see formation reaction 4.4) enthalpies obtained for each ligand combination and protein environment are depicted in Fig. 7.3. This data, together with the free energies, is available in the appendix, Table 10.1.

Overall, both metals are very prone to binding the active site composed by three ligands, in all the range of dielectrics inside the protein.

The intrinsic propensity of the thermodynamic reaction (blue symbols), is very favourable. The affinity goes up to -670 kcal/mol for Al(III) and -360 kcal/mol for Mg(II). In this case the reaction is driven primarily by favorable charge-charge interactions between the positively charged metal complex and the negatively charged active site.

The charge of the active site (-3, -2 or -1) regulates this affinity, which increases with the charge (in absolute value). This is particularly remarkable in the case of Al(III), as the formation enthalpies obtained are -700 kcal/mol, -570 kcal/mol and -400 kcal/mol, respectively. Mg(II), on the other hand, has similar affinity for -3 and -2 charged ligand combinations (-380 kcal/mol and -350 kcal/mol, respectively). The interaction with the three negatively charged ligands is still more favourable than with two negatively charged ligands, but, the energy gain is smaller, since, each metal-ligand bond is weaker in the former, due to the strong charge transfer to Mg(II). The affinity for -1 charged ligand combinations falls around -230 kcal/mol.

These differences are smothered when environmental effects are included. It was already seen in previous chapters and in literature [4], that increasing the solvent exposure of the metal binding site attenuates the energy gain of the water/ligand exchange because the desolvation penalty of the charged reactants exceeds the solvation free energy gains of the less charged products. Consequently, the reaction energy decreases in absolute value as the more solvent accessible is the area studied.

The lower the net charge in the binding site, the desolvation penalty will be less important, since the charge difference between reactants and products is smaller in this case. In resume, we have two opposed driving forces. On one side, the favourable electrostatic interactions between positively charged metal and the binding site favours the most negatively charged ligand combinations. Instead, they are the most affected by the desolvation penalty. Due to the balance between these two forces, the affinity difference arising from the binding site charge is less pronounced as the solvent exposure increases. Thus, even in gas phase the presence of three negatively charged ligands highly enhances the metal/ligand exchange, in the most solvent exposed areas of the protein, the affinity is similar regardless the ligand combination.

Although charge is the dominant factor, the nature of the ligands chosen also affects the formation energy of the complexes. Among all the ligands

studied, the acetate is the only one which has two binding atoms, thus, it can bind the metal cation via one of the carboxylate oxygen atoms (monodentate mode) or both oxygen atoms (bidentate mode). The mode of carboxylate binding is known to play an important role in recognition of the native metal cofactor and thus, the function of metalloproteins [5].

In gas phase, both metals present the same affinity order for the three acetate complexes. The results show a preference of the metals for monodentate acetates, where the free oxygen of the monodentate acetate is stabilized by the interactions with the water molecules of the first shell [5]. The most favorable formation is that corresponding to the 3M complex, followed by 2MB, M2B and 3B. The energy gap between complexes is around 10 kcal/mol for both metals, except the 3B complex for Mg(II), which is 30 kcal/mol less stable than the M2B one.

The charge of the magnesium ion is remarkably reduced by the attachment of three acetates, two of them being bidentate, and thus, binding the remaining free oxygen destabilizes further the complex. This does not happen with Al(III) since it can accept more charge than Mg(II), and the gap between 3B and M2B complexes remains similar in this case. The difference between the complexes decreases as we increase the solvent exposure. The preference of monodentate acetates over bidentates is also seen in dianionic and monoanionic cavities.

In general, when a methylthiolate ligand is included in the binding site, the behaviour is similar to the rest of -3 charge binding sites, even though the formation energies are not so favoured as for three acetate binding sites. The larger size of the S atom results in steric constrains that elongate the bonds, making the interactions weaker. This is reflected specially in Mg(II) complexes, due to the metals low charge and bigger size, where in the most solvent accessible areas of the protein the formation energies are lower than for any other complexes, and the bond lengths increase. This agrees with the fact that in nature, sulfur atoms are seldom found in Mg(II) binding sites.

Between the neutral ligands, as expected, the preferred ligand is methylimidazole, and the less favoured one is the methanol. The latter presented specially low affinity in monoanionic cavities, and in the most solvent exposed areas of the protein (ε=20, 78), its formation was thermoneutral or even unfavourable for Al(III) complexes.

7.2.3 Metal exchange reaction

The energy balance of the exchange reaction (see reaction 4.6), the exchange energy, will indicate the likehood for the hydrated Al(III) to substitute a Mg(II) already attached to a binding site in a protein.

In this case we did not consider the methylthiolate ligands, since they are very rarely found in natural Mg(II) binding sites, along with the difficulties experimented when characterizing Mg(II) complexes with methylthiolate ligands (see previous section).

The exchange enthalpies obtained are depicted in Fig. 7.4, and all the data is presented in detail in Table 10.2 of the appendix.

In general, the exchange reaction is energetically very probable to occur. In gas phase, it can be as favourable as -340 kcal/mol, for the binding sites with three negatively charged ligands. Again, the charge of the cavity plays a major role in the thermodynamics of the reaction. The charge difference between both metals makes the exchange much more favourable the more negative is the active site of the protein.

As solvation effects are included, the desolvation penalty for Al(III) complexes is higher than for Mg(II) ones, because the charge difference between reactants and products is more remarked for the former. So, as the dielectric constant value of the site increases, the capacity of aluminium to substitute magnesium decreases, and at some extent, becomes unfavourable. If we have a monoanionic cavity (filled symbols), in relatively solvent-exposed area the exchange will not be favorable. Dianionic cavities also disfavour the exchange in totally solvent exposed area (green symbols) when two bidentate acetates are present in the complex, for acetamide and methanol.

In gas phase, the exchange energy in triply charged binding sites is also most favoured when three bidentate acetates are considered. Charge transfer is highest in these conformation, what favours the attachment of trivalent cations [6]. In the most solvent exposed areas, the preferred conformation for exchange is 3M because of the environmental effect.

When one methylimidazole is present in our active site, the most likely conformation to undergo metal exchange is when one of the acetates is monodentate and the other bidentate. In the rest of structures containing one or two neutral ligands, the exchange is most favoured when the acetates are monodentately bound.

7.3 Conclusions

Previous extensive surveys of the protein data bank have concluded that most common natural occurring Mg(II) protein binding sites are formed by three ligands, at least one of them being an acetate [1]. Consequently, in this chapter we have studied the affinity of both metals, Mg(II) and Al(III), for these active sites and also their selectivity towards the metal. The negative charge of the cavity has been varied by adding negatively charged ligands, since it has been seen that in biological systems the net charge of the binding pocket

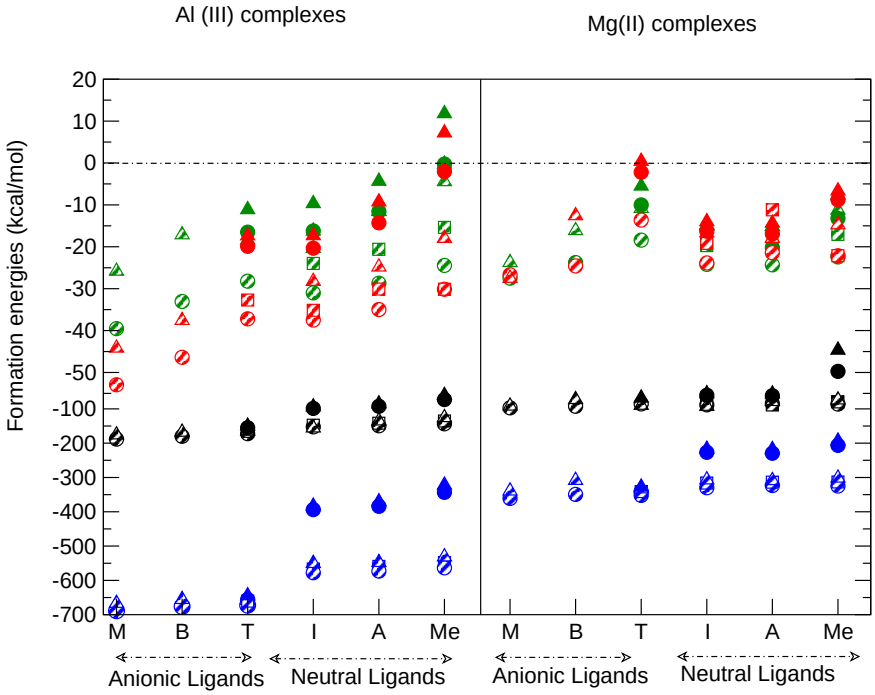

Fig. 7.3 Formation reaction enthalpies of the complexes, in kcal/mol. Filled symbols stand for the complexes containing one acetate plus two ligands defined in the X-axis. Stripped symbols stand for complexes formed by two acetates plus one ligand defined in the X-axis. Triangles stand for bidentate acetates, and circles monodentate acetates. The square stripped symbols denote structures with one monodentate and one bidentate acetates. Note that the energy scale changes at -50 kcal/mol. Blue symbols stand for the gas phase data, black ones for the ε=4, the red for ε=20 and the green ones for aqueous phase enthalpies.

contributes to the selective binding of higher charged metals against much higher concentration of less charged metals [7].

Both metals present favourable binding affinities, regardless of the ligand combination, in all the protein environments studied. As an exception, monoanionic cavities containing two methanol ligands gave unfavourable binding energies towards Al(III) in the most solvent exposed areas of the pro-

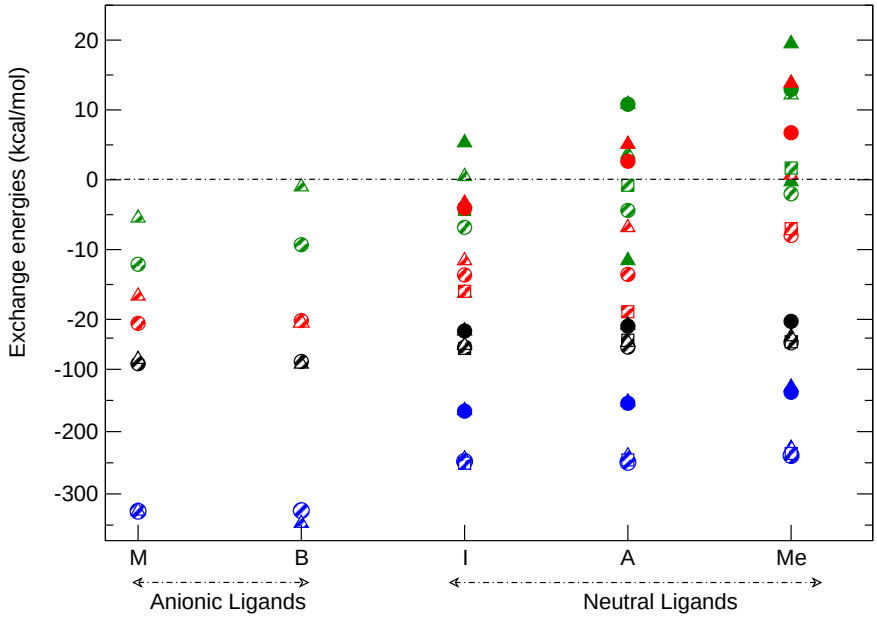

Fig. 7.4 Exchange reaction enthalpies of the complexes, in kcal/mol.Filled symbols stand for the complexes containing one acetate plus two ligands defined in the X-axis. Stripped symbols stand for complexes formed by two acetates plus one ligand defined in the X-axis. Triangles stand for bidentate acetates, and circles monodentate acetates. The square stripped symbols denote structures with one monodentate and one bidentate acetates. Note that the energy scale changes at -20 kcal/mol. Blue symbols stand for the gas phase data, black ones for the ε=4, the red for ε=20 and the green ones for aqueous phase enthalpies.

teins, due to the high polarizability of the site and the low affinity for methanol ligands.

Carboxylate has been seen to be the preferred negatively charged ligand, and the highest affinity is achieved in binding sites containing three acetates (net charge -3), specially Al(III), which is obviously a better charge acceptor than Mg(II).

Preference for monodentate binding mode has been detected, in accordance with the literature, where it has been found that from all the Mg(II) binding sites with first shell acetate ligands, only one Mg(II) active site was found to contain bidentately bound carboxylates [8, 9]. Additionally, the presence of a monodentate acetate in the binding helps the Mg/Al substitution. The more acetates in the binding site, the more likely the exchange to occur, since Al(III) can accept more carboxylates in its first coordination shell [5].

As compared to previous ligand combinations (see chapter 4), the addition of a neutral ligand in an monoanionic or dianionic cavity (consisting of one acetate and one neutral ligand or two acetates, respectively) promotes the affinity of both metals, becoming favourable to bind even in the most solvent exposed areas. This addition also favors the substitution in dianionic cavities, which was unfavourable in the most solvent exposed areas of the protein, when consisting of only two acetates. Nevertheless, the Mg/Al exchange possibility remains unfavourable in the most solvent exposed areas for monoanionic cavities.

Finally, the shorter bond lengths of Al(III) as compared to Mg(II) have been confirmed for all the complexes, due to the higher charge and smaller size of Al(III). This may be the cause of the low exchange rate of ligands in sites served by Al(III), due to its enhance rigidity. The latter is claimed to be the reason for the blockage of Al(III) bound proteins [10].

References

1 T. Dudev, J. A. Cowan, C. Lim, J. Am. Chem. Soc. 121 (1999) 7665.

2 A. Katz, J. Glusker, G. Markham, C. Bock, J. Phys Chem B 102 (1998) 6342–6350.

3 D. Tunega, Haberhauer, M. Gerzabek, H. Lischka, J. Phys. Chem A 104 (2000) 6824–6833.

4 T. Dudev, C. Lim, J. Am. Chem. Soc. 128 (2006) 1553–1561.

5 T. Dudev, C. Lim, J. Am. Chem. Soc. 128 (2006) 10541–10548.

6 T. Dudev, L. Chang, C. Lim, J. Am. Chem. Soc. 127 (2005) 4091–4103.

7 J. Falke, S. Drake, A. Hazard, O. Peersen, Q. Rev. Biophys. 27 (1994) 219–290.

8 T. Dudev, C. Lim, J. Phys. Chem. B 108 (2004) 4546–4557.

9 T. Dudev, C. Lim, Acc. Chem. Res. 40 (2007) 85–93.

10 T. Gerczei, Z. Bocskei, E. Szabo, B. Asboth, G. Naray-Szabo, Int. J. Biol. Macro. 25 (1999) 329.

8
Further insight on Mg(II)/Al(III) exchange in natural Mg(II) protein binding sites

8.1
Introduction

This chapter focuses on the Mg(II) exchange by Al(III) in its natural binding sites. The discussion will be based on the data obtained in previous chapters, along with a careful consideration of the characteristics that magnesium usually presents in natural binding sites.

Previous extensive surveys [1] of the Protein Data Bank (PDB) for the ligands present in Mg(II) binding sites have concluded the following:

1. Mg(II) is always partially hydrated in the binding site.
2. The negatively charged amino acid side chains found are Aspartate and Glutamate (43 %)
3. The non-charged Serine and Threonine (3.9 %), Asparagine and Glutamine (2.8 %), Hystidine (2.8 %) and Tyrosine (0.6 %) amino acid side chains are also found.
4. Backbone carbonyl groups are found in the 10.1 % of the binding sites.
5. No sulfur containing amino acid side chains have been characterized so far.

In previous chapters we have established that, despite the high affinity of the metals for the negatively charged methylthiolate, the nature of the complexes encountered suggests the low probability of finding a sulfur atom in the first hydration shell of the metals, specially for magnesium. Therefore, in accordance with the results of the PDB survey, combinations containing a methylthiol were not pursued further.

The presence of one negatively charged carboxylate is ubiquitous in Mg(II) for naturally occurring PDB protein binding sites [2]. Also binding sites consisting of three carboxylates or two carboxylates and one neutral ligand, are very common combinations found [2] in Mg(II) binding sites.

These characteristics are in accordance with our results in previous chapter. Therefore, in this chapter we will consider the binding sites containing one ligand, one acetate plus a second ligand, and two acetates plus a third ligand.

The free energy of the exchange reaction (see reaction 4.6) will shed light on the required energetics for the substitution of Mg(II) by Al(III) to take place.

Both Mg(II) and Al(III) will be considered to have the same binding site, as a first approach on the possibility for Mg/Al exchange. Subsequent alterations in the first binding shell can be originated by Al, which are beyond the scope of this work as are specific for each protein. Moreover, it has been experimentally determined that there are some cases where the binding site does not undergo further alteration after Mg/Al substitution, being this enough to block the protein [3].

Besides, the affinity of a metal for a binding site depends on the solvent accessibility of the site within the whole protein. Metal ions bind usually in sites surrounded by non-polar hydrophobic groups, that is, regions of low dielectric constants. In other words, as inferred from available X-ray structures, metal binding sites are usually buried [4–8].

The metal exchange can take place in two different ways. Firstly, one can imagine that the incoming metal arrives at the protein site hydrated, and then the exchange occurs in the environment set up by the protein cavity [9]. This might happen in cation channels and transporters [10], where there is sound evidence that metals, and in particular magnesium [11], retain a degree of hydration upon entering the ion conduction pore of the protein. Conversely, for other binding sites the exchange mechanism considers the metal arriving directly from solution and the replaced one going to solution (thus the dielectric constant for the hydrated cations will always be that of water).

Simulation of the former type of metal exchange will be carried our by imposing the same dielectric constant to all the four terms of reaction. Simulation of the latter metal exchange process will be carried out by imposing ε=78 to both hydrated cations and a different ε to simulate the environment of the binding site for the ligand surrounded species [12].

Although the selection of the dielectric constant values for modeling protein environments is arbitrary, based on earlier sections (see previous chapters), we have chosen ε=4 for a buried protein environment and ε=20 for a partially buried protein environment. Naturally, ε=78 stands for the fully solvent accessible environment.

8.2 Results

The calculated free energies, in kcal/mol, for the Mg(II)/Al(III) exchange reaction within the protein cavity are shown in Fig. 8.1. Concomitantly, Fig. 8.2,

shows the free energies for the exchange reaction when metals are taken up from the aqueous environment.

Symbols on the abscissa stand for the ligands of the considered binding sites. Thus, M, B, I, A, and Me stand for monodentate acetate, bidentate acetate, methylimidazole, acetamide and methanol, respectively.

The hollow symbols correspond to the single ligand complexes, and the filled symbols to the two ligand complexes, where one ligand always corresponds to a monodentate acetate, and the second is denoted on the x-axis. Finally, the striped symbols denote the complexes with two monodentate acetates together with the ligand indicated on the x-axis.

8.2.1 Metal exchange within the protein cavity.

Consider the case of a hydrated Al(III) cation approaching the binding site of protein already served by Mg(II). The thermodynamical requirement for the substitution of Mg(II) by the incoming Al(III) cation to take place is that the ΔG of the exchange reaction must be negative. The calculated free energies of the Mg(II) cation exchange by Al(III) for all the single ligand complexes are negative when no environmental effects are considered (ε=1). A remarkable difference is found for the negative ligand Mg(II)/Al(III) exchange energy of around -140 kcal/mol (see the blue hollow circles corresponding to M and B on the left-hand-side of Fig. 8.1) and the neutral ligands ranging from -30 to -10 kcal/mol (see the blue hollow circles corresponding to I, A and Me on the right-hand-side of Fig. 8.1). This is a direct consequence of the larger interaction energy of Al(III) with negatively charged ligands as compared to Mg(II).

In a buried protein site (ε=4) metal exchange is favorable only for the negatively charged acetate ligand (see the M and B black hollow up-triangles) with exchange free energies of -27 kcal/mol for the monodentate binding and -20 kcal/mol for the bidentate binding. Neutral ligands have positive metal exchange free energies (see the I, A and Me black hollow up-triangles).

At higher dielectrics, the metal exchange from single ligand protein binding sites is not energetically favored even for the negatively charged acetate ligand, because the hard Al(III) metal cation has a large hydration free energy and therefore leaving the highly polarizable hydration shell for the less polarizable protein ligands environment is very unfavorable. Consequently, the Mg(II)/Al(III) exchange free energies for dielectric constants ε=20 and ε=78, which simulate a partially buried and a fully water accessible sites, respectively, are all positive (see the red hollow down triangles and the green hollow diamonds, respectively).

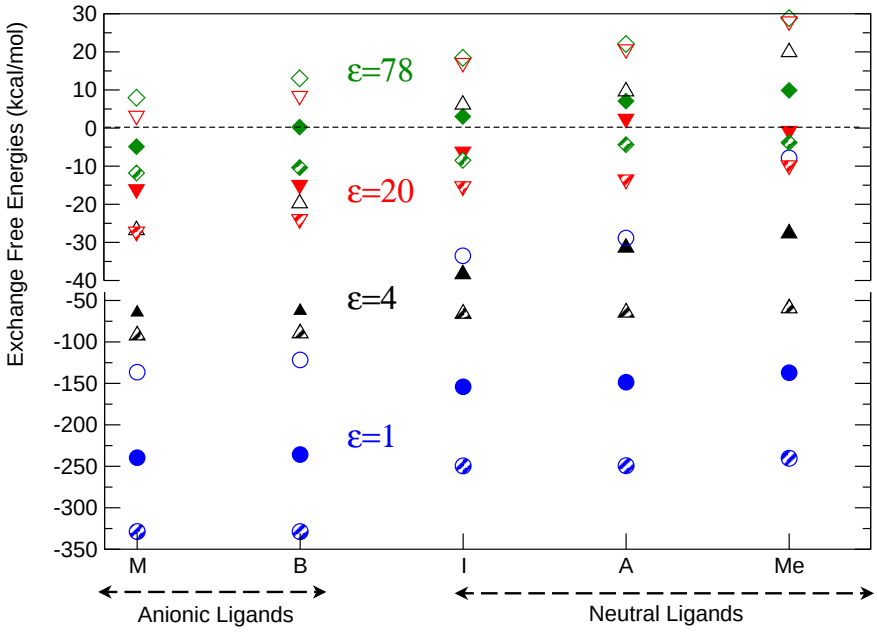

Fig. 8.1 Metal exchange reaction free energies of the reaction (4.6) for selected dielectric constant values. Circles stand for fully buried sites (ε=1), diamonds for fully solvent exposed sites (ε=78) and the up triangles and down triangles for the dielectric constant values 4 and 20, respectively. The hollow symbols correspond to the single ligand complexes, and the filled symbols to the two ligand complexes, where one ligand always corresponds to a monodentate acetate, and the second is denoted on the x-axis. Finally, the striped symbols denote the complexes with two monodentate acetates together with the ligand indicated on the x-axis. Notice that the energy scale changes at -40 kcal/mol.

Consider now binding sites with two ligands (filled symbols in Fig. 8.1) one of which is a monodentate acetate and the other one either a monodentate acetate (M), a bidentate acetate (B), a methylimidazole (I), an acetamide (A) or methanol (Me). Clearly, Mg(II)/Al(III) metal exchange, as compared with single ligand binding sites, is more favorable at all dielectric constants. Observe that it is only for those binding sites located in the fully solvent exposed areas (ε=78) that the metal exchange reaction is unfavorable (notice that the filled green diamonds of Fig. 8.1 are positive).

Finally we have considered protein binding sites made of two monodentate carboxylates and a third ligand of the same type as above. The Mg(II)/Al(III) metal exchange energies are shown in Fig. 8.1 by the striped symbols. The metal exchange is predicted to be highly favorable for buried sites (ε=4, 20).

Regarding the most solvent exposed area of the protein, the metal exchange reaction is also energetically favored in a fully water exposed environment, for all the binding site types investigated.

8.2.2
Metal exchange between the protein cavity and the aqueous environment.

Consider now the Mg(II)/Al(III) exchange when both hexahydrated cations, Mg(II) and Al(III) lie in an aqueous environment (ε=78) and the protein binding site is simulated by the explicit consideration of the ligands $L_1, \ldots, L_n$ and a lower dielectric constant. The calculated ΔG's for such a reactions are shown in Fig. 8.2.

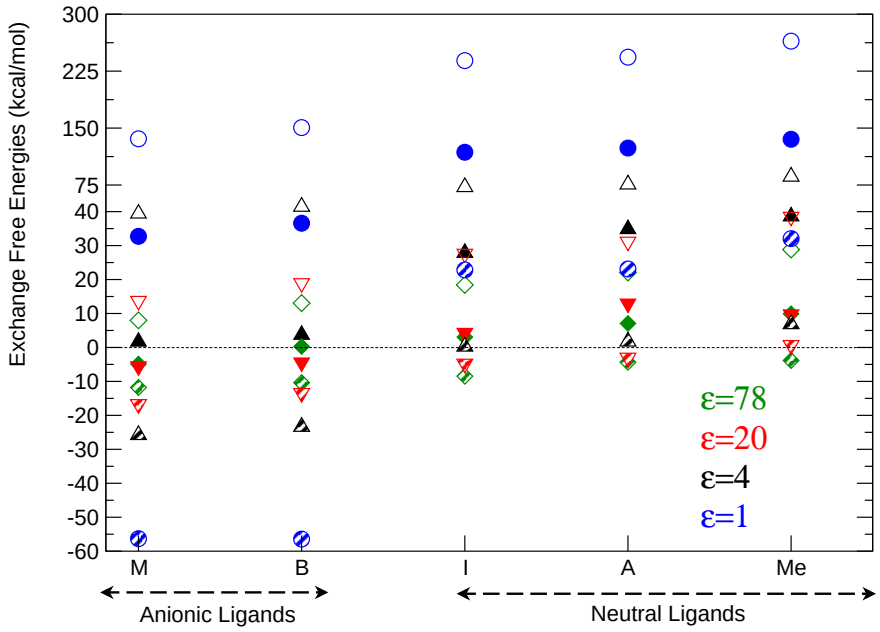

Fig. 8.2 Metal exchange reaction free energies of the reaction (4.6) for selected dielectric constant values. Circles stand for fully buried sites (ε=1), diamonds for fully solvent exposed sites (ε=78) and the up triangles and down triangles for the dielectric constant values 4 and 20, respectively. The hollow symbols correspond to the single ligand complexes, and the filled symbols to the two ligand complexes, where one ligand always corresponds to a monodentate acetate, and the second is denoted on the x-axis. Finally, the striped symbols denote the complexes with two monodentate acetates together with the ligand indicated on the x-axis. Notice that the energy scale changes at 40 kcal/mol.

Inspection of Fig. 8.2 reveals that the Mg(II)/Al(III) exchange is substantially less favorable than when the hydrated metal ion positions itself in the protein cavity and then the exchange takes place at the site. The latter mechanism has been discussed in Section 8.2.1.

Observe that for buried protein sites (ε=4) the substitution of Mg(II) by Al(III) will most favorably occur at sites containing two monodentate acetate ligands and one more acetate ligand either monodentate of bidentate (see striped black up-triangles of Fig. 8.2). Less buried sites (ε=20) allow the substitution also from sites consisting of two monodentate acetate ligands and one third methylimidazole (I) or acetamide (A) neutral ligand (see the striped red down-triangles of Fig. 8.2). Observe that for the fully accessible solvent environment (ε=78), the substitution can also occur at binding sites having methanol as the third ligand (see the green striped diamonds of Fig. 8.2).

Mg(II)/Al(III) substitution at binding sites consisting of one monodentate acetate ligand an additional acetate either monodentate or bidentate is only allowed at partially buried sites (ε=20) with a ΔG less than -10 kcal/mol (see the red filled down-triangles at the left hand site of Fig. 8.2).

8.3 Conclusions

Hydrated Al(III) can displace Mg(II) from protein binding sites most favorably when the binding sites are located in poorly solvent exposed areas.

The displacement reaction at these protein buried sites, is driven primarily by favorable Coulombic interactions between the larger positive charge of Al(III) and the negatively charged carboxylate ligands of the site. Negatively charged ligands, therefore, enhance the metal exchange. In particular, we have found that monodentate acetate side chains yield large negative free energies for the Mg(II)/Al(III) metal exchange reaction.

Increasing the solvent exposure of the binding site attenuates the free energy gain of the water/ligand exchange in the coordination shell of the metal because the desolvation penalty of the charged reactants exceeds the solvation free energy gain of the non charged or less charged products. Recall that *desolvation* in former of the two exchange mechanisms considered, consists of the removal of the cation's hydration shell, whereas in the latter mechanism *desolvation* includes also the extraction of the hexahydrated moiety from the aqueous environment. The hydrated Al(III), due to its larger charge, has a considerably higher desolvation penalty than Mg(II). This constrains the Mg(II)/Al(III) substitution in the most solvent exposed areas, overcoming the higher affinity of the aluminum cation for the ligands, for the former mechanism. In the latter, the balance between the ligand affinity of the cation and its desolvation energy is more subtle.

These two opposite tendencies are clearly reflected in Fig. 8.1 and 8.2. Our calculations suggest that Mg(II) and Al (III) can exchange their first coordination shells, *i.e:* Al(III) takes Mg(II)'s ligands and Mg(II) gets the hydration shell of the incoming hexahydrated Al(III), in the gas phase (ε=1). Observe that all blue symbols of Fig. 8.1 correspond to negative exchange free energies.

However, protein environment modifies this behavior substantially. When a buried protein site is considered and consequently the dielectric constant of the environment increased as to model the polarizability of the protein cavity (typical ε values in proteins sites [4–8] vary between 2 and 4), more ligands are required for the substitution to occur. In particular, the Mg(II)/Al(III) exchange, when both hexahydrated cations are placed in an aqueous phase, requires the presence of three ligands, two of which must be acetates and the third one either another acetate or a neutral ligand like methylimidazole or acetamide for partially buried sites (ε=20).

The metal exchange is more favorable in a stepwise mechanism. Namely, first, the hydrated Al(III) leaves the aqueous phase and positions itself within the protein binding site. Then the metal exchange occurs at the binding site, which in our modeling is characterized by a low dielectric constant (ε=4-20). Under these circumstances, even single neutral ligand binding sites might provide with the appropriate protein environment for the exchange process to be accomplished (see Fig. 8.1).

Finally, in the most solvent exposed areas, metal exchange could occur only in the three-ligand binding sites (three acetates or two acetates and a neutral ligand).

Interestingly, these are the ligands present in the most frequent protein binding sites [2] served by Mg(II), and also the proteins experimentally seen to be affected by Al(III) (as mentioned in the introduction) fulfill the conditions for substitution to be thermodynamically favoured.

Additionally, the location of Mg(II) in natural binding sites of proteins is very diverse, as it appears in several different dielectric environments. In the present work we have found that depending on the number and nature of the ligands and on the type of exchange mechanism, the exchange is favoured to occur at different polarizabilities, so none of the possible protein areas can be discarded.

Finally, recall that bond shortening has been observed upon Al(III) attachment to the binding site in previous chapters. This feature has also been addressed experimentally, resulting in the loss of enzymatic activity [3].

References

1 T. Dudev, Y. Lin, M. Dudev, C. Lim, J. Am. Chem. Soc. 125 (2003) 3168–3180.

2 T. Dudev, J. A. Cowan, C. Lim, J. Am. Chem. Soc. 121 (1999) 7665.

3 T. Gerczei, Z. Bocskei, E. Szabo, B. Asboth, G. Naray-Szabo, Int. J. Biol. Macro. 25 (1999) 329.

4 L. Rulisek, Z. Havlas, J. Phys. Chem. A 106 (2002) 3855.

5 T. Dudev, C. Lim, J. Phys. Chem. B 108 (2004) 4546–4557.

6 T. Simonson, J. Am. Chem. Soc. 20 (1998) 4875–4876.

7 T. Simonson, C. L. Brooks, J. Am. Chem. Soc. 118 (1995) 8452–8458.

8 T. Simonson, D. Perahia, Proc. Natl. Acad. Sci. U.S.A. 4 (1992) 1082–1086.

9 T. Dudev, C. Lim, J. Phys. Chem. B 104 (2000) 3692–3694.

10 P. Bernardi, Physiol. Rev. 79 (1999) 1127.

11 V. Lunin, E. Dobrovetsky, G. Khutoreskaya, R. Zhang, A. Joachimiak, D. Doyle, A. Bochkarev, M.E.Maguire, A. Edwards, C. Koth, Nature 440 (2006) 833.

12 T. Dudev, C. Lim, J. Am. Chem. Soc. 128 (2006) 10541–10548.

13 H. Meiri, E. Banin, M. Roll, A. Rousseau, Progress in Neurobiology 40 (1993) 89–121.

14 C. S. Babu, T. Dudev, R. Casareno, J. Cowan, C. Lim, J. Am. Chem. Soc. 125 (2003) 9318–9328.

Part 4 Concluding Remarks

Few structural data regarding Al(III) complexes with biological compounds is available in literature [1,2], including those relevant for elucidating the biochemistry of Al(III) in protein environments. In this thesis, ample structural information is reported, regarding the binding of Al(III) and Mg(II) with the most common ligands found in proteins, considering the various combinations and different number of ligands that can be found in a metal binding site. This information might be useful in modeling the binding of aluminium to specific proteins [3,4].

Aluminium, as expected for a "hard" ion, has shown to favour binding to oxygen and nitrogen groups, in particular negatively charged oxygens. Therefore, the negatively charged acetate and the neutral methylimidazole, followed by formamide and methanol (both neutral) have been seen to be preferred for binding Al(III). This implies that the preferred amino acids to bind Al(III) in proteins should be Aspartate, Glutamate and Histidine, and in a lesser extent Asparagine, Glutamine, backbone carbonyl groups, Serine, Threonine and Tyrosine. This behaviour parallels that of Mg(II), which shows the same ligand preference.

Overall, our results point out that for the acetate, the monodentate way of binding is the preferred for aluminium in all cases. In principle, trivalent cations are better charge acceptors than divalent ions, and in particular, the trivalent La(III) has been seen to show a preference for bidentate carboxylate [6]. However, in our case the size prevails over the charge, for La(III) is large enough as to accommodate bidentate carboxylic groups with tiny sterical hindrance. Al(III), on the other hand, favours the monodentate binding rather than bidentate binding, due to its small size, which provides not enough room in its coordination sphere or bidentate mode complexation [5,6]. We have always considered water-rich metal complexes, where the metal-free carboxylate oxygen atoms interact with the metal-bound water molecules; therefore, the monodentate is stabilized as compared to the bidentate mode. In fact, monodentate carboxylate binding mode is the most common one found in natural Mg(II) binding sites. Our results are in accordance with this fact, as monodentate binding of the carboxylate has been seen to be, overall, the preferred one [7].

The binding of the metals to the bioligands is mainly dictated by the favourable Coulomb interactions between the positively charged cation and the negatively charged or neutral ligands, and the solvation free energies of the products and reactants in the dielectric environment considered. Al(III), due mainly to its high charge, has a strong tendency of binding these bioligands, but its solvation free energy is also very high. The delicate balance of these forces regulates the affinity of the metal for the binding sites in the corresponding dielectric environment.

Therefore, the presence of negatively charged ligands highly enhances the attachment of aluminium to the binding site, being most favored in low dielectric environments. We can consider that aluminium will prefer to bind proteins (low dielectric environment) rather than small low weight molecules, in an aqueous environment. Nevertheless, the formation of aluminium complexes in both gas and aqueous phases is promoted when the number of available ligands increases. In particular, binding sites with two acetates or three ligands (at least one of them being an acetate) are energetically favored to bind aluminium in the whole range of dielectric constants in our calculations. Accordingly, experimental works have revealed that simple bidentate carboxylic ligands such as lactic acid, oxalic acid or amino acids weakly keep Al(III) in solution via complex formation, while tridentate small organic species which can bind the metal provide higher stability [8–10]. In fact, the best chelators for Al(III) are multidentate ligands with negative oxygen donors [11]. The main example is the citrate, which, with three donor groups bound to aluminium, is the main low weight molecule which carries aluminium in blood [12].

This can also be applied to peptides. Aluminium will bind peptides in solution, if there are enough ligands available and depending on the environment [3, 13, 14], and the length of the peptide, will be able of causing conformational changes and aggregation.

In buried protein zones Al(III) has been seen to attach binding sites with only one ligand, but, still, the preferred binding sites are those presenting three ligands, at least one of them being acetate. The latter is the most common case found in natural proteins, for which Al(III) has shown high affinity, and very large formation free energies.

We can therefore suggest this kind of binding sites in proteins that interact with Al(III). The large binding strength estimated and the low exchange rate of Al(III) suggests that, in consequence, the binding site of the protein can be blocked. Accordingly, Al(III) has been seen to block the active centre of the trypsin, for which the coordination suggested involves a serine, a histidine and an aspartate [15].

Even if four ligand binding sites have not been studied in this case, the outlined tendency suggests that, aluminium will be able to attach to binding sites with four ligands with similar or more strength than those with three ligands. Four acetates might be the maximum number of monodentate acetates that Al(III) could bind [16]. Consequently, we can suppose that, as happened with the magnesium, the attachment of a fourth acetate in the first hydration shell might not involve such a large energy gain as compared to the third, and that the energy difference with the addition of a non charged ligands would also be small in this case. Thus, we can say that the binding sites presenting four or more ligands, acetates being between 1 and 3, might be very favourable for aluminium, even in the most solvent-exposed areas of the protein. The

binding site in the transferrin is one of these cases, where the metal binds two tyrosines, one histidine, one aspartate and a bicarbonate ion.

Regarding the ability of Al(III) to substitute Mg(II), we have seen in the previous chapter that it largely depends on the environment and substitution mechanism. Observe, nevertheless, that the metal exchange is likely to happen in Mg(II)'s binding sites and, probably, in binding sites with more than three ligands available. Between the Mg-dependent enzymes inhibited or altered by aluminium, some of them as acetilcholinesterase, alkaline phosphatase, or adenylate cyclase, fulfill this conditions, so, the substitution is possible from the thermodynamical point of view. Due to the charge difference between both metals, the key factor on the selectivity of one binding site for one metal or another can rely on the negatively charged acetates, as it happens in the engineered EF-hand calcium binding sites containing three Asp/Glu side chains (with a net ligand charge of -3), which preferably bind Ca(II) against a much higher background concentration of monovalent cations such as Na(I) and K(I) [17]. Mg(II) natural binding sites, as remarked previously, are not usually very specific, so the entering of another metal with higher affinity for the site is probable. One of the reasons for which Mg(II) is so widely used in biological reactions might because it 'weakly' binds its binding sites. This permits to enter and exit the protein easily. Al(III), in the case which is able to arrive to the active site and bind stronger than Mg(II) would certainly not have this easy entering and exiting the binding site property, and undoubtedly, would lead to the misfunctioning of the biological species.

References

1 A. Salifoglou, Coord. Chem. Rev. 228 (2002) 297–317.

2 A. K. Powell, S. L. Heath, Coor. Chem. Rev. 149 (1996) 59–80.

3 D. Hollender, A. Karoly-Lakatos, P. Forgo, T. Kortvelyesi, G. Dombi, Z. Majer, M. Hollosi, T. Kiss, A. Odani, J. Inorg. Biochem. (2006) 351–361.

4 R. E. Bongini, S. Culver, K. M. Elkins, J. Inorg. Biochem. (2007) 1251–1264.

5 A. Katz, J. Glusker, G. Markham, C. Bock, J. Phys. Chem. B 102 (1998) 6342–6350.

6 T. Dudev, C. Lim, Acc. Chem. Res. 40 (2007) 85–93.

7 T. Dudev, C. Lim, J. Phys. Chem. B 108 (2004) 4546–4557.

8 C. Exley (Ed.), Aluminium and Alzheimer's disease, Elsevier, Amsterdam, 2001.

9 T. Kiss, I. Sovago, R. B. Martin, Inorg. Chem. (1991) 2130–2132.

10 P. Rubini, A. Lakatos, D. Champmartin, T. Kiss, Coord. Chem. Rev. 228 (2002) 137–152.

11 R. A. Yokel, Coord. Chem. Rev. 228 (2002) 97–113.

12 A. J. A. Aquino, D. Tunega, G. Haberhauer, M. H. Gerzabek, H. Lischka, Chem. Phys. Phys. Chem. 3 (2001) 1979.

13 M. Kilyen, P. Forgo, A. Lakatos, G. Dombi, T. Kiss, N. Kotsakis, A. Salifoglou, J. Inorg. Biochem. 94 (2003) 207–213.

14 T. Kiss, M. Kilyen, A. Lakatos, F. Evanics, T. Kortvelyesi, G. Dombi, Z. Majer, M. Hollosi, Coord. Chem. Rev. 228 (2002) 227–236.

15 P. Zatta, C. Bordin, M. Favarato, Arch. Biochem. Biophys. 303 (1993) 407–411.

16 T. Dudev, C. Lim, J. Am. Chem. Soc. 128 (2006) 1553–1561.

17 J. Falke, S. Drake, A. Hazard, O. Peersen, Q. Rev. Biophys. 27 (1994) 219–290.

Part 5 Appendix

9
Tables corresponding the Plots in the chapter 6

Tab. 9.1 Gas phase and aqueous phase (in *italics*) geometries (in Å) of the complexes described along the text. X-O_l is the bond length of the acetate's oxygen and the metal cation. X-L_2 is the bond length formed between the second ligand and the metal, while X-O_w is the average of the bonds formed between the metal cation and the water molecules of the complex (the standard deviation was in all cases less than 5% of the mean value). Values in parenthesis have been taken from the literature.

	Al (III)			Mg (II)		
	X-O_l	X-L_2	X-O_w	X-O_l	X-L_2	X-O_w
2M	1.939	1.939	1.927	2.056	2.056	2.131
	(1.957 [a], 1.811[b])	(1.957 [a], 1.811[b])				
	1.861(1.929 [a])	*1.866 (1.986 [a])*	*1.939*	*2.051*	*2.049*	*2.118*
MB	(bi) 1.929	1.890	1.945	(bi)2.119	2.036	2.139
	(bi) 1.935	*1.842*	*1.935*	*(bi)2.132*	*2.049*	*2.119*
2B	1.904	1.909	1.980	2.090	2.120	2.160
	(1.933 [a], 1.893[b])	(1.933 [a], 1.893 [b])				
	1.920 (1.953 [a])	*1.931 (1.933[a])*	*1.916*	*2.111*	*2.116*	*2.101*
TM	1.937	2.299	1.982	2.050	2.570	2.320
	1.883	*2.318*	*1.964*	*2.054*	*2.517*	*2.138*
TB	1.939	2.251	2.022	2.121	2.514	2.170
	1.959	*2.145*	*1.967*	*2.143*	*2.476*	*2.139*
MeM	1.871	1.953	1.945	2.021	2.103	2.117
	1.846	*1.941*	*1.917*	*2.038*	*2.097*	*2.085*
MeB	1.881	1.898	1.979	2.071	2.070	2.142
	1.921	*1.883*	*1.921*	*2.108*	*2.049*	*2.098*
AM	1.886	1.876	1.956	2.027	2.047	2.135
	1.849	*1.855*	*1.941*	*2.038*	*2.047*	*2.113*
AB	1.900	1.822	1.979	2.102	2.020	2.135
	1.929	*1.826*	*1.929*	*2.126*	*2.023*	*2.098*
IM	1.885	1.971	1.966	2.033	2.159	2.135
	1.861	*1.981*	*1.932*	*2.041*	*2.160*	*2.113*
IB	1.899	1.935	1.995	2.101	2.125	2.156
	1.931	*1.931*	*1.943*	*2.119*	*2.130*	*2.118*

[a] taken from ref [6].
[b] taken from ref [5].

Tab. 9.2 Formation enthalpies and free energies (in kcal/mol) corresponding to the water/ligand exchange as described in reaction 3 of the manuscript. ^{g} superscipt stands for gas phase and ^{aq} for aquoeus phase properties. Figures in *italics* have been taken from the literature. The enthalpies have been plotted in Figure 2 of the manuscript.

	Aluminum (III)				Magnesium (II)			
	ΔH_f^g	ΔG_f^g	ΔH_f^{aq}	ΔG_f^{aq}	ΔH_f^g	ΔG_f^g	ΔH_f^{aq}	ΔG_f^{aq}
2M	-561.9 *-552.5*[a]	-559.64-*551.7*[a]	-19.26 *-16.3*[a]	-15.63 *-14.7*[a]	-324.43	-320.04	-14.24	-10.75
MB	-545.75	-554.62	-7.00	-15.87	-312.61	-318.88	-9.87	-16.14
2B	-527.3 *-510.4*[a]	-546.38 *-531.8*[a]	1.27 *6.8*[a]	-17.79 *-11.7*[a]	-298.47	-316.71	-4.04	-22.28
TM	-541.27	-542.1	-7.66	-8.49	-311.91	-309.55	-5.52	-3.16
TB	-525.97	-537.31	1.22	-10.13	-297.90	-307.23	-0.53	-9.86
MeM	-341.78	-341.28	3.45	-0.56	-205.92	-204.18	-7.7	-10.46
MeB	-317.64	-327.46	14.04	-0.30	-192.31	-200.62	-0.44	-13.25
AM	-363.61	-361.22	-1.19	1.20	-216.61	-212.62	-9.86	-5.87
AB	-344.44	-353.43	8.02	-0.97	-206.01	-213.14	-3.86	-10.99
IM	-370.25	-368.94	-5.6	-4.29	-217.57	-214.82	-10.08	-7.33
IB	-350.49	-357.51	3.78	-3.23	-204.49	-212.79	-4.59	-12.89

[a] taken from ref [6].

Tab. 9.3 Metal exchange energies and free energies (in kcal/mol) as described by reaction 4. The enthalpies have been plotted in Figure 3 of the manuscript.

	$\Delta H^{g}_{Mg/Al}$	$\Delta G^{g}_{Mg/Al}$	$\Delta H^{aq}_{Mg/Al}$	$\Delta G^{aq}_{Mg/Al}$
2M	-237.47	-239.60	-5.02	-4.88
MB	-233.15	-235.75	2.87	0.27
2B	-228.84	-229.56	5.30	4.48
TM	-229.36	-232.54	-2.14	-5.32
TB	-228.07	-230.09	1.74	-0.27
MeM	-135.86	-137.10	11.15	9.90
MeB	-125.33	-126.84	14.48	12.96
AM	-146.99	-148.60	8.67	7.07
AB	-138.43	-140.28	11.87	10.02
IM	-152.68	-154.12	4.48	3.04
IB	-146.00	-144.72	8.38	9.66

Tab. 9.4 Formation free energies (in kcal/mol) as described in reaction 3 for selected values of the dielectric constant ϵ. Values plotted in Figure 5 of the manuscript.

	Aluminum (III)								Magnesium (II)							
	ΔH				ΔG				ΔH				ΔG			
	ϵ=2	ϵ=4	ϵ=20	ϵ=78	ϵ=2	ϵ=4	ϵ=20	ϵ=78	ϵ=2	ϵ=4	ϵ=20	ϵ=78	ϵ=2	ϵ=4	ϵ=20	ϵ=78
2M	-283.33	-143.61	-30.38	-19.26	-281.07	-141.35	-28.12	-15.63	-161.53	-81.21	-16.46	-14.24	-157.14	-76.82	-12.07	-10.75
MB	-271.51	-135.14	-25.34	-7.00	-280.38	-144.01	-34.21	-15.87	-153.17	-70.35	-8.12	-9.87	-159.44	-76.62	-14.39	-16.14
2B	-256.94	-123.37	-16.47	1.27	-276.02	-142.45	-35.55	-17.79	-143.18	-68.10	-8.84	-4.04	-161.42	-86.34	-27.08	-22.28
TM	-277.76	-141.14	-30.93	-7.66	-267.88	-131.26	-21.05	-8.49	-150.89	-72.12	-8.9	-5.52	-148.53	-69.76	-6.54	-3.16
TB	-254.73	-121.06	-13.81	1.22	-266.07	-132.40	-25.15	-10.13	-140.93	-64.93	-4.42	-0.53	-150.23	-74.23	-13.72	-9.86
MeM	-164.73	-77.09	-6.59	3.45	-164.23	-76.59	-6.09	-0.56	-101.38	-50.69	-10.26	-7.7	-99.64	-48.95	-8.52	-10.46
MeB	-146.80	-63.42	2.71	14.04	-156.62	-73.24	-7.11	-0.30	-84.10	-36.10	1.49	-0.44	-92.41	-44.41	-6.82	-13.25
AM	-168.36	-75.39	-2.62	-1.19	-176.21	-83.24	-10.47	1.20	-108.42	-55.85	-13.72	-9.86	-104.43	-51.86	-9.73	-5.87
AB	-164.31	-75.65	-4.53	8.02	-173.30	-84.64	-13.52	-0.97	-100.62	-50.32	-10.7	-3.86	-107.75	-57.45	-17.83	-10.99
IM	-184.11	-91.83	-17.07	-5.6	-182.80	-90.52	-15.76	-4.29	-107.86	-54.92	-12.31	-10.08	-105.11	-52.17	-9.56	-7.33
IB	-169.16	-80.39	-9.39	3.78	-176.18	-87.41	-16.41	-3.23	-98.98	-48.96	-9.36	-4.59	-107.28	-57.26	-17.66	-12.89

Tab. 9.5 Metal exchange free energies (in kcal/mol) as described in reaction 4 for selected values of the dielectric constant ϵ. Values plotted in Figure 6.

	ΔH				ΔG			
	ϵ=2	ϵ=4	ϵ=20	ϵ=78	ϵ=2	ϵ=4	ϵ=20	ϵ=78
2M	-121.80	-62.40	-13.92	-5.02	-123.93	-64.53	-16.05	-4.88
MB	-118.35	-59.89	-12.32	2.87	-120.95	-62.49	-14.92	0.27
2B	-113.67	-55.18	-7.54	5.30	-114.49	-56.00	-8.36	4.48
TM	-120.45	-62.60	-15.61	-2.14	-122.57	-64.72	-17.73	-5.32
TB	-113.80	-56.13	-9.39	1.74	-115.82	-58.15	-11.41	-0.27
MeM	-63.35	-26.4	3.67	11.15	-64.59	-27.64	2.43	9.90
MeB	-55.11	-19.73	8.81	14.48	-55.55	-20.17	8.37	12.96
AM	-70.17	-29.77	0.87	8.67	-71.78	-31.38	-0.74	7.07
AB	-63.69	-25.33	6.17	11.87	-65.54	-27.18	4.32	10.02
IM	-76.25	-36.91	-4.76	4.48	-77.69	-38.35	-6.2	3.04
IB	-70.18	-31.43	-0.03	8.38	-68.90	-30.15	1.25	9.66

10
Tables corresponding the Plots in the chapter 7

Tab. 10.1 Formation enthalpies and free energies (in *italics*) (in kcal/mol) corresponding to the water/ligand exchange as described in reaction 3 of the manuscript. ^{g} superscipt stands for gas phase and ^{aq} for aquoeus phase properties, while ^{4} and ^{20} stand for dielectrics 4 and 20. The enthalpies have been plotted in Figure 3 of the manuscript.

	Aluminum (III)				Magnesium (II)			
	ΔE_f^g	ΔE_f^4	ΔE_f^{20}	ΔE_f^{aq}	ΔE_f^g	ΔE_f^4	ΔE_f^{20}	ΔE_f^{aq}
3M	-688.74 *-683.40*	-188.23-*182.89*	-52.95-*47.6*	-39.54 *-34.21*	-361.0-*354.8*	-97.14-*90.9*	-26.68 *-20.4*	-27.5 *-21.2*
2MB	-676.05-*682.15*	-180.02-*186.12*	-46.39 *-52.5*	-33.05 *-39.16*	-349.40-*353.39*	-92.55-*96.54*	-24.58 *-28.57*	-23.76-*27.75*
M2B	-666.72 *-682.73*	-175.79 *-191.8*	-44.16 *-60.17*	-25.82-*41.83*	-339.26-*354.06*	-91.77-*106.57*	-27.51-*42.31*	-20.36-*35.15*
3B	-655.39 *-679.69*	-167.92-*192.22*	-37.58-*61.88*	-17.12 *-41.41*	-308.32-*336.49*	-72.59-*100.76*	-12.57 *-40.74*	-16.12 *-44.29*
2M-T	-672.32-*669.28*	-172.28-*169.24*	-37.21-*34.17*	-28.21-*25.17*	-352.29-*347.39*	-85.58-*80.68*	-13.63-*8.73*	-18.41-*13.51*
MB-T	-660.39-*668.2*	-165.52-*173.33*	-32.71-*40.52*	-22.44-*30.25*				
M-2T	-655.74-*654.7*	-155.16 *-154.17*	-19.89-*18.90*	-16.5-*15.5*	-340.61-*337.10*	-73.98 *-70.47*	-2.20 *1.31*	-10.00-*6.49*
B-2T	-644.69-*655.45*	-150.03-*160.79*	-17.36-*28.12*	-11.12 *-21.87*	-327.89-*335.46*	-68.29-*75.86*	0.42-*7.15*	-5.49 *-13.05*
2M-I	-577.82-*573.36*	-152.59-*148.13*	-37.48-*33.02*	-31.01-*26.56*	-330.00-*323.88*	-88.30-*82.18*	-23.85-*17.73*	-24.20-*18.09*
MB-I	-566.73-*571.96*	-147.62-*152.85*	-35.16-*40.39*	-23.97-*29.19*	-316.20-*321.13*	-81.21-*86.14*	-19.19-*24.12*	-19.71 *-24.64*
2B-I	-550.37-*567.81*	-138.00-*155.44*	-28.24-*45.68*	-14.28 *-31.72*	290.15*230.33*	-76.49-*92.39*	-16.67-*32.57*	-14.75-*30.65*
2M-A	-572.87-*567.5*	-149.25-*143.88*	-34.97-*29.6*	-28.71 *-23.33*	-323.63-*318.28*	-84.75-*79.4*	-21.42-*16.07*	-24.32-*18.97*
MB-A	-559.16-*564.52*	-141.88-*147.24*	-30.09-*35.45*	-20.6-*25.97*	-313.68-*317.75*	-88.68-*92.75*	-11.18-*15.25*	-19.81-*23.88*
2B-A	-547.76-*564.05*	-135.04-*151.33*	-24.81 *-41.10*	-11.51 *-27.8*	-308.98-*323.41*	-78.29-*92.72*	-17.97-*32.4*	-15.22-*29.65*
2M-Me	-563.51-*559.88*	-143.49-*139.86*	-30.13 *-26.5*	-24.44-*20.81*	-325.05-*319.61*	-85.94-*80.5*	-22.14-*16.7*	-22.43-*16.99*
MB-Me	-548.14-*555.61*	-135.43-*142.9*	-25.06-*32.53*	-15.37-*22.83*	-313.11-*319.59*	-79.65-*86.13*	-18.05 *-24.53*	-17.05-*23.53*
2B-Me	-531.26-*549.42*	-125.32-*143.48*	-17.99-*36.15*	-4.44 *-22.6*	-301.61-*317.81*	-73.79-*89.99*	-14.72-*30.92*	-11.24 *-27.44*
M-2I	-393.75-*390.22*	-98.77-*95.24*	-20.34-*16.81*	-16.23 *-12.71*	-226.61-*222.34*	-60.22-*55.95*	-16.28 *-12.01*	-74.93*22.25*
B-2I	-383.37-*390.26*	-93.95-*100.84*	-17.33 *-24.22*	-9.68-*13.73*	-217.36-*223.05*	-55.72-*61.41*	-13.99 *-19.68*	-14.98-*20.68*
M-2A	-384.04-*378.33*	-92.47-*86.76*	-14.28-*8.57*	-11.57-*5.86*	-229.49-*222.42*	-61.56-*54.49*	-16.93 *-9.86*	-20.22-*13.14*
B-2A	-370.72-*376.06*	-85.22-*90.56*	-9.27-*14.61*	-4.35 *-9.69*	-218.22-*223.2*	-56.49-*61.47*	-14.36 *-19.34*	-15.16-*20.15*
M-2Me	-343.29-*342.11*	-72.91-*71.73*	-2.04-*0.86*	-0.27 *0.92*	-206.34-*202.636*	-49.74-*46.04*	-8.79 *-5.09*	-13.22 *-9.519*
B-2Me	-322.11-*331.54*	-60.70-*70.13*	7.2 *-2.23*	11.79 *2.36*	-193.65-*201.9*	-44.65-*52.9*	-6.65 *-14.90*	-7.7-*15.95*

Tab. 10.2 Metal exchange enthalpies and free energies (in *italics*) (in kcal/mol) as described by reaction 4. The enthalpies have been plotted in Figure 4 of the manuscript. ^{g} superscipt stands for gas phase and ^{aq} for aquoeus phase properties, while ^{4} and ^{20} stand for dielectrics 4 and 20.

	$\Delta E^{g}_{Mg/Al}$	$\Delta E^{4}_{Mg/Al}$	$\Delta E^{20}_{Mg/Al}$	$\Delta E^{aq}_{Mg/Al}$
3M	-327.70 *-328.64*	-91.09-*92.03*	-26.27-*27.21*	-12.08-*13.01*
2MB	-326.65-*328.76*	-87.47-*89.58*	-21.81-*23.92*	-9.30-*11.41*
M2B	-327.46-*328.67*	-84.02-*85.23*	-16.65-*17.86*	-5.47-*6.68*
3B	-347.08-*343.20*	-95.34-*91.46*	-25.02-*21.14*	-1.00*2.88*
2M-I	-247.82 *-249.48*	-64.29-*65.95*	-13.63 *-15.29*	-6.81-*8.47*
MB-I	-250.53 *-250.83*	-66.41-*66.71*	-15.97-*15.97*	-4.26 *-4.56*
2B-I	-243.56-*245.10*	-61.52-*63.06*	-11.58 *-13.12*	0.47-*1.07*
2M-A	-249.24-*249.21*	-64.50-*64.47*	-13.55 *-13.52*	-4.39-*4.36*
MB-A	-245.47-*246.78*	-53.19-*54.50*	-18.90-*20.21*	-0.79-*2.09*
2B-A	-238.78-*240.65*	-56.75-*58.62*	-6.84 *-8.71*	3.71*1.85*
2M-Me	-238.45-*240.27*	-57.54-*59.36*	-7.98 *-9.80*	-2.01-*3.05*
MB-Me	-235.03 *-236.02*	-55.78-*56.77*	-7.01-*8.00*	1.68*0.7*
2B-Me	-229.64 *-231.60*	-51.52-*53.48*	-3.26 *-5.22*	6.8*4.84*
MI	-167.14 *-167.88*	-38.55-*39.29*	-4.06 *-4.80*	58.7-*34.96*
BI	-166.01-*167.21*	-38.23-*39.43*	-3.34-*4.54*	5.30 *4.10*
MA	-154.55 *-155.91*	-30.91-*32.27*	2.65*1.29*	8.65*7.28*
BA	-152.5 *-152.86*	-28.73-*29.09*	5.09 *4.73*	10.81 *10.46*
MMe	-136.96-*139.47*	-23.18-*25.69*	6.74 *4.23*	12.95 *10.44*
BMe	-128.47 *-129.65*	-16.05-*17.23*	13.85 *12.67*	19.49 *18.31*

Tab. 10.3 Gas phase and aqueous phase (in *italics*) geometries (in Å) of the complexes described along the text. X-O_l is the average bond length of the acetate's oxygen and the metal cation. X-L_2 is the average bond length formed between the second ligand and the metal, while X-O_w is the average of the bonds formed between the metal cation and the water molecules of the complex.

	Al (III)			Mg (II)		
	X-O_l	X-L_2	X-O_w	X-O_l	X-L_2	X-O_w
3M	1.8972		1.9469	2.0912		2.1452
	1.9024		*1.9434*	*2.1075*		*2.1314*
2MB	1.8772	(bi) 1.9658	1.9503	2.0517	(bi) 2.1807	2.1854
	1.8774	*(bi) 1.9786*	*1.9299*	*2.0774*	*(bi) 2.1666*	*2.1287*
M2B	1.8110	(bi) 1.9561	2.0346	2.0266	(bi) 2.1521	2.2975
	1.8159	*(bi) 1.9640*	*1.9543*	*2.0111*	*(bi) 2.1569*	*2.1374*
3B	1.9402			2.1415		
	1.9372			*2.1431*		
2M-T	1.9018	2.3459	1.9898	2.0870	2.6472	2.1632
	1.9008	*2.3505*	*1.9855*	*2.0896*	*2.6455*	*2.1515*
MB-T	1.8714 ((bi) 1.9936)	2.3081	2.0377			
	1.8972 ((bi) 2.0003)	*2.3135*	*1.9757*			
M-2T	1.8685	2.3435	2.0942	2.1253	2.5919	2.2046
	1.8871	*2.3638*	*2.0350*	*1.8871*	*2.3638*	*2.0350*
B-2T	1.9904	2.3073	2.1658	2.1956	2.5483	2.2801
	2.0090	*2.3360*	*2.0392*	*2.1801*	*2.5652*	*2.2221*
2M-I	1.9615	2.0252	2.0650 (-OH 1.84)	2.0745	2.1938	2.1488
	1.8933	*2.0161*	*1.9426*	*2.0793*	*2.1888*	*2.1475*
MB-I	1.9139 ((bi) 1.9624)	1.9795	2.0999 (-OH 1.8048)	2.0720 ((bi) 2.1379)	2.1896	2.1636
	1.8810 ((bi) 1.9647)	*1.9627*	*1.9446*	*2.0814 ((bi) 2.1538)*	*2.1934*	*2.1145*
2B-I	1.9287	1.9361	2.0206	2.1287	2.1490	2.2111
	1.9477	*1.9523*	*1.9425*	*2.1390*	*2.1491*	*2.1270*
2M-A	1.9098	1.9110	2.0416 (-OH 1.8366)	2.0578	2.1721	2.1300
	1.8865	*1.8964*	*1.9483*	*2.0828*	*2.1112*	*2.1266*
MB-A	1.9256 ((bi) 1.9548)	2.0266	2.0485(-OH 1.8077)	2.0332 ((bi) 2.1438)	2.1018	2.1406
	1.8776 ((bi) 1.9629)	*1.8635*	*1.9395*	*2.0718 ((bi) 2.1492)*	*2.0733*	*2.1239*
2B-A	1.9277	1.8705	1.9860	2.1253	2.0622	2.1822
	1.9449	*1.8513*	*1.9244*	*2.1351*	*2.0574*	*2.1088*
2M-Me	1.9332	2.0134	2.0421 (-OH 1.8279)	2.0589	2.1441	2.1332
	1.8734	*1.9545*	*1.9372*	*2.0632*	*2.1464*	*2.1262*
MB-Me	1.8956 ((bi) 1.9322)	2.0103	1.9804 (-OH 1.8247)	2.0155 ((bi) 2.1310)	2.1473	2.1343
	1.8416 ((bi) 1.9543)	*1.9467*	*1.9235*	*2.0428 ((bi) 2.1476)*	*2.1337*	*2.1121*
2B-Me	1.8882	1.9265	1.9861	2.0753	2.1368	2.0963
	1.9262	*1.9150*	*1.9172*	*2.1154*	*2.1255*	*2.0732*
MI	1.9128	2.0181	2.0437 (-OH 1.8086)	2.0451	2.1945	2.1499
	1.8780	*2.0087*	*1.9531*	*2.0635*	*2.1993*	*2.1385*
BI	1.9200	1.9641	2.0348	2.1053	2.1523	2.1874
	1.9521	*1.9687*	*1.9589*	*2.1443*	*2.1618*	*2.1411*
MA	1.8667	1.8610	2.0178 (-OH 1.9270)	2.0738	2.0791	2.1219
	1.8836	*1.8681*	*1.9527*	*2.0897*	*2.0476*	*2.1187*
BA	1.9348	1.8486	1.9996	2.1310	2.0420	2.1507
	1.9517	*1.8585*	*1.9386*	*2.1526*	*2.0707*	*2.1121*
MMe	1.8747	1.9773	2.0059 (-OH 1.7797)	2.0309	2.1074	2.1257
	1.8454	*1.9478*	*1.9209*	*2.0470*	*2.0866*	*2.1174*
BMe	1.8882	1.9265	1.9861	2.0753	2.1368	2.0963
	1.9262	*1.9150*	*1.9172*	*2.1154*	*2.1255*	*2.0732*